

An Improved Wide-Band System Equivalent Technique for Real Time Digital Simulators

by

Yuefeng Liang

A Thesis

Submitted to the Faculty of Graduate Studies in Partial Fulfillment
of the Requirements for the Degree of

Doctor of Philosophy

Department of Electrical and Computer Engineering
University of Manitoba
Winnipeg, Manitoba

Copyright©2011 by Yuefeng Liang

Author's Declaration

I hereby declare that I am the sole author of this thesis. This is a true copy of the thesis, including any required final revisions, as accepted by my examiners. I understand that my thesis may be made electronically available to the public.

Abstract

This thesis introduces a new modeling approach that allows very large power systems to be modeled on a real time electro-magnetic transients (EMT) digital simulator with reduced hardware costs. The key step in achieving this is the development of an improved wide-band multi-port equivalent, which reduces a large power network into a small manageable equivalent model that preserves wideband behaviors.

This approach has a foundation method that use a two part equivalent in which the high frequency behavior of the equivalenced network is represented by a terminating frequency dependent network equivalent (FDNE), with the low frequency behavior being modeled using a detailed Transient Stability Analysis (TSA) model that only models the electromechanical behavior. This approach allowed the modeling of medium size electric regions up to hundreds of buses in real time.

This thesis extends the equivalent by implementing a reduced order of the detailed electromechanical TSA equivalent mentioned above. Coherency based reduction is used for the electromechanical model of the power network to be equivalenced, and is implemented as a Transient Stability Analysis (TSA) type electromechanical equivalent. A challenge in implementing the FDNE is to ensure that it is a passive network, as otherwise its inclusion could lead to unstable simulation. This thesis also introduces a practical procedure to enforce passivity in the FDNE.

The validity of the proposed technique is demonstrated by comparing the approach with detailed electromagnetic simulations of the well-known 39 bus New England system and a modified 39 bus system with an HVDC infeed with coupling between the dc line and an adjacent ac line, in addition to a 108 bus ac system. The power of the method is demonstrated by the real-time simulation of a large system with 2300 buses and 139 generators. It has been shown that this approach has the potential to increase by at least one order of magnitude the size of the network that can be modeled and thus on a real time electro-magnetic transients (EMT) digital simulator with reduced hardware costs.

Acknowledgments

I would like to express my sincere gratitude and appreciation to Prof. Ani Gole for his invaluable guidance and encouragement throughout the course of this research work.

I am also indebted to Prof. Udaya D. Annakkage, Dr. Ming Yu, Dr. Yi Zhang and Mr. In-Kwon Park for many fruitful discussions of the research and expert programming guidance of the RTDS.

Thanks are forward to my fellow students in the Power Group and my colleagues in RTDS, for the friendly, helpful and enlightening atmosphere, which makes the research work enjoyable. Especially I would like to express my gratitude to Dr. Xi Lin for his help to this work.

Here I am also grateful to the Alberta ISO for providing the original data which was modified to derive the 2300 bus system. Thanks are given to Andrew Isaacs and Garth Irwin of Electranix Inc., for their useful suggestions.

My special appreciation goes to my beloved families for their love, endless support and encouragement in this venture.

Financial supports from the Industrial Research Chairs (IRC) program of the Natural Sciences and Engineering Research Council (NSERC) of Canada, the Network Centre of Excellence MITACS, and the RTDS Technologies Inc. are gratefully acknowledged.

Table of Contents

AUTHOR’S DECLARATION	II
ABSTRACT	III
ACKNOWLEDGMENTS.....	IV
TABLE OF CONTENTS	V
LIST OF FIGURES.....	VII
LIST OF TABLES	IX
CHAPTER 1: INTRODUCTION	1
1.1 DIGITAL TIME DOMAIN SIMULATION IN POWER SYSTEM STUDIES	1
1.2 REAL TIME DIGITAL SIMULATOR	2
1.3 THE DYNAMIC BEHAVIOURS OF POWER SYSTEMS.....	3
1.4 ELECTROMAGNETIC TRANSIENT (EMT) AND TRANSIENT STABILITY ANALYSIS (TSA) SIMULATIONS ..	5
1.4.1 <i>Electromagnetic Transient (EMT) Model</i>	5
1.4.2 <i>Transient Stability Analysis (TSA) Model</i>	6
1.4.3 <i>Difference between EMT and TSA model</i>	7
1.5 BACKGROUND AND OBJECTIVES FOR DEVELOPING THE EQUIVALENT	7
1.5.1 <i>Hybrid Simulation Approaches</i>	8
1.5.2 <i>Hybrid wide band two part equivalent</i>	9
1.5.3 <i>The Objective of the Research</i>	10
1.6 DYNAMIC SYSTEM EQUIVALENT IN POWER SYSTEM	10
1.6.1 <i>Need for a Special Multi-Port Wide-Band Equivalent for the RTDS</i>	13
1.7 ORGANIZATION OF THIS REPORT.....	14
CHAPTER 2: ELECTROMECHANICAL LOW FREQUENCY DYNAMIC SYSTEM EQUIVALENT TECHNIQUES	16
2.1 MODAL ANALYSIS APPROACH IN POWER SYSTEM STUDIES	16
2.2 DIFFERENT TECHNIQUES FOR LOW FREQUENCY ELECTROMECHANICAL DYNAMIC EQUIVALENTS	21
2.2.1 <i>Modal-Based Approach</i>	22
2.2.2 <i>Coherency-Based Group Approach</i>	23
2.2.3 <i>Estimation Approach</i>	24
2.2.4 <i>Modal-Coherency Approach</i>	25
CHAPTER 3: FREQUENCY DEPENDENT NETWORK EQUIVALENT AND PASSIVITY ENFORCEMENT	27
3.1 FREQUENCY DEPENDENT NETWORK EQUIVALENT (FDNE)	27
3.1.1 <i>Rational Polynomial Function</i>	29
3.1.2 <i>Vector Fitting</i>	30
3.2 DETERMINATION OF $Y_{ex}(j\omega)$	33
3.3 MODELING $Y_{ex}(j\omega)$ IN THE EMT PROGRAM	33
3.4 PASSIVITY ENFORCEMENT OF THE FDNE.....	34
3.4.1 <i>The Passivity Criterion</i>	35
3.4.2 <i>Constrained Optimization Based Passivity Enforcement [49]</i>	36
3.4.3 <i>A Practical Procedure of Passivity Enforcement</i>	37
CHAPTER 4: AN IMPROVED TWO PART WIDE BAND EQUIVALENCING TECHNIQUE FOR RTDS	40
4.1 THE SCHEME OF AN IMPROVED TWO PART WIDE BAND EQUIVALENCING TECHNIQUE FOR RTDS	40
4.2 PROCEDURES OF COHERENCY BASED DYNAMIC SYSTEM EQUIVALENT	43
4.2.1 <i>Definition of the internal and external areas</i>	43

4.2.2	<i>Coherency Identification</i>	43
4.2.3	<i>Reduction of generator buses</i>	44
4.2.4	<i>Reduction of load buses</i>	44
4.2.5	<i>Aggregation of Generating Unit</i>	45
4.3	METHODS FOR COHERENCY IDENTIFICATION	45
4.3.1	<i>Time domain simulation method</i>	46
4.3.2	<i>Weak Link Method (WL)</i>	46
4.3.3	<i>Two Time Scale Method (TS)</i>	50
4.4	APPLICATION TO IEEE (NEW ENGLAND) 39 BUS SYSTEM	54
4.5	COHERENCY BASED NETWORK REDUCTION	57
4.6	TRANSIENT STABILITY ANALYSIS (TSA) EQUIVALENT WITH THE FDNE	64
CHAPTER 5: AGGREGATION OF GENERATING UNITS.....		68
5.1	OPTIMIZATION BASED AGGREGATION TECHNIQUES	68
5.1.1	<i>Frequency Domain Optimization</i>	69
5.1.2	<i>Time Domain Optimization [54][56]</i>	73
5.2	DIRECT AGGREGATION TECHNIQUES.....	76
5.2.1	<i>Synchronic Modal Equivalencing Approach</i>	77
5.2.2	<i>Structure Preservation Algorithm</i>	77
5.2.3	<i>The Logarithmic Average Method</i>	77
5.2.4	<i>Aggregation Method for the Generator and Its Controls in the Proposed Work</i>	78
CHAPTER 6: IMPLEMENTATION STRUCTURE OF THE PROPOSED EQUIVALENT.....		82
6.1	SCHEMATIC STRUCTURE OF THE PROPOSED EQUIVALENT	82
6.2	BOUNDARY DATA CONVERSION	85
6.3	TSA SOLUTION.....	90
6.4	EXAMPLE	93
CHAPTER 7: SIMULATION CASES AND VALIDATIONS FOR THE PROPOSED EQUIVALENT ON THE RTDS PLATFORM.....		97
7.1	SIMULATION RESULTS FOR THE EIGHT BUS SYSTEM	97
7.2	TEST SYSTEMS AND VALIDATION.....	99
7.2.1	<i>Simulation of a 39-Bus AC System Using Two Port Equivalent</i>	100
7.2.2	<i>Simulation of 39 bus system with coupled AC/DC lines</i>	105
7.2.3	<i>Simulation of a 108 bus System Using One Port Equivalent</i>	107
7.2.4	<i>Simulation of a 2300 Bus System Using One Port Equivalent</i>	109
7.2.5	<i>The Efficiency of the Proposed Algorithm</i>	112
CHAPTER 8: CONCLUSION AND FUTURE WORK.....		113
8.1	THE CONTRIBUTION TOWARD THE REDUCED TRANSIENT STABILITY ANALYSIS (TSA) EQUIVALENT MODEL.....	113
8.2	THE CONTRIBUTION TOWARD THE FDNE WITH PASSIVITY ENFORCEMENT	115
8.3	DIRECTIONS FOR FUTURE RESEARCH	116
APPENDIX A: WEAK LINK METHOD.....		118
(A1)	THEORY OF WEAK LINK METHOD	118
(A2)	IMPLEMENTATION ALGORITHM OF WEAK LINK METHOD	119
(A3)	AN EIGHT BUS SYSTEM IMPLEMENTATION EXAMPLE OF THE WEAK LINK METHOD	121

List of Figures

Figure 1.1	Time Frames of Power System Dynamics	3
Figure 1.2	R, L , C in EMT Model	5
Figure 1.3	A Wide Band Two Parts Equivalent for RTDS.....	9
Figure 1.4	Internal System and External Systems	11
Figure 3.1	External Network as Seen From the Boundary Bus.....	28
Figure 3.2	FDNE Fitting Example.....	34
Figure 3.3	FDNE Passivity Enforcement.....	37
Figure 3.4	Passivity Enforcement Procedures	39
Figure 4.1	An Improved Wide Band Two Parts Equivalent for the RTDS	41
Figure 4.2	The Definition of Internal System and External System.....	43
Figure 4.3	Reduction of Generator Buses.....	44
Figure 4.4	Reduction of Load Buses.....	45
Figure 4.5	Dynamic Aggregations of Generators	45
Figure 4.6	TSAT Simulation Result for Fault on Bus 29	46
Figure 4.8	Eight Bus Test System.....	50
Figure 4.9	Coherent Groups of IEEE 39 Test System.....	56
Figure 4.10	TSAT Time Domain Simulation Results	57
Figure 4.11	Coherency Based Bus Reduction	58
Figure 4.12	TSA Equivalent of the External System.....	65
Figure 5.1	Generating Unit Model.....	69
Figure 5.2	Resultant Exciter by Weighting Individual Exciters	70
Figure 5.3	Simplified Equivalent Exciter Model.....	71
Figure 5.4	Simplified exciter model for large step input.....	72
Figure 5.5	Time Domain Simulation Method.....	73
Figure 5.6	Coherent Area Input-Output Model	74

Figure 5. 7	IEEE Type1 Excitation System Model.....	76
Figure 5. 8	Scheme of Synchronic Modal Equivalencing Approach.....	77
Figure 5. 9	Aggregation of the Exciters.....	80
Figure 5. 10	Aggregated and Equivalent Frequency Response	81
Figure 6. 1	General Structure of the Equivalent Scheme.....	83
Figure 6. 2	Signal Flow of the Proposed Scheme.....	84
Figure 6. 3	Multi-port Norton Equivalent Circuit.....	85
Figure 6. 4	Instantaneous and phasor value conversion	87
Figure 6. 5	Implementation of the EMT/TSA conversion.....	88
Figure 6. 8	The Implementation of the Scheme in RTDS	95
Figure 6. 9	Implementation of coherency-based TSA in RTDS.....	96
Figure 7. 1	Simulation Results of #2 Bus Voltage	98
Figure 7. 2	Simulation Results of #3 Bus Voltage	98
Figure 7. 3	Simulation Results of #1 Generator Power	99
Figure 7. 4	The New England IEEE 39 Bus test system	100
Figure 7. 5	Simulation Results of #29 Bus Voltage	101
Figure 7. 6	Simulation Results of #9 Generator Power	102
Figure 7. 7	The Transient of #9 Generator	102
Figure 7. 8	Simulation Results of #28, #29 Bus Voltage.....	103
Figure 7. 9	Simulation Results of #9 Generator	104
Figure 7. 10	The Ac/Dc Coupling System.....	105
Figure 7. 11	DC Link Voltage of AC/DC Coupling System	106
Figure 7. 12	One Port Equivalent in RTDS for a 108 Bus System.....	107
Figure 7. 13	Generator Speed	108
Figure 7. 14	2300 Bus System.....	110
Figure 7. 15	T Line Power with Fault on Bus 1473.....	110
Figure 7. 16	T Line Power with Fault on Bus 18473.....	111

List of Tables

Table 4. 1	L Matrix of 8 Bus System.....	54
Table 4. 2	L Matrix of 39 Bus System.....	55
Table 7. 1	Generator Speed Curve Data	109
Table A- 1	State Matrix of the Eight Bus System	122
Table A- 2	Off Diagonal Summation of the State Matirx	122

Chapter 1: Introduction

1.1 Digital Time Domain Simulation in Power System Studies

Power system networks are generally regarded as the most complex structures ever built by human beings. They cover very large geographic areas and are served by many utilities. In a typical power system, there are tens of thousands of buses, transmission lines, transformers, generators etc. All these power system components work together in one large network to supply the necessary power to the public.

The scales of power system networks are very large and the structures and components are very complicated, making it very difficult to build and maintain a scaled down physical model of a power system with appropriate accuracy.

These characteristics of modern power systems require sophisticated analysis tools for the system study. Typically, these tools are based on digital time domain simulation. The digital time domain simulation can be understood as a set of algorithms run on computers, on which the nonlinear differential equations are solved by using step-by-step numerical integration techniques. By appropriately choosing the models, algorithms and time step sizes, power system behaviors can be well simulated, predicted and studied.

There are two major types of digital time domain simulation tools used in power system studies. They have been developed separately since the 1960s. The first one is the electromechanical transient simulation, which is also well known as Transient Stability Analysis (TSA). These types of simulation tools are mainly used for predicting whether or not a large power system can regain an acceptable equilibrium point (stable and secure) after being subjected to large disturbances (short circuit fault, disconnection of lines, transformers, generators, malfunction of controls etc., or so called ‘contingencies’ [1]). In such studies, the dynamic behaviors of power system components and the dynamic interactions between them which can cause large energy flow variations are of main concern.

The second one is electromagnetic transient (EMT) simulation, which focuses on simulating the detailed behavior of the components of the power system, such as voltage

spikes, current surges and harmonics etc. As power electronic devices are widely used in the power system, simulating very detailed switching transients has become one of the major applications of EMT simulation tools [2]. These will be described in more detail later.

1.2 Real Time Digital Simulator

Recently, it has become possible to implement EMT algorithms on Real-time simulators using parallel processing computers [3]. The Real Time Digital Simulator (RTDS) is a real time implementation of an EMT simulation. The power system to be simulated is divided into parts by utilizing the traveling wave characteristic of transmission lines. A specially designed powerful parallel computation platform is used to solve the nonlinear differential equations. In this way, the size of the system to be simulated is not limited by one processor or one computer. It has been shown that Real Time Digital Simulators (RTDS) are able to model very large system with the parallel hardware size growing approximately linearly with the system size [4]. This means that the cost of the computing platform also grows with the system size, and hence real-time simulators are typically used to study systems with a few hundred buses or less.

RTDS is playing an increasing role in power system studies and equipment tests by manufacturers, universities, research institutes and power system utilities. Using highly parallel, ultra-fast computer architectures, these simulators are able to model large electrical networks in real-time. To simulate the power system in real time is not just to save computation time; more importantly, actual protective relays and control equipments can be connected to the RTDS in a close of loop and be tested as if they are in a real power system [5][6].

However, in order to achieve real time speed, the RTDS makes some computational compromises. For example, the interpolation technique [7] is used in EMT simulations to accurately reproduce switch behavior. But it is hard to implement it on the RTDS because of the constraints imposed by maintaining the real time speed. As the RTDS uses multiprocessor parallel computing streams to do its calculations, it requires a large amount of computation resource.

The RTDS has the ability to handle large systems [4]. But its capability for accurately

reproducing dynamic and transient behavior of large systems is often limited by the burden of additional hardware requirements, which can make the required computing hardware prohibitively expensive for many customers. For example, a rack (the processing unit in the RTDS) has the ability to handle a 22 node (3 phase) system [8]. For a 108 bus system, 5 racks are needed to model the whole system in detail, which could be a high cost. This is why there always is a demand for making system equivalents for the RTDS.

Developing automated methods for making system equivalents for the RTDS is a difficult task. This research potentially paves the way for RTDS to simulate a very large power system (i.e., a system with thousands of buses). It will expand the scope for using the RTDS and make the RTDS more powerful and flexible for customers.

1.3 The Dynamic Behaviours of Power Systems

Power system dynamic behavior is a combination of various transient phenomena. A rough classification of these phenomena is given in Figure 1.1.

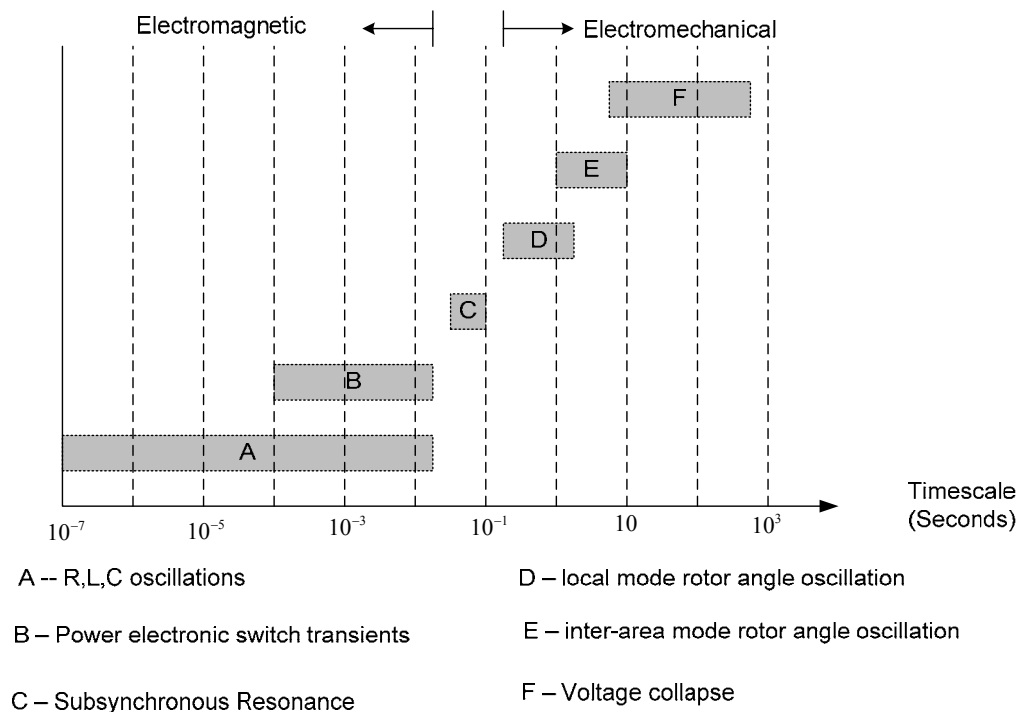


Figure 1.1 Time Frames of Power System Dynamics

Here the categories are developed from the point of view of the power system time domain simulation, and they are described below.

A: To simulate higher frequency resonances caused by resistive, inductive or capacitive (R, L, C) elements. The network components, such as transmission lines, cables, transformers, shunt capacitors, shunt reactors, filters etc. need to be represented by partial and ordinary differential equations. Both the linear and nonlinear characteristics should be modeled. Depending on the phenomena to be studied, some components might need to be modeled in very great detail. For example, in lightning studies, the transformer might be modeled as a distributed component instead of a lumped component.

B: To simulate power electronic switching transients, the converters need to be modeled in detail, in which semiconductor switches are explicitly modeled [9]. Traditionally, phenomena A and B are called electromagnetic transients.

C: Sub-synchronous resonance is the result of the interactions between the mechanical torsional dynamics of generator rotors and the machine electrical windings and external electrical network. The mechanical characteristic of the rotor as a construction of several rotating masses has to be modeled in the form of differential equations; the network also has to be modeled as differential equations.

D & E: There is no clear distinction between the local mode rotor angle oscillation and the inter-area mode rotor angle oscillation. However, local mode rotor angle oscillations mainly involve generators in a small area, and involve the rotor angle oscillation of a single power plant against the rest of the power system. The oscillation frequencies of such oscillations are higher than in the inter-area mode. To study local mode rotor angle oscillations, there might be a couple of generators and the corresponding exciters and stabilizers that need to be modeled in detail. To study inter-area mode rotor angle oscillations, larger number of generators that are located in a large area need to be modeled in detail; generator governors as well as loads and the supplementary controls of HVDC and FACTS play important roles in these phenomena. In both these phenomena, electromagnetic transients play less important roles and can often be neglected.

F: In voltage collapses, network elements that control the voltage are no longer able to control the voltage and instability occurs. Load characteristics play critical roles in these phenomena; auto transformer tap changers, excitation systems, protective controls and load shedding relays are the important system elements that need to be modeled in appropriate detail.

1.4 Electromagnetic Transient (EMT) and Transient Stability Analysis (TSA) Simulations

As mentioned in section 1.1 due to the complexity and large scale of modern power systems digital time domain simulation tools, electro-magnetic transient (EMT) programs and transient stability analysis (TSA) programs, have become significant tools in power system studies.

1.4.1 Electromagnetic Transient (EMT) Model

EMT models are the most detailed with all transmission as well electromechanical components modeled using detailed differential equations. The differential equations corresponding to linear components (reactor, capacitor etc.) are represented by a circuit equivalent consisting of a constant conductance in parallel with a history current term [10] which is based on the trapezoidal rule of integration as shown in Figure 1. 2.

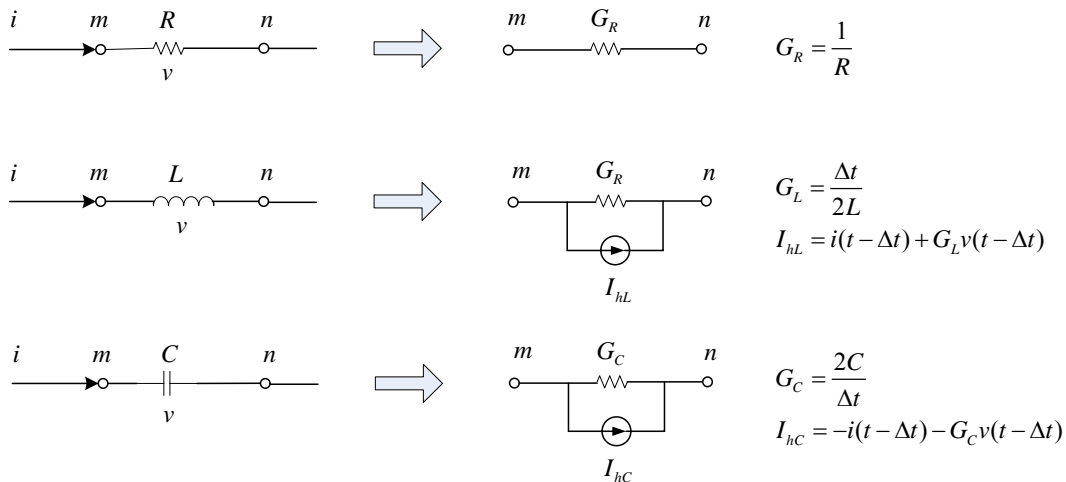


Figure 1.2 R, L, C in EMT Model

The value of the history current term is determined only by past (history) information. The system equations are built by using the standard nodal approach [7]. All the network elements can thus be reduced to the Norton equivalent form similar to that of Figure 1. 2. The equation to solve the entire network is assembled by standard nodal analysis procedures to give (1. 1)

$$[Y] \cdot V = J + J_h \quad (1. 1)$$

where Y is the system admittance matrix, J is the externally injected(real) current source, J_h is the history current source.

Every phase of the power system network is modeled separately in EMT simulation, so all unbalanced components and behavior can be modeled and simulated. The common time step which EMT simulation uses is $50 \mu s$. With this time step, most transients of the power system can be captured. The frequency range of applicability can be from dc to hundreds of kilohertz. Typically EMT simulation has been used to study switching transients; transients triggered by lightning and equipment faults and analyze operation of power-electronics based power system equipment such as HVDC converters and FACTS Controllers.

The trapezoidal integration rule is applied for solving the differential equations. It is stability-preserving for linear systems. That means a large time step will not cause numerical instability during the integration, though the results might lose accuracy.

Typically EMT simulation covers phenomena for A to C in Figure 1.1. EMTP and PSCAD/EMTDC are typical examples of commercially available off-line EMT solvers. As mentioned in section 1.2 the RTDS is the real time implementation of the EMT algorithm.

1.4.2 Transient Stability Analysis (TSA) Model

On the other hand, in TSA programs the transmission lines and other network impedances are represented as algebraic “phasor models” and the dynamic modeling is confined to rotating machines, exciters, governors and turbines and a few other elements. The TSA model is more approximate than EMT model and only considers the fundamental frequency electrical behavior. The three phase AC system is assumed to

be balanced. Hence it is represented by the positive sequence single line network. The unbalance of the network is ignored. The effect of an unbalanced fault is modeled by effective impedances in the positive sequence network.

As high frequency dynamics are ignored, a larger integration step (typically half a cycle) is possible and large power systems with 50,000 or more buses can be modeled.[11] Hence, traditionally TSA models have been used to study rotor angle deviations and determine transient stability performance following system disturbances. Other fast transients whose time frames are shorter than the simulation time step are neglected.

TSA simulation commercial software, like PSS/E, TSAT and BPA, are widely used in the power industry. They are used to study power system transient stability [12]. These are the phenomena from D to F in Figure 1.1, especially phenomena D and E.

1.4.3 Difference between EMT and TSA model

There are essential differences between EMT and TSA simulation. The TSA simulation is formulated in the fundamental frequency, positive sequence, and phasor domain. On the other hand, in EMT simulation, real physical values such as instantaneous voltage and current are directly computed. No matter how small the time step is, TSA simulation cannot simulate the phenomena from A to C in Figure 1.1. By the nature of the TSA simulation, waveform distortions, harmonics, accurate switch behavior, network oscillations etc. cannot be studied.

In theory, EMT simulation can cover all the phenomena from A to F in Figure 1.1. But its simulation length is often limited to one to two seconds due to large computational needs. In such short periods the phenomena from D to F in Figure 1.1 are not revealed or are only partly revealed.

1.5 Background and Objectives for developing the Equivalent

As mentioned in section 1.4, EMT models are the most detailed with all transmission as well electromechanical components modeled using detailed differential equations. The frequency range of applicability can be from dc to hundreds of kilohertz. A drawback of the high level of detail is that the computational burden is high, which on conventional single-processor computer platforms, limits the size and study interval of the system.

While in TSA programs, the transmission lines and other network impedances are represented as algebraic “phasor models” and the dynamic modeling is confined to rotating machines, exciters, governors and turbines and a few other elements. As high frequency dynamics are ignored, a larger integration step (typically half a cycle) is possible and large power systems with 50,000 or more buses can be modeled in reduced detail. Hence, traditionally, TSA models have been used to study rotor angle deviations and determine transient stability performance following system disturbances; and EMT simulation has been used to study switching transients, transients triggered by lightning and equipment faults and analyze operation of power-electronics based power system equipment such as HVDC converters and FACTS Controllers.

1.5.1 Hybrid Simulation Approaches

In many studies, it is possible to partition the study system into an internal and external system. The internal system is of greater interest and is modeled with all its components represented in complete detail. Faults or other disturbances are applied within this internal system. The remainder of the study system can be modeled as an external system which is a simplified equivalent. This reduces the number of buses to a manageable and affordable number. The challenge in this approach lies in developing an equivalent which from the internal system’s point of view is accurate over the entire frequency range of interest. This equivalent must be able to replicate the responses of the external system to disturbances in the internal system with reasonable accuracy, but with much reduced computation resources.

Previous approaches to meet this challenge on off-line as well as real-time were the ‘hybrid simulation’ methods that modeled the internal system with an EMT and the external system with a TSA algorithm [13]-[17] and interfaced them together. Such approaches neglect the high frequency behaviors of the external system [13]-[15].

Typically these approaches require the inclusion of surrounding boundary area around the internal system of interest to be included in the EMT part of the model. This is because placing the TSA too close to the internal system would result in significant error in the representation of the high frequency transients in the internal system. This considerably increases the size of the internal system to be modeled in detail in the EMT

program. Some other approaches [16][17] do include a simple equivalent modeled using several parallel R,L,C branches, but it is a single port equivalent that cannot represent the full multiport frequency dependent behaviour.

1.5.2 Hybrid wide band two part equivalent

Recently, in order to preserve both the fast and slow transient responses of the external system, a ‘wide band two part’ equivalent technique for RTDS was proposed as part of the PhD research of X.Lin at the University of Manitoba [18]. The general idea of this technique is similar to those ‘hybrid simulation’ mentioned above but it overcomes some drawbacks of the previous approaches. It is illustrated in Figure 1.3.

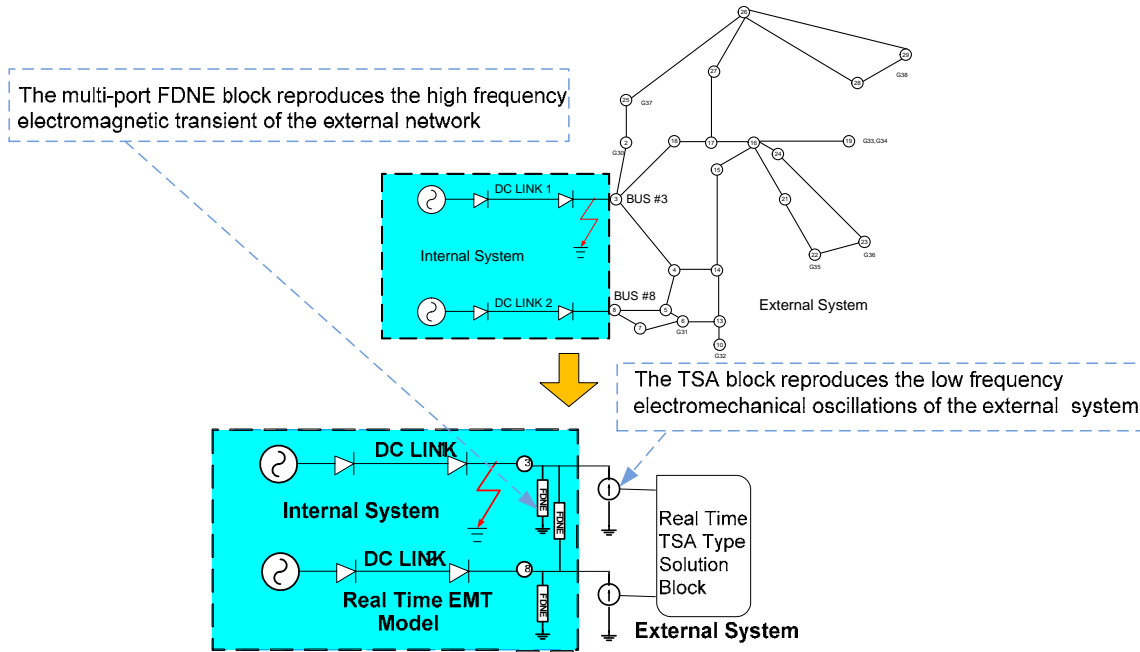


Figure 1.3 A Wide Band Two Parts Equivalent for RTDS

The first part is a Frequency Dependent Network Equivalent (FDNE). With approximations and simplifications, the external system can be seen as a linear network connected with some dynamic sources (generators). The concept of FDNE is to make a model which can be simulated in the time domain and has a similar frequency response as the linear external network and hence has a similar time domain response as the

external network. This model should be computationally more efficient than the full external model. In order to do this, the frequency response of the external system is firstly obtained from the power flow data. Then a vector fitting algorithm [19] is employed to derive the rational function approximation of the external network. Finally this derived rational function is simulated in the time domain as a frequency dependent impedance using the EMT simulation method [7][10].

The second part is an equivalent in the form of a group of controlled Norton equivalent current sources. This part represents equivalent currents seen from the boundary buses which are produced by generators in the external network. A TSA type solution block is implemented in RTDS to control the dynamic variation of these current sources.

1.5.3 The Objective of the Research

In this previous approach, using the FDNE did result in a significantly reduced model for representing the high-frequency behaviour. The TSA block, however, was still modeled with every component being separately represented, resulting in a very large model for the electromechanical part of the simulation. Although this approach reduced the computational hardware required for simulating a large system significantly, it was still impractical to model very large systems.

The main objective of this research is to develop an improved multi-port wide-band system equivalent technique based on the previous work for the RTDS by determining approaches to further reduce the low frequency TSA model into a simpler equivalent by identifying and collapsing generator units that show coherent swings. It extends the capability of the RTDS by enabling the simulation of cases with thousands of buses at reasonable cost.

The passivity issue, which is a challenge in implementing the FDNE, is also looked into. A non-passive FDNE included in the EMT model could result in unstable simulation. A practical procedure to enforce passivity in the FDNE is also proposed.

1.6 Dynamic System Equivalent in Power System

As a major objective, the TSA dynamic equivalent will be developed for the RTDS.

This section gives a short introduction of the dynamic system equivalent for a power system and the need for a special wide-band equivalent for the RTDS.

The scale of a modern power system is so large that it is neither practical nor necessary for any digital time domain simulation tools to run large power system model in which all the components are modeled in detail [20]. In addition occasionally from the confidential consideration the full detailed model cannot be disclosed. Hence it is a common practice to represent the whole system with one internal system and one or more external systems. The basic concept of such a system equivalent can be illustrated by Figure 1.4, which shows the example of the New England IEEE Test System [21]. The system is divided into one internal system and one external system. The internal system contains 11 buses, 5 loads, 4 generators, 12 branches and 4 transformers. There are 29 buses, 14 loads, 6 generators, 24 branches and 10 transformers in the external system.

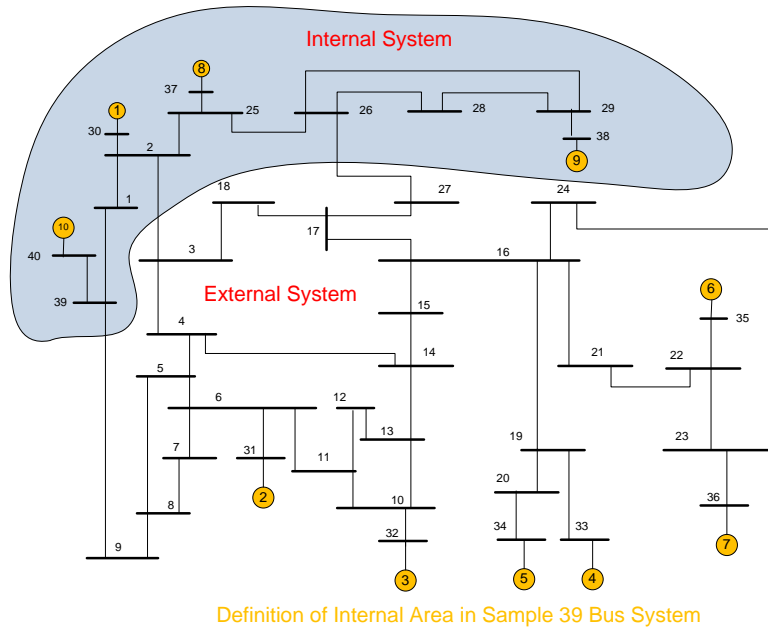


Figure 1.4 Internal System and External Systems

The internal system is the system which we are interested in. So the components in it, such as generators, controls, high voltage direct current (HVDC) devices etc, are modeled in full EMT detail. Faults or other disturbances are applied within this internal system. The external systems are those which we have less interest in. As mentioned earlier, the power system is an interconnected network and the behavior of the internal system is

influenced by the interactions between the internal system and the external system. The external system is not necessarily to be studied in detail, but in order to simulate interactions with high accuracy; the straightforward approach is to model it in full detail.

This detailed modeling results in very high computational resource use. In order to reduce the computational burden, engineers look for a simplified model, which still maintains acceptable accuracy. This simplified model should be able to replicate the responses of the external system to the changes in the internal system with reasonable accuracy, but demand much less computational resource.

The adequacy of the simplified model depends on the phenomena to be studied. In general this could be classified into static and dynamic equivalent. They are explained below.

A static equivalent represents a network, which contains many buses but only a few boundary buses. It uses a reduced network that contains only the boundary buses and a few of the original buses. This allows large areas of major interconnected systems to be represented in studies. It also achieves improved computational speed in simulations by removing buses and branches that influence system behavior, but are not of specific interest [11]. This kind of equivalent is used mainly in power flow analysis. It does not represent any dynamic behavior (A, B, C, D and E) of the equivalent system shown in Figure 1.1.

The existence of large-scale, interconnected power systems may require that even local transient stability studies include representation of an extensive network to accurately simulate dynamic behavior. Consequently, in many cases the transmission lines and machines are modeled, not because they are under investigation, but simply because they will affect the behavior of the area under investigation. So in order investigate the transient stability of a study area the whole area should be modeled in detail. For some cases of large-scale interconnected power systems, this is impossible or uneconomical.

This requires another kind of equivalencing technique. It is not only required to retain the static characteristic (power flow), but also the dynamic characteristic (transient behavior) of the external system. This kind of equivalent is called a 'dynamic system

equivalent' in contrast with the 'static system equivalent' mentioned above. There are different kinds of dynamic equivalent techniques depending on what kind of dynamic behavior is to be investigated. This could be broadly classified into three categories:

(a) High frequency equivalents for studies of the high frequency electromagnetic transient from A to C in Figure 1.1. These approaches attempt to model the frequency dependent terminal admittance of a network using either a lumped parameter circuit model or a rational function model [42]-[48].

(b) Low frequency equivalents for studies of the low frequency electromechanical oscillation from D to F in Figure 1.1. These models are used in simulating transient rotor angle stability of synchronous machines (transient stability simulation). Most of the research efforts in this area have been in 1970s and 1980s when the computing power was dramatically less than today. Now they are still needed when the influence of the power electronics devices on low frequency oscillations is simulated using EMT type simulations [20]-[41].

(c) Wide-band equivalents for studies that involve both low frequency electromechanical and high frequency electromagnetic behaviors from A to F in Figure 1.1. The proposed work is a wide-band equivalent which is composed of both high and low frequency equivalent techniques [18].

In recent years with the rapid evolution in computing technologies, the cost of the computer is becoming increasingly cheaper, while at the same time, its calculation speed and storage capacity is becoming more powerful. At the first glance this suggests there should be less and less need to use equivalent techniques in the digital time domain simulation software. To some extent this is true, especially for off-line TSA commercial simulation software. The whole system can probably be modeled in detail using modern simulation tools with a high performance computer.

1.6.1 Need for a Special Multi-Port Wide-Band Equivalent for the RTDS

However, with the Real Time Digital Simulator (RTDS), the situation is different as discussed below. For the RTDS the simulation has to be finished within the real transient time. In fact the RTDS can run continuously, without any specified termination time, and should be able to replicate real physical world phenomena accurately. Hence the RTDS

are capable of modeling the fast high frequency events which are the traditional domain of EMT programs, it can also be used to study lower frequency electromechanical oscillations. This implies that the RTDS should capture all the dynamic behavior in Figure 1.1. It has been shown that the RTDS is able to model very large system with the parallel computer size growing approximately linearly with the system size [4]. In other words the cost of the computing platform which is mentioned in section 1.2 also grows with the system size, and hence real-time simulators are typically used to study systems with a few hundred buses or less. This is the basis for the demand for system equivalents in the RTDS.

Traditionally, as mentioned in section 1.4, EMT simulation focuses on the fast behaviors ($>10\text{Hz}$). TSA simulations, on the other hand, concentrate on generator oscillations. For these, the most important consideration is to preserve the slow behaviors ($0.2\sim 2\text{Hz}$). However, the real time nature of the RTDS demands both the fast and slow behaviors of the system (A to F in Figure 1.1) to be modeled. These equivalent techniques for RTDS must be able to cover a wide frequency range. In other words, it should be a multi port wide band equivalent technique. Such a technique is developed in this thesis.

1.7 Organization of this Report

In Chapter 1, the background information of the digital time domain simulation in power system studies, the dynamic system equivalent, RTDS, and the research background and objectives are presented.

In Chapter2, the modal analysis approach is introduced. Then different low frequency electromechanical dynamic equivalent techniques are discussed.

In Chapter 3, the concept of FDNE and its implementation are introduced. The passivity enforcement is also investigated and a practical procedure developed in this thesis to ensure passivity of FDNE is described.

In Chapter 4, the proposed improved wide band two-part equivalent technique is illustrated. Then each component procedure of the coherency-based dynamic equivalent technique is discussed and two coherency identification methods are studied. Finally the

implementation of the proposed improved wide-band equivalent technique is introduced.

In Chapter 5, the techniques about aggregating generators are introduced.

In Chapter 6, the implementation of the improved two parts equivalent is interpreted. Firstly its structure is explained and then the boundary data conversion and TSA network solution with dynamic system equivalent are illustrated. The scheme of the proposed wide band equivalent technique on the RTDS platform is also introduced.

In Chapter 7, the simulation cases and validations are illustrated.

In Chapter 8, the summary and future works are proposed.

Chapter 2: Electromechanical Low Frequency Dynamic System Equivalent Techniques

The previous chapter introduced the need for an improved two part equivalent, one which represents the high frequency electromagnetic transient part (FDNE) and the other which represents the low frequency electromechanical dynamic part (coherency-based TSA equivalent).

This chapter describes techniques for developing the low frequency electro-mechanical dynamic system equivalent. The methods described herein are later adapted for the reduced TSA dynamic equivalent being designed for the RTDS as described in the previous chapter.

Various techniques for low frequency electro-mechanical dynamic equivalencing have been investigated for over 30 years, for the purpose of obtaining dynamic equivalents from full system models in a systematic and rigorous manner. They can be roughly divided into three categories which include modal, coherency-base and estimation methods.

Modal analysis [12] has proven to be the most practical way to analyze small signal stability problems. It is also used as the basis for the coherency identification method described later in this research. A brief introduction is provided below.

2.1 Modal Analysis Approach in Power System Studies

The concept of state is fundamental to the state-space approach. The state of a system represents the minimum amount of information about the system at any instant in time t_0 that is necessary so that its future behavior can be determined without reference to the input before t_0 [12].

Any set of n linearly independent system variables may be used to describe the state of the system. These are referred to as the state variables; they form a minimal set of dynamic variables that, along with the inputs to the system, provide a complete description of the system behavior. Any other system variables may be determined from

the knowledge of the state.

The system state may be represented in an n -dimensional Euclidean space called the state space. When we select a different set of state variables to describe the system, we are in effect choosing a different coordinate system. Whenever the system is not in equilibrium or whenever the input is non-zero, the system state will change with time. The set of points traced by the system state in the state space as the system moves is called the state trajectory.

The behavior of a dynamic system, such as a power system, may be described by a set of first order nonlinear ordinary differential equations in the following state-space form [12].

$$\dot{x} = f(x, u) \quad (2. 1)$$

x is a n -dimensional state vector

f is a n -dimensional nonlinear function

u is a r -dimensional input vector

The outputs of the system are nonlinear functions of the state and input vectors

$$y = g(x, u) \quad (2. 2)$$

y is an m -dimensional output vector

g is an m -dimensional nonlinear function

At steady state, the system is at an equilibrium point x_0 satisfying

$$f(x_0, u_0) = 0 \quad (2. 3)$$

When there is a small perturbation about the equilibrium point

$$x = x_0 + \Delta x, u = u_0 + \Delta u \quad (2. 4)$$

The state equation becomes the following form

$$\dot{x} = \dot{x}_0 + \Delta \dot{x} = f[(x_0 + \Delta x), (u_0 + \Delta u)] \quad (2. 5)$$

For small perturbations, $f(x,u)$ can be expressed in terms of its Taylor's series expansion. Terms involving second and higher order powers of Δx and Δu may be neglected.

$$\begin{aligned}\dot{\Delta x} &= A\Delta x + B\Delta u \\ \Delta y &= C\Delta x + D\Delta u\end{aligned}\tag{2.6}$$

Where A, B, C, D are the Jacobins of the system. A is also referred to as the state matrix or the plant matrix.

$$\begin{aligned}A &= \begin{bmatrix} \frac{\partial f_1}{\partial x_1} & \dots & \frac{\partial f_1}{\partial x_n} \\ \dots & \dots & \dots \\ \dots & \dots & \dots \\ \frac{\partial f_n}{\partial x_1} & \dots & \frac{\partial f_n}{\partial x_n} \end{bmatrix} & B &= \begin{bmatrix} \frac{\partial f_1}{\partial u_1} & \dots & \frac{\partial f_1}{\partial u_n} \\ \dots & \dots & \dots \\ \dots & \dots & \dots \\ \frac{\partial f_n}{\partial u_1} & \dots & \frac{\partial f_n}{\partial u_n} \end{bmatrix} \\ C &= \begin{bmatrix} \frac{\partial g_1}{\partial x_1} & \dots & \frac{\partial g_1}{\partial x_n} \\ \dots & \dots & \dots \\ \dots & \dots & \dots \\ \frac{\partial g_m}{\partial x_1} & \dots & \frac{\partial g_m}{\partial x_n} \end{bmatrix} & D &= \begin{bmatrix} \frac{\partial g_1}{\partial u_1} & \dots & \frac{\partial g_1}{\partial u_n} \\ \dots & \dots & \dots \\ \dots & \dots & \dots \\ \frac{\partial g_m}{\partial u_1} & \dots & \frac{\partial g_m}{\partial u_n} \end{bmatrix}\end{aligned}\tag{2.7}$$

The following are the definitions of the state matrix eigenproperties.

- Eigenvalues and eigenvectors

$$\begin{aligned}A\varphi &= \lambda\varphi \\ \psi A &= \lambda\psi\end{aligned}\tag{2.8}$$

- λ is an eigenvalue
- φ is the right eigenvector associated with λ
- ψ is the left eigenvector associated with λ

- Modal matrices

$$\begin{aligned}\Phi &= [\varphi_1 \quad \varphi_2 \quad \dots \quad \varphi_n] \\ \Psi &= [\psi_1^T \quad \psi_2^T \quad \dots \quad \psi_n^T]^T\end{aligned}\quad (2.9)$$

- Φ is the right eigenvector matrix
- Ψ is the left eigenvector matrix

- Relationships

$$\begin{aligned}A\Phi &= \Phi\Lambda, \quad \Phi\Psi = I \\ \Phi^{-1}A\Phi &= \Lambda\end{aligned}\quad (2.10)$$

I is the unit matrix and Λ is a diagonal matrix:

$$\Lambda = \text{diag}[\lambda_1 \quad \dots \quad \lambda_n] \quad (2.11)$$

- The concept of modes

The mode is a very important concept in modal analysis. In frequency domain, a mode refers to a real eigenvalue or a pair of conjugate complex eigenvalues. Analysis of the linearized system model is the perfect tool to obtain characteristics of individual modes.

In time domain, a mode is a sinusoidal component in a time response that has a single frequency and damping, together with other attributes of the sinusoid (amplitude and phase angle). By its dynamic nature, a power system inherently consists of many modes.

- Right Eigenvector and Mode Shape

A transformation of a variable from X to Z is made in order to eliminate the cross coupling between state variables. The state transformation is considered

$$X = \Phi Z \quad (2.12)$$

State space equation in Z is a set of decoupled differential equations

$$\dot{Z} = \Phi^{-1}A\Phi Z = \Lambda Z \quad (2.13)$$

Time domain response is the following:

$$Z_i(t) = Z_i(0)e^{\lambda_i t} \quad (2.14)$$

Where $Z_i(0) = \Psi_i X(0)$ is the initial condition

The response of the original state vector is

$$X(t) = \Phi Z(t) \quad (2.15)$$

A state variable is related to individual modes by

$$X_i(t) = \Phi_{1i}Z_1(t) + \Phi_{2i}Z_2(t) + \dots + \Phi_{ji}Z_j(t) + \dots + \Phi_{ni}Z_n(t) \quad (2.16)$$

Φ_{ji} is the i^{th} element in the right eigenvector Φ_j .

If $\Phi_{ji} = 0$, the j^{th} mode is unobservable in X_i .

If Φ_{ji} is large, the j^{th} mode will show up strongly in X_i .

Therefore, Φ_j determines the mode shape of the j^{th} mode.

Left Eigenvector and Participation Factors

A mode is related to individual state variables by

$$Z_i(t) = \Psi_{j1}X_1(t) + \Psi_{j2}X_2(t) + \dots + \Psi_{ji}X_i(t) + \dots + \Psi_{jn}X_n(t) \quad (2.17)$$

Ψ_{ji} is the i^{th} element in the left eigenvector Ψ_j

if $\Psi_{ji} = 0$, the j^{th} mode cannot be controlled by X_i

if Ψ_{ji} is large, the j^{th} mode is largely determined by X_i

One problem in directly using right and the left eigenvectors individually for identifying the relationship between the states and the modes is that the elements of the eigenvectors are dependent on units and scaling associated with the state variables. As a solution to this problem, a matrix called the participation matrix (P), which combines the right and left eigenvectors as follows is proposed in reference [22]-[24] as a measure of the association between the state variables and the modes.

$$P = [p_1 \quad p_2 \quad \cdot \quad \cdot \quad \cdot \quad p_n]$$

$$p_i = \begin{bmatrix} p_{1i} \\ p_{2i} \\ \cdot \\ \cdot \\ \cdot \\ p_{ni} \end{bmatrix} = \begin{bmatrix} \Phi_{1i} \Psi_{i1} \\ \Phi_{2i} \Psi_{i2} \\ \cdot \\ \cdot \\ \cdot \\ \Phi_{ni} \Psi_{in} \end{bmatrix} \quad (2.18)$$

The element $p_{ki} = \Phi_{ki} \Psi_{ik}$ is termed the participation factor. It is a measure of the relative participation of the k th state variable in the i th mode, and vice versa.

Φ_{ki} is the element on the k th row and i th column of the modal matrix Φ , also the k th entry of the right eigenvector Φ_i

Ψ_{ik} is the element on the i th row and k th column of the modal matrix Ψ , also the k th entry of the left eigenvector Ψ_i

Since Φ_{ki} measures the activity of x_k in the i th mode and Ψ_{ik} weighs the contribution of this activity to the mode, the product p_{ki} measures the net participation. The effect of multiplying the elements of the left and right eigenvectors is also to make p_{ki} dimensionless (independent of the choice of units).

2.2 Different Techniques for Low Frequency Electromechanical Dynamic Equivalents

Early work on this area includes the development of the modal equivalents approach in the late 1970's [22]-[26]. This approach eliminates some modes which are deemed to have a negligible effect on the internal system.

Another approach developed by Electric Power Research Institute (EPRI) in the 1970's was based on the concept of coherency [27]-[36]. Coherency means that certain groups of generators tend to swing together for remote disturbances and can therefore be represented by a single equivalent machine. Based on this theory, the DYNEQ [21][28] program was developed for EPRI, in which coherency was determined by comparing the angle responses for simplified linear time simulations. In 1993, Ontario Hydro developed

a new dynamic equivalencing program (DYNRED)[20][29], which included the techniques from the DYNEQ program as well as some fault independent coherency identification methods, such as the weak link [30] and two-time scale [31]-[35] methods. It has some similar ideas to the modal-coherency technique in [41].

The estimation method [37]-[40] determines equivalent parameters with minimum values of the cost function. It is useful because it is a straightforward method and its idea can be used in other applications, such as aggregating generators controls [20][29]. It is not widely used because it is time consuming and has implementation difficulty. It was just tested with a thirteen machine system. The basic idea of this approach is introduced next.

2.2.1 Modal-Based Approach

The modal approach is based on the fact that the dynamic response of a linear system is built up from the contributions of the natural modes of the system. A linear model is used to approximate the response of the external system, where the perturbations are assumed to have small magnitudes. Typically certain natural modes dominate this response for the following reasons.

The initial conditions and the system structure are such that certain modes are particularly excited and also have a significant effect on the internal system.

Some modes may be too slow or too fast to have a significant effect on the response in the time frame of interest.

As a result, the modal analysis technique accomplishes system reduction by determining the natural modes of the external system and eliminating the state variables corresponding to the modes which are deemed to have a negligible effect on the internal system. Some results indicate, however, that substantial savings can be obtained by using unreduced modal dynamic equivalents due to the computational efficiency of their structures [25]. The modal technique has been tested on fair-sized systems of up to about 1300 bus bars and computational savings of 50-60% (compared to using the full model) have been obtained [26].

The modal methods have a rigorous mathematical basis. They provide a good insight

into the various modes of oscillations present in the system. The modal technique has the potential for controlling the size of the equivalent in a systematic manner. In contrast to the coherency equivalent, the quality of the modal equivalent does not depend on the aptness of the perturbation etc. chosen to construct the equivalent.

However, there are several objections raised against the modal approach in spite of its theoretical soundness. These objections are the followings.

Performing the complete eigen-analysis of the system required by this method is very time consuming and has a large cost.

The modal equivalent cannot be represented in terms of actual power system components (e.g., interconnections will develop in the reduced system that have no counterpart in the actual power system). Therefore these equivalents cannot be used directly in standard transient stability programs.

2.2.2 Coherency-Based Group Approach

The coherency approach is based on the empirical observation that following a disturbance certain groups of generators tend to swing together, or in other words, in a post fault transient only some machines close to the fault location respond with fast inter-machine oscillations while other machines more distant from the fault swing together in groups with “in phase” slow motion (usually 0.2 to 2 Hz). These kinds of “in phase” motions of generators can be defined as coherency.

The definition of a coherent group of generating units for a given perturbation is a group of generators oscillating with the same angular speed, and with terminal voltages in a const complex ratio. Thus the generating units belonging to a coherent group can be attached to a common bus and if necessary through an ideal complex ratio transformer.

The dynamic equivalent of a coherent group of generating units is a single generating unit that exhibits the same speed, voltage and total mechanical and electrical power as the group during any perturbation where those units remain coherent.

In coherency methods, coherent groupings of machines are obtained by analyzing the system response to a perturbation. An equivalent of the external system is then obtained by replacing each such coherent group of machines by a large equivalent machine.

This approach has the following advantages:

The coherency technique does not need any special interfacing with the internal system model, because the equivalent is in the form of a model of an actual physical component as used in stability programs.

The coherency technique has been tested on large systems of 11,028 bus bars and 2,553 generators [36]. It has been found to be cost - efficient and reasonably accurate.

Engineers have generally favored coherency methods, because the coherency equivalents are described in terms of the original physical system components. Hence the engineer can evaluate the validity of the equivalent and supply approximate data, if necessary, for remotely connected utilities by drawing on past experience. No modifications to existing stability programs are necessary for using coherency equivalents. Nonlinearity can be introduced in the equivalent machine model, thus extending the validity of the coherency equivalents for large disturbances.

However the coherency technique suffers from the following disadvantages:

The conventional coherency technique is a purely empirical technique. A theoretical justification for aggregation based on the proposed definitions of coherency has not been given.

The quality of the equivalent obtained is dependent on the perturbation chosen to determine coherency, but it is difficult to lay down guidelines for choosing the most appropriate perturbation.

2.2.3 Estimation Approach

In the estimation approach, complete information on the external system is not required. The dynamic equivalent for the external system is computed from a priori information and operating data in such a way that the reduced model (structure and parameters) best fits the available information in some specified sense. The following is a brief introduction for this method [37].

First, from preliminary studies, some reduced order models are found for the external system. The final choice of the model is determined by the uniqueness of the equivalent parameters with minimum values in the cost function.

Then the original system and the equivalent system equations are written in the same linear form

$$\begin{aligned}\dot{x} &= Ax + Dd \\ y &= Hx\end{aligned}\tag{2. 19}$$

where x is the state vector, y is the output vector, d is the intentional disturbance, A is the system matrix, H is the output matrix, and D is the disturbance matrix.

The order of the equivalent system, however, is greatly reduced. For the estimation, the equations are written as (2. 20)

$$\begin{aligned}\dot{\tilde{x}}(\alpha) &= A(\alpha)\tilde{x}(\alpha) + Dd \\ \tilde{y}(\alpha) &= \tilde{H}(\alpha)\tilde{x}(\alpha)\end{aligned}\tag{2. 20}$$

where \tilde{x} , \tilde{y} , \tilde{A} and \tilde{H} are all functions of the equivalent parameter vector α which is being estimated.

An error function of the quadratic form (2. 21) is chosen as the cost function, where R is the weighting matrix, y is the measurement selected to form the cost function.

$$J = \int_{t_0}^t [y - \tilde{y}(\alpha)]' R [y - \tilde{y}(\alpha)] dt\tag{2. 21}$$

In [38] and [39] similar principle is used. The main idea is to search for the best parameter vector which minimizes an error index that is taken to be a square function of the difference between the measured output and the calculated output. In [40], recorded disturbances are analyzed to get the equivalent parameters.

This kind of method has just been tested with small system and not been widely used by industry.

2.2.4 Modal-Coherency Approach

As discussed above, both modal and coherency approaches have some advantages and disadvantages. An ideal equivalent approach would be to use the sound theoretical basis of modal analysis complemented by the attractive form of the coherency equivalent.

The electro-mechanical modes of a power system are classified in terms of area and sub-area modes etc. This allows these modes to be ordered into a hierarchical tree structure. The coherent groups of generators are derived from this modal tree structure [41]. This technique has some similarities to techniques used in the dynamic equivalencing program (DYNRED) [20][29]. They both use modal analysis for coherency identification, then with the obtained coherent groups; the conventional coherency-based techniques are used for dynamic equivalent.

The coherency-based equivalent technique has been widely used in the industry in TSA programs. The model size can be expanded to very large networks (thousands of buses) with model reduction using coherency-based dynamic equivalents [20]. Generators are grouped into equivalent generators by their coherency and can be directly used in a conventional TSA program. In this research, the frame of the coherency-based method is used. For the conventional coherency-based technique, the coherency identification is based on the empirical observation that following a disturbance, certain groups of generators tend to swing together. It is therefore fault dependent. In order to overcome this disadvantage, the weak link (WL) [30] and two time scale (TS) [31]-[35] methods are employed for the coherency identification. They are based on the linearized state matrix of the power system and hence are fault independent. They will be given detailed discussion in section 4.3.2 and 4.3.3.

Chapter 3: Frequency Dependent Network Equivalent and Passivity Enforcement

The previous chapter discussed existing techniques for developing the low frequency electromechanical dynamic system equivalent. Such techniques only model the low-frequency behavior. Another main concern of this thesis is the high frequency electromagnetic transient equivalent which is represented using a frequency dependent network equivalent (FDNE). This chapter begins with a brief description of existing FDNE approaches. It then presents a contribution of this thesis, which is the adaptation of a previous approach to a new procedure that ensures passivity in the developed equivalent. Passivity is an important attribute of many physical systems and means that the system does not produce power when excited with a source.

3.1 Frequency Dependent Network Equivalent (FDNE)

With approximations and simplifications, the external AC system can be seen as a linear network with some dynamic sources (Generators, nonlinear loads, etc) connected to it. The FDNE is implemented as a multi-port admittance matrix with rational polynomial elements (in the Laplace or s -domain) embedded into the EMT solution. The frequency response characteristic of this admittance closely matches the frequency response behavior of the entire external network (ignoring non-linearities) over the selected frequency range (typically from a few Hz to several kHz). As the elements are rational polynomial functions, they can be readily converted to time-domain differential equations and included in the EMT simulation [10]. This model should be computationally more efficient than the entire original network model.

The modeling, which assumes linearity of the considered external system, is normally based on an admittance formulation which defines the relation between voltages V and currents I on the boundary buses of the system shown in Figure 3. 1.

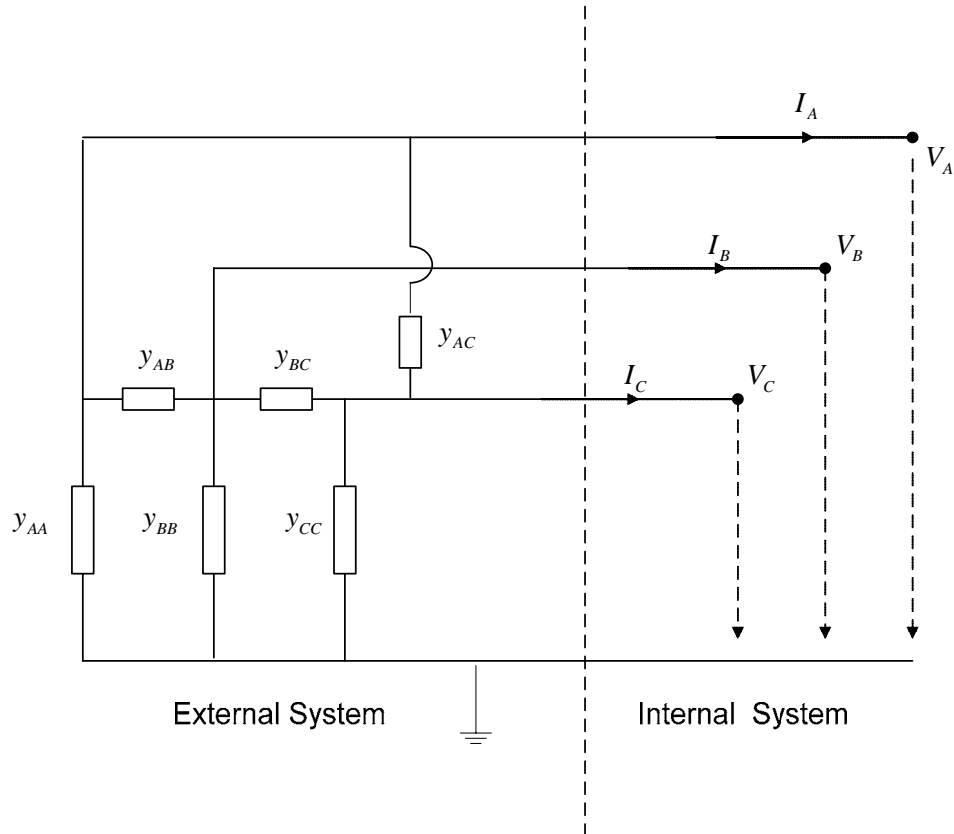


Figure 3.1 External Network as Seen From the Boundary Bus

The individual branch in Figure 3. 1 is derived from the self and mutual impedances observed at the boundary. Each of them is a frequency dependent admittance;

$$Y_{ex}(j\omega) = \frac{I(j\omega)}{V(j\omega)} \quad (3.1)$$

Earlier work in this area tried to replace the original network with an equivalent network consisting of lumped R,L,C components whose values are determined in the way that the equivalent network has essentially the same frequency response as the original network[42][43]. However, in many cases, the external network consists of distributed parameter components such as transmission lines. To fit such complex frequency response characteristics, a very large R, L, C component count becomes troublesome. With digital computers, it becomes possible to use the more direct method of polynomial functions and now the R, L, C method is no longer used.

The solution using polynomial functions is finding a good polynomial function

approximation for the known frequency response admittance characteristic of the external system by fitting it with appropriate order:

3.1.1 Rational Polynomial Function

The form of the rational polynomial function is:

$$f_{fit}(s) = \frac{a_0 + a_1s + a_2s^2 + \dots + a_Ns^N}{1 + b_1s + b_2s^2 + \dots + b_Ns^N} \quad (3.2)$$

where $a_0, a_1, \dots, a_N, b_1, b_2, \dots, b_N$ are real numbers.

The equivalent orthogonal polynomial form is:

$$f_{fit}(s) = g_0 + sh_0 + \sum_{k=1}^N \frac{c_k}{s - a_k} \quad (3.3)$$

As the frequency response $Y_{ex}(j\omega)$ of the external system can either be measured or calculated at an arbitrarily large number of frequency points

$$Y_{ex}(j\omega_i) = G_i + jB_i, \quad (i = 1 \dots M) \quad (3.4)$$

M is the number of the frequency points, which is normally much larger than N , the order of $f_{fit}(s)$ in (3.2) or (3.3).

For (3.2) at each frequency point the equivalent $f_{fit}(j\omega_i)$ need to be approximately equal to the frequency response $Y_{ex}(j\omega_i)$:

$$f_{fit}(j\omega_i) = \frac{a_0 + a_1j\omega_i + a_2(j\omega_i)^2 + \dots + a_N(j\omega_i)^N}{1 + b_1j\omega_i + b_2(j\omega_i)^2 + \dots + b_N(j\omega_i)^N} = G_i + jB_i \quad (i = 1 \dots M) \quad (3.5)$$

In (3.5) G_i, B_i and ω_i are given, $a_0 \dots a_N, b_1 \dots b_N$ are variables and needed to be determined. The number of the variables is $2N + 1$. Because M is much bigger than N this is an over-determined linear equation set and can be solved by standard least square algorithms.

The difficulty of solving such a problem is that these equations are badly scaled and ill conditioned due to the powers of ω in the equations. Especially when a high order approximation needs to be used, or a wide range frequency response needs to be fitted.

In contrast to the form of the polynomial function (3. 2), the orthogonal polynomial function (3. 3) has much smaller coefficients. In (3. 3), g_0 and h_0 are real numbers. a_k and c_k can be either real or conjugate complex pair. The difficulty of fitting (3. 3) is that the unknown coefficient c_k appears in the denominators, which makes the fitting a nonlinear form.

For (3. 3) at each frequency point the equivalent $f_{fit}(j\omega_i)$ need to be approximately equal to the frequency response $Y_{ex}(j\omega_i)$:

$$f_{fit}(j\omega_i) = g_0 + j\omega_i h_0 + \sum_{k=1}^N \frac{a_k}{j\omega_i - c_k} = G_i + jB_i \quad (i=1 \cdots M) \quad (3. 6)$$

Given a set of initial values of g_0, h_0, a_k, c_k the nonlinear equation (3. 6) can be linearized at the initial point by using the first derivatives of g_0, h_0, a_k, c_k , and a set of linear equations can be solved using standard linear least square techniques. The results can be used for updating g_0, h_0, a_k, c_k and then the nonlinear equation (3. 6) can be linearized at the new point. This can be done iteratively until converging.

Early work [44] reported in literature used frequency domain computed data to fit parameters to the model in (3. 2). In [45][46], the ill-conditioning problems are overcome by dividing the frequency response into sections and other techniques, such as adaptive weighting, iterations step adjustment, etc. A time domain approach to obtain the fitted function (3. 3) using Prony analysis is presented in [47]. Recently a more powerful vector fitting technique has been proposed [19][48]. The basic concept of this algorithm is described as follows:

3.1.2 Vector Fitting

As discussed in section 3.1.1, the actual transfer function $f(s)$ is assumed to be known as in (3. 4). The purpose of vector fitting is to approximate $f(s)$ with a rational fitting function $f_{fit}(s)$ as in (3. 7) below.

$$f(s) \approx f_{fit}(s) = g_0 + sh_0 + \sum_{k=1}^N \frac{a_k}{s-c_k} = h_0 \frac{\prod_{k=1}^N (s-s_k)}{\prod_{k=1}^N (s-c_k)} \quad (3.7)$$

Introduce a rational function $\sigma(s)$, which has arbitrary given poles d_1, d_2, \dots, d_N :

$$\sigma(s) = 1 + \sum_{k=1}^N \frac{b_k}{s-d_k} = \frac{\prod_{k=1}^N (s-y_k)}{\prod_{k=1}^N (s-d_k)} \quad (3.8)$$

Function $\sigma(s)$ is required to satisfy the condition that $\sigma(s)$ and $f_{fit}(s) \cdot \sigma(s)$ have the same poles d_k , ie:

$$f_{fit}(s) \cdot \sigma(s) = l_0 + m_0 s + \sum_{k=1}^N \frac{e_k}{s-d_k} = m_0 \frac{\prod_{k=1}^N (s-x_k)}{\prod_{k=1}^N (s-d_k)} \quad (3.9)$$

However, seeing that $f_{fit}(s)$ has poles c_k and $\sigma(s)$ has poles d_k , it is also true that :

$$f_{fit}(s) \cdot \sigma(s) = h_0 \frac{\prod_{k=1}^N (s-z_k)}{\prod_{k=1}^N (s-c_k)} \cdot \frac{\prod_{k=1}^N (s-y_k)}{\prod_{k=1}^N (s-d_k)} \quad (3.10)$$

For arbitrary given poles d_1, d_2, \dots, d_N , the necessary condition for $f_{fit}(s) \cdot \sigma(s)$ and $\sigma(s)$ having the same poles is that:

$$\prod_{k=1}^N (s-y_k) = \prod_{k=1}^N (s-c_k) \quad (3.11)$$

It means the zeros of $\sigma(s)$ should be equal to the poles of $f_{fit}(s)$.

The frequency characteristic of $f(s)$ is known as a frequency spectrum. At a sample frequency point $\omega = \omega_i$, equation (3.8), (3.9) and (3.10) can be reorganized as:

$$f_{fit}(j\omega_i) \approx f(j\omega_i) = v_i + jw_i \quad (3.12)$$

$$f(s) \cdot \sigma(s) \approx f_{fit}(s) \cdot \sigma(s) = l_0 + m_0 s + \sum_{k=1}^N \frac{e_k}{s - d_k} \quad (3.13)$$

$$(v_i + jw_i) \cdot \left(1 + \sum_{k=1}^N \frac{b_k}{j\omega_i - d_k} \right) \approx l_0 + m_0 j\omega_i + \sum_{k=1}^N \frac{e_k}{j\omega_i - d_k} \quad (3.14)$$

With arbitrary given poles d_1, d_2, \dots, d_N , equation (3.14) is a linear equation with the unknown b_k, l_0, m_0, e_k . Writing equation (3.14) at a series of given frequency point, an over-determined linear problem can be obtained (because the number of the frequency points is much larger than the number of the unknowns):

$$\left\{ \begin{array}{l} (v_1 + jw_1) \cdot \left(1 + \sum_{k=1}^N \frac{b_k}{j\omega_1 - d_k} \right) \approx l_0 + m_0 j\omega_1 + \sum_{k=1}^N \frac{e_k}{j\omega_1 - d_k} \\ (v_2 + jw_2) \cdot \left(1 + \sum_{k=1}^N \frac{b_k}{j\omega_2 - d_k} \right) \approx l_0 + m_0 j\omega_2 + \sum_{k=1}^N \frac{e_k}{j\omega_2 - d_k} \\ \vdots \\ \vdots \\ \vdots \\ (v_M + jw_M) \cdot \left(1 + \sum_{k=1}^N \frac{b_k}{j\omega_M - d_k} \right) \approx l_0 + m_0 j\omega_M + \sum_{k=1}^N \frac{e_k}{j\omega_M - d_k} \end{array} \right. \quad (3.15)$$

As all the unknowns b_k, l_0, m_0, e_k appear in the numerator, equation (3.15) can be solved by standard linear least square techniques. In this way, the original nonlinear problem of finding the poles of $f_{fit}(s)$ is converted to a linear problem of finding the residues of $f_{fit}(s) \cdot \sigma(s)$ and $\sigma(s)$.

The process of vector fitting can thus be summarized as below:

Arbitrarily select a set of poles d_1, d_2, \dots, d_N .

Construct equation (3.15) and use a standard linear least square technique to solve it, find the residues of $\sigma(s)$.

The poles of $f_{fit}(s)$ can be derived by calculating the zeros of $\sigma(s)$. This should theoretically end the search. However, by observations, it has been determined that the process can be repeated to improve the fitting accuracy, as follows:

Replace the previous poles d_1, d_2, \dots, d_N by the new poles of $f_{fit}(s)$, then go back to step 2), start the next iteration until converged.

With the converged poles of $f_{fit}(s)$, the residues of $f_{fit}(s)$ can be found by solving a linear least square problem.

3.2 Determination of $Y_{ex}(j\omega)$

The first step in implementing the FDNE is to obtain the frequency dependent multi-port, three-phase Norton admittance $Y_{ex}(j\omega)$ as seen from the boundary buses. $Y_{ex}(j\omega)$ can be obtained by representing all the transmission lines and cables in the network by Bergeron model [10] in EMTP (or by pi-section models) and transformers and generators by suitable leakage or other inductances. Standard network reduction techniques for obtaining Norton equivalents can be applied to obtain the multi-port $Y_{ex}(j\omega)$. In the absence of more information, the capacitance and inductance per unit length of all transmission lines can be estimated from fundamental frequency data available in the load-flow model [18]. Further refinements are possible if more detailed frequency domain data on some of the lines and cables are available.

3.3 Modeling $Y_{ex}(j\omega)$ in the EMT program

The procedure of implementing $Y_{ex}(j\omega)$ in the EMT simulation is to fit $Y_{ex}(j\omega)$ with a rational function in the s-domain referred as $Y_{fit}(s)$ as discussed in section 3.1. This s-domain transfer function form of the admittance is directly converted into the standard “current-source admittance formulation” in the EMT program and becomes part of the main EMT solution [10]. Here, a “vector fitting” [19][48] algorithm is used to select the coefficients of the polynomial numerator and denominator terms of the rational function elements of $Y_{fit}(s)$. The Vector Fitting method is an efficient method to implement a least-squared error fit between a frequency response plot and a rational transfer

function [18][19][48].

An example of the fitting is shown in Figure 3. 2, where the solid and dashed line respectively are plots of the original and fitted frequency response of the magnitude and phase of a typical matrix element of the admittance matrix $[Y_{4,6}(j\omega)]$ of the 39 bus New England System shown in Figure 7. 4. As can be seen, an accurate fit can be achieved.

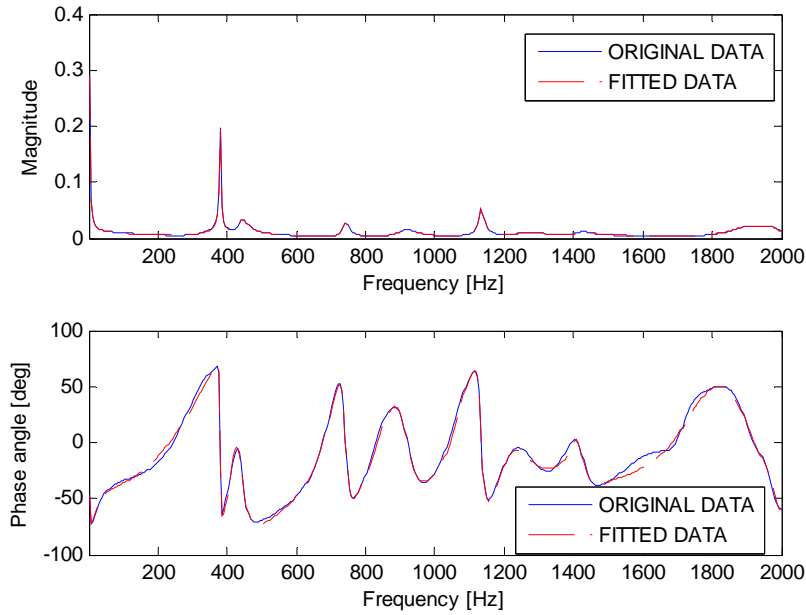


Figure 3. 2 FDNE Fitting Example

3.4 Passivity enforcement of the FDNE

As mentioned above, each element of $Y_{ex}(j\omega)$ is independently fitted with a transfer function. However, inherent approximations in the fitting process may cause $Y_{fit}(s)$ to have passivity violation at certain frequency ranges [49]. This means that the network equivalent would have negative power consumption in those frequency ranges; which is in reality, not possible. Passivity requires that eigenvalues of the real part (conductance) of the admittance matrix $Y_{ex}(j\omega)$ must be positive definite (PD) at any frequency [49]. The earlier approach to ensuring passivity of the FDNE [18] was to identify frequency regions of passivity violation and then do a more refined and tighter fitting in those regions. While this eliminated many of the passivity violation cases, it was

not foolproof.

This thesis adopts an alternate improved formulation based on [49], which enforces passivity using linearization and constrained optimization. A frequency scan of the eigenvalues of the fitted function $Y_{fit}(s)$ is carried out and if the scan shows any eigenvalues with negative real parts, the coefficients of the elements of $Y_{fit}(s)$ are perturbed till the violations disappear. An optimization problem is formulated in which the objective function is a combination of fitting error and PD constraint violation. Solving the problem yields a passive $Y_{fit}(s)$ with an acceptable fitting error. The following discusses the passivity criterion and this passivity enforcement technique in more mathematics detail.

3.4.1 The Passivity Criterion

From the boundary buses, a linear network can be seen as a frequency dependent admittance matrix $Y(j\omega)$. For a single three-phase port interface, this matrix is a 3×3 complex matrix. For a double three-phase ports interface, this matrix is a 6×6 complex matrix. The value of entries in the matrix varies with frequency.

This frequency dependant network matrix $Y(j\omega)$ can be included in a time domain EMT simulation as a frequency dependent network equivalent by approximation its admittance matrix $Y(j\omega)$ using rational functions in the frequency domain [19][48]. The frequency domain transfer function $Y_{fit}(s)$ is directly converted into the standard “current-source admittance formulation” in the EMT program and becomes part of the main EMT solution [10].

Passivity means the circuit should always absorb power at any frequency. It should be noted that even though the elements of $Y_{fit}(s)$ have been fitted using stable poles the circuit can be non-passive [49]. When such a circuit is connected to other external circuit elements, the simulation can sometimes become unstable. The following is a simple explanation of the passivity criterion and passivity enforcement procedures in this work.

For an admittance matrix Y

$$i = Yv \quad (3.16)$$

For any complex vector v the power absorbed by the admittance matrix Y can be calculated as:

$$P = \text{Re}\{v^* Y v\} = \text{Re}\{(v^* (G + jB)v)\} = \text{Re}\{v^* G v\} \quad (3. 17)$$

In (3. 17) the asterisk $*$ denotes the transpose conjugate function. From (3. 17) it is seen that the absorbed power P will be positive only if all eigenvalues of G have positive values. It should be noted that G is a symmetric, real matrix hence all eigenvalues of G are real. Thus a criterion for passivity is that $G = \text{Re}\{Y\}$ be positive definite.

3.4.2 Constrained Optimization Based Passivity Enforcement [49]

This approach is based on post-processing of the original fitting rational function which is obtained from “Vector Fitting” [19][48]. The rational function is given in pole-residue form (3. 18):

$$Y_{fit,i,j}(s) = \sum_{m=1}^N \frac{R_m}{s - a_m} + D + sE \quad (3. 18)$$

Passivity implies that the eigenvalues of the real part of the admittance matrix Y are positive for all frequencies.

$$\text{eig}\left(\text{Re}\left\{\sum_{m=1}^N \frac{R_m}{s - a_m} + D + sE\right\}\right) > 0 \quad (3. 19)$$

This passivity criterion is enforced by perturbing the model parameters so that the perturbed Y matrix is passive; while at the same time minimizing the change to the original ration function.

$$\Delta Y = \sum_{m=1}^N \frac{\Delta R_m}{s - a_m} + \Delta D \cong 0 \quad (3. 20)$$

$$\text{eig}(\text{Re}(Y + \Delta Y)) > 0 \quad (3. 21)$$

A constrained optimization problem is formulated from (3. 20) and (3. 21) in which the objective function is a combination of fitting error and passivity criterion. Solving the problem yields a passive $Y_{fit}(s)$ with an acceptable fitting error [49].

Figure 3. 3 (a) shows the real part of one eigenvalue (solid line) of the originally fitted matrix $[Y_{fit}(s)]$ of the New England System (see Figure 7. 4). The negative excursion around the 2 kHz range signifies a passivity violation. On application of the above procedure, the violation disappears (dotted line). The fitting error plot of Figure 3. 3(b) indicates that the correction is achieved without significant deterioration in the quality of fit in comparison with the original fit.

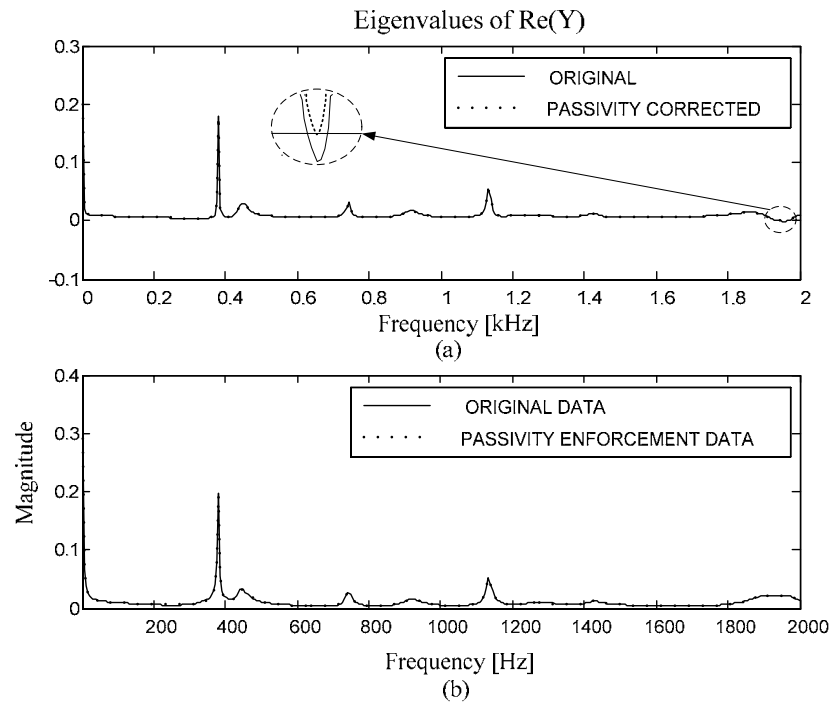


Figure 3. 3 FDNE Passivity Enforcement

3.4.3 A Practical Procedure of Passivity Enforcement

The experience of getting $Y_{fit}(s)$ has shown that the following procedure may alleviate the passivity violation to a great extent, so that minimal perturbation is needed for any residual small violations. They are the followings:

- 1) Using different initial poles and more iteration for getting new poles in the fitting process.
- 2) Giving more weight to the passivity violation regions during the fitting process.
- 3) Doing a more refined and tighter fitting for those passivity violation regions.

The above passivity enforcement method perturbs the original fit. In order to

minimize this perturbation, it is preferable to make the original fit itself have as few passivity violation regions as possible.

The procedure which combines the above experience based approach and constrained optimization approach is outlined below and flowcharted in Figure 3. 4.

- 1) The order (the highest power of the Laplace coefficient) in the fitted function $[Y_{fit}(s)]$ can be selected by the user. The procedure attempts to try a number of different orders over a range. This range is estimated by counting the number of peaks in the frequency response plot and selecting a range $[n_{low} \ n_{high}]$ that brackets this number.
- 2) The order n of the model is varied over the range $[n_{low} \ n_{high}]$, and for each n , a fitted model $Y_{fit_n}(s)$ is obtained. The fitting error is stored in a vector V_{error} for each of these orders.
- 3) From the lowest pole number to the highest pole order in the range $[n_{low} \ n_{high}]$ which is obtained from step (1), the fitting process to get the fitted model $[Y_{fit}(s)]$ is called.
- 4) The fitted model $[Y_{fit}(s)]$ which has the smallest fitting error is chosen as the first candidate. Then this element is deleted from the error vector V_{error} . Check the passivity violation of the fitted model $[Y_{fit}(s)]$.
- 5) If the fitted model $[Y_{fit}(s)]$ is passive, then this can be used directly in the EMT time domain simulation.
- 6) If the fitted model has a relative large passivity violation region, then a fitting process is called again, using more refined frequency response and allocating more weight to the violation region. Then the passivity violation for the new fitted model $[Y_{fit}(s)]$ is re-checked.
- 7) If there is no passivity violation, the fitted model can be used in the EMT

time domain simulation.

- 8) When the passivity violation becomes relatively small, then the constrained optimization method mentioned above is applied to get a passive fitted model at the same time ensuring small fitting error.
- 9) If the passivity violation region is still relative big, then go to 3) to pick the error vector. V_{error} is inspected, and the model with the smallest error(which now happens to be the one with the next smallest error) due to the deletion of the smallest error in step (3) is selected as the next candidate. This procedure is iterated until a passive model with acceptable fitting error is found.

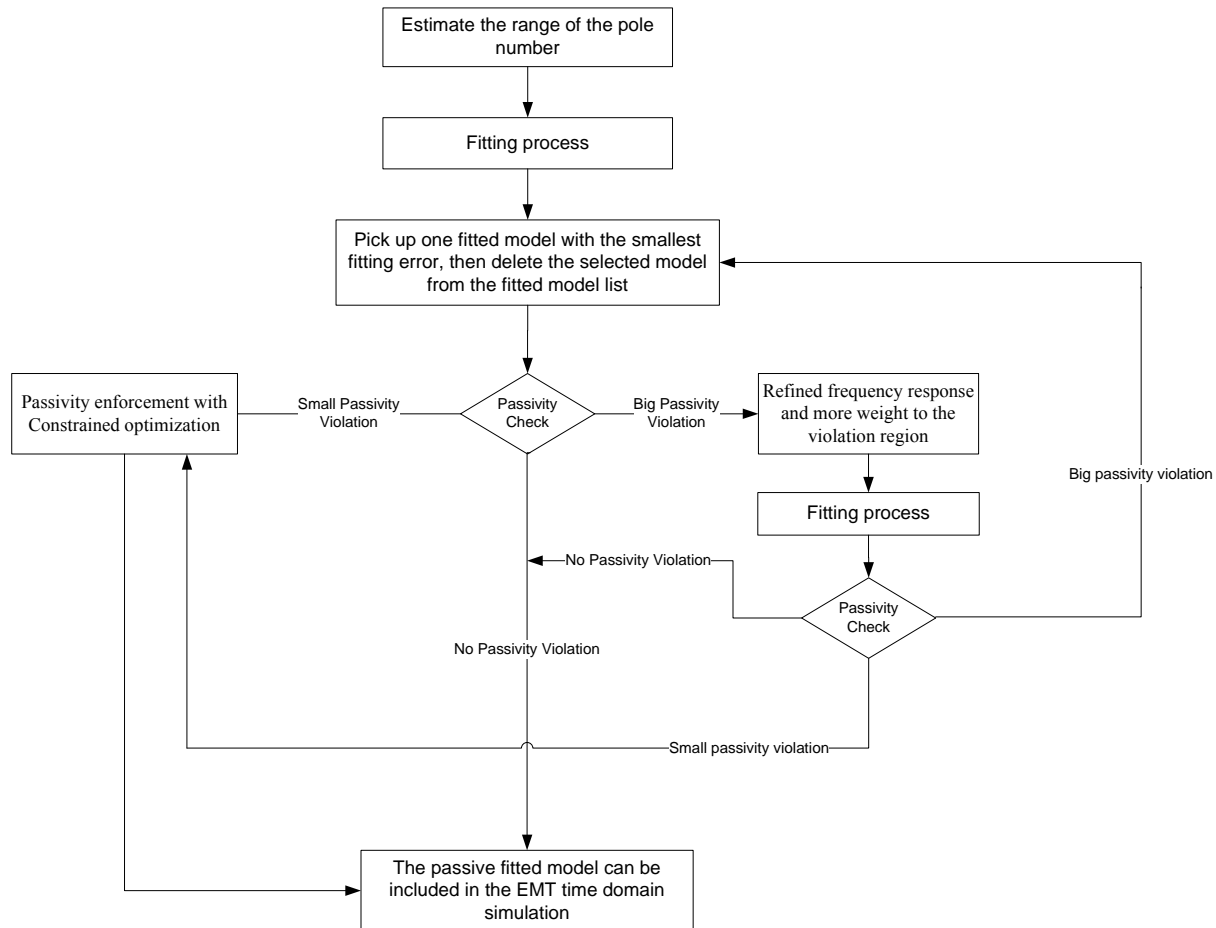


Figure 3. 4 Passivity Enforcement Procedures

Chapter 4: An Improved Two Part Wide Band Equivalencing Technique for RTDS

As described in Chapter 1, in order to enable RTDS to handle a very large size of power system, an improved wide band two part equivalent that considers both the high and low frequency behaviors of the equivalenced large system is proposed.

The coherency based dynamic equivalent technique was adapted to construct the low frequency electromechanical equivalent. The high frequency equivalent is implemented by converting the fitted rational function admittance into a time domain representation. These procedures are discussed below.

4.1 The Scheme of an Improved Two Part Wide Band Equivalencing Technique for RTDS

The proposed equivalent is illustrated in Figure 4.1. In earlier work in this area, Lin et al [18] developed a two part equivalent in which the high frequency behaviour of the reduced network was implemented using a multi-port frequency dependant network equivalent (FDNE); whereas the low frequency electro-mechanical behaviour was implemented by conducting a transient stability solution of the *unreduced* network. Using FDNE considerably reduced the size of the network to be represented by the real-time EMT model. The TSA block, however, was still the full network, resulting in a very large model for the electromechanical part of the simulation. This limited the size of the largest network that could be modeled to several hundred buses. The proposed equivalent extends this previous work through the addition of the following features making it possible to make wide-band equivalents of several thousands of buses:

- 1) Implementation of a reduced order transient stability model for representing the electro-mechanical behaviour.
- 2) Improvement to the FDNE algorithm with a guaranteed passive model.

The aim of FDNE is making a model which can be simulated in the time domain and at higher frequencies (ranging from tens of Hz to several kHz) has closely matches the frequency response of the external network (ignoring non-linearities) and hence produces

near-identical transients as the original network for any excitation applied at its boundaries, i.e., in the internal network. It is embedded into the EMT solution as a multi-port admittance and becomes a part of the main EMT solution. The FDNE can be obtained by fitting the frequency response characteristic of the original network using least-square or vector fitting [19][48]. The nonlinear, low frequency dynamic characteristics are represented by a reduced TSA solution block, in which the external network is represented by a coherency based dynamic equivalent thereby reducing the size of the modeled network, thus permitting the consideration of very large networks. This block interfaces to the EMT solution through a controlled current source, in a manner similar to that shown by Lin et al [18].

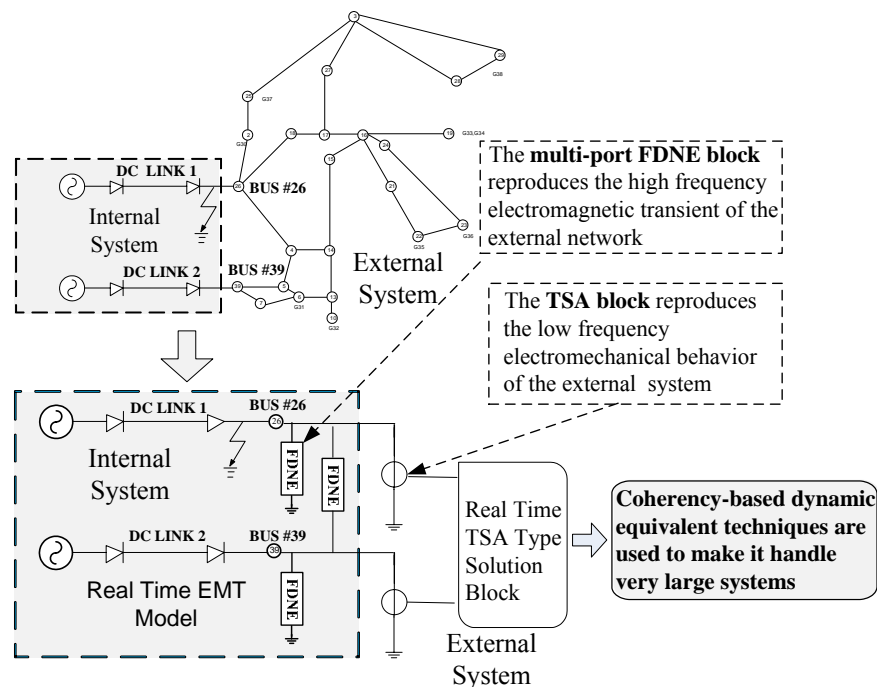


Figure 4.1 An Improved Wide Band Two Parts Equivalent for the RTDS

When a disturbance occurs in the internal system, the response of the external system is the combination of complex transients which includes high frequency phenomena as well as low frequency phenomena.

Among these transients, the linear part of R, L, C oscillations can be reproduced by the FDNE, but the nonlinear part has to be neglected [19]. FDNE is a linear

approximation, and cannot produce any nonlinear response. Hence the power electronic switching transients of the external system have to be neglected and the power electronic converters have to be replaced by their fundamental frequency approximations. The equivalent has to be passive and linear at all frequencies. If there are power electronic converters in the external system which are close to the boundary, neglecting their transients may not be advisable. But for remote converters it is probably acceptable, since the fast transients are damped out quickly due to the electrical distance and make no significant impact at the boundary.

In the earlier approach of Lin et al [18] the electromechanical response of the network was modeled with a full detailed TSA model. While this model permitted the analysis of many phenomenon associated with fundamental frequency behavior such as inter-area mode oscillations and voltage collapses. It still required large amount of computing resources. Hence, to model very large networks, it is advisable to make an equivalent even for the TSA part. Therefore, the proposed equivalent structure can cover a wide-band frequency range with reduced hardware computation.

In summary, the proposed two part equivalent largely covers the entire frequency range. The fast, linear, passive and frequency dependant characteristics are represented by the FDNE. The slow, nonlinear, fundamental frequency dynamic characteristics are represented by a reduced TSA solution. However this improved two part equivalent still has to address a potential problem, in that occasionally the FDNE shows numerical instability due to errors in the curve fitting process [49]. This problem is solved by including passivity enforcement procedure described in the pervious chapter.

The Coherency-based dynamic equivalent technique has been widely used in the industry in TSA programs. Model size can be expanded to very large networks (thousands of buses) with model reduction using coherency-based dynamic equivalents. Generators are grouped into equivalent generators by their coherency and can be directly used in a conventional TSA program. This equivalent technique will be adapted and used in the proposed two part equivalent for RTDS and its detailed procedures will be introduced in the following section.

4.2 Procedures of Coherency Based Dynamic System Equivalent

There are five steps in the coherency based dynamic system equivalent [28]. They are described in the following five sub-sections.

4.2.1 Definition of the internal and external areas

The internal system is defined as the union of all areas of most interest to the user. It could have several different parts glued together by external system elements. The external system is the remainder of the network not included in the internal system. Details of the structure of the external system are not relevant. Usually the internal system is selected by the user. However, sometimes there are regions of the network with power electronic components etc, which cannot be satisfactorily included in an external equivalent. Hence additional region sometimes have to be included in the internal system.

The system in Figure 4. 2 is the New England Test System. The entire system is divided into one internal system and one external system. The internal system contains 11 buses, 5 loads, 4 generators, 12 branches and 4 transformers. There are 29 buses, 14 loads, 6 generators, 24 branches and 10 transformers in the external system.

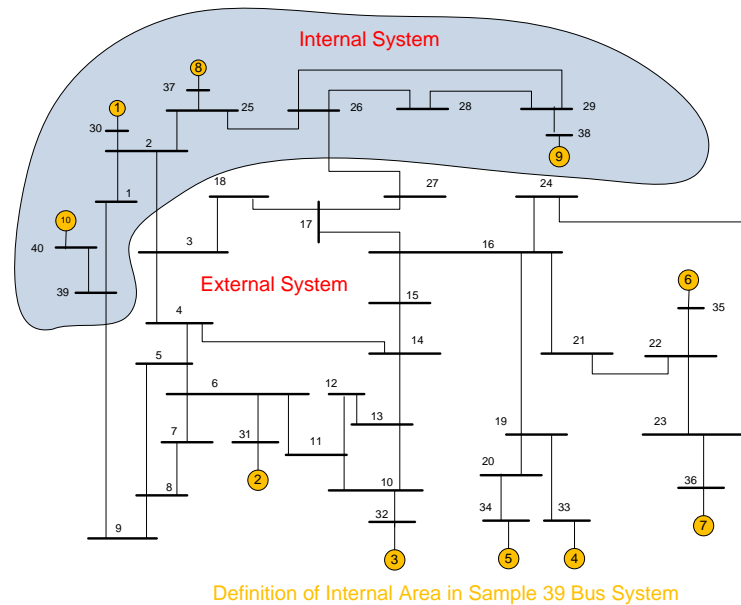


Figure 4. 2 The Definition of Internal System and External System

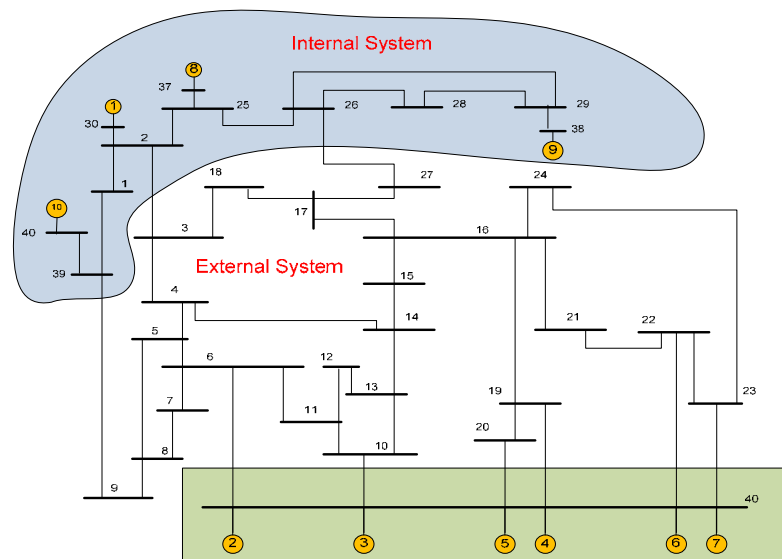
4.2.2 Coherency Identification

Coherency identification is a very important step in equivalencing the external network as mentioned in Chapter 2. Coherent groupings of machines are obtained by

analyzing the system response to a perturbation or from the point of modal analysis. An equivalent of the external system is then obtained by replacing each such coherent group of machines by a large equivalent machine. These detailed methods will be described in section 4.3.

4.2.3 Reduction of generator buses

From coherency identification the coherency groups of the system can be determined. Now we can replace the several individual buses of any coherent group with a single bus. This is shown in Figure 4. 3 and details will be explained in section 4.5.

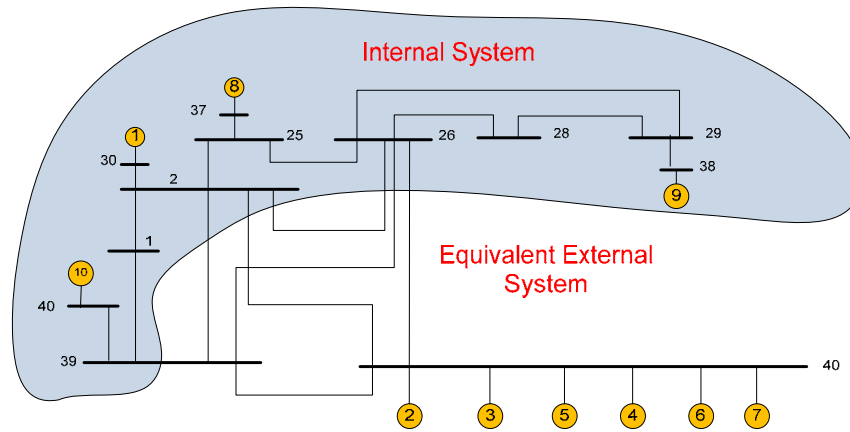


System Configuration After Coherency Based Reduction of Generator Buses

Figure 4. 3 Reduction of Generator Buses

4.2.4 Reduction of load buses

After aggregating generator terminal buses the network admittance matrix is reduced further. This procedure is shown in Figure 4. 4 and details will be explained in section 4.6.

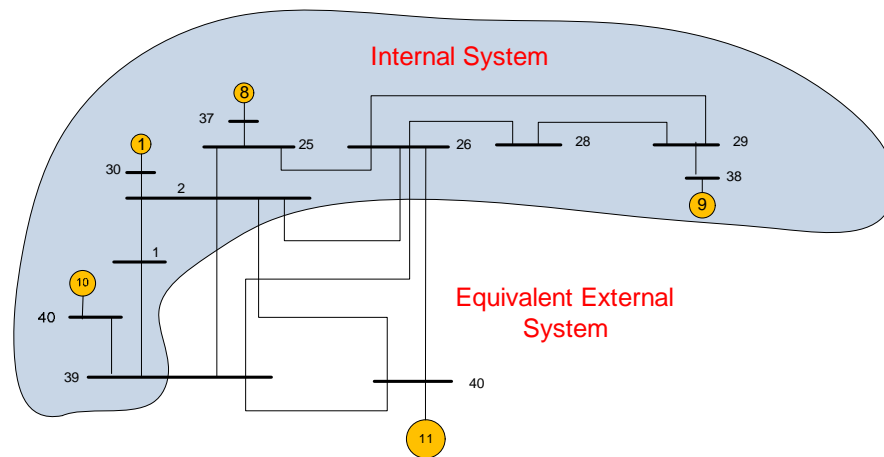


System Configuration After Gaussian Elimination of Load Buses

Figure 4.4 Reduction of Load Buses

4.2.5 Aggregation of Generating Unit

In this step all coherent generators and their controls can be aggregated into one equivalent generator. Then the individual generators in the group are replaced by the equivalent generator. This is shown in Figure 4.5 and the details will be explained in Chapter 5.



System Configuration After Dynamic Aggregation of Generating Unit Models

Figure 4.5 Dynamic Aggregations of Generators

4.3 Methods for coherency identification

As described in Chapter 2, there are several methods for the coherency identification. The most intuitive method is to compare the generators' swing curves after a typical disturbance. This method is called time domain simulation. This method is fault dependent and experience based. In this research, this method is not used for coherency

identification but is used as verification for other coherency identification methods. In this research weak link (WL) [30] and two time scale (TS) [31]-[35] methods are used for coherency identification. These two methods will be explained in detail in section 4.3.2 and 4.3.3.

4.3.1 Time domain simulation method

Time domain simulation is accomplished by comparing the swing curves under typical disturbances based on full or simplified and linearized power system models. For example, in the system (Figure 4. 2), a three bus fault at bus 29 is simulated for 0.05 s and cleared by opening line 26-29 using TSAT (A commercial transient stability analysis software). Units 2, 3,4,5,6 and 7 can be determined to be coherent for this fault according to Figure 4. 6

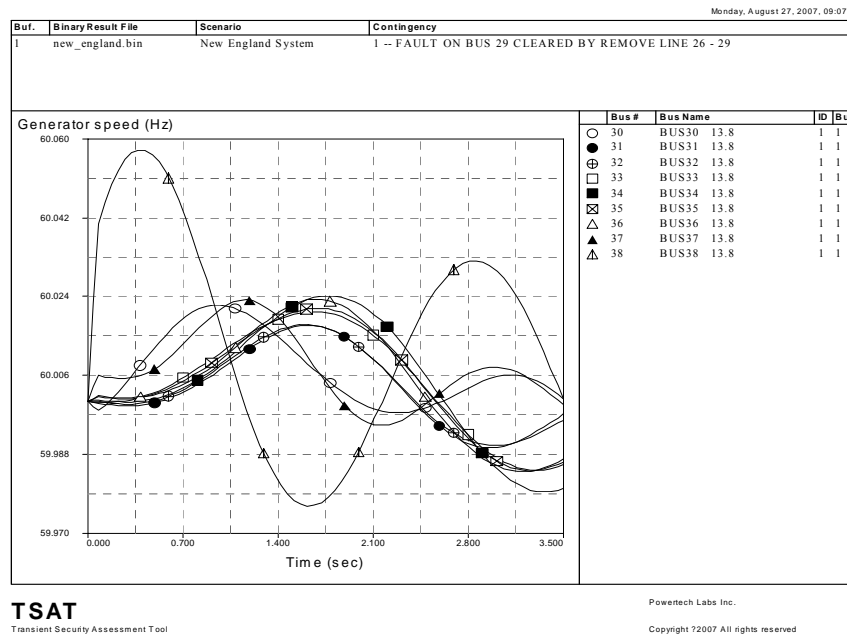


Figure 4. 6 TSAT Simulation Result for Fault on Bus 29

4.3.2 Weak Link Method (WL)

The weak link method [30] identifies the coherent groups by determining the weakly coupled subsystems from the system state matrix. The coupling between two subsystems comprises the terms of a ‘coupling factor’. The coupling factor is used in algorithm groups for the set of machines which are strongly coupled or are coherent. This is an analytical method and is fault independent. Since it needs to analyze the system state

matrix, the discussion will begin with an introduction of the linearized system model.

4.3.2.1 The Linearized system model

Since excitation and governor systems only modify the damping of the transients and do not significantly change natural frequencies and mode shapes [27], the classical representation of the synchronous machines can be used in the coherency identification.

The linearized swing equations of i -th machine can be written as

$$\Delta \dot{\delta}_i = \Delta \omega_i \quad (4.1)$$

$$\Delta \dot{\omega}_i = -V_{qi} \Delta I_{qi} / (2H_i) \quad (4.2)$$

where $\delta_i, \omega_i, H_i, V_{qi}, I_{qi}$ are respectively the rotor angle, angular velocity, inertia constant, q axis terminal voltage and current of machine i .

With $X = [\Delta \delta_1, \Delta \omega_1, \Delta \delta_2, \Delta \omega_2, \dots, \Delta \delta_n, \Delta \omega_n]^t$, (4.1) and (4.2) can be rewritten in the matrix form as

$$\dot{X} = CX + D\Delta I_{q\Delta} \quad (4.3)$$

where $\Delta I_{q\Delta} = [\Delta I_{q1} \quad \Delta I_{q2} \quad \dots \quad \Delta I_{qn}]^t$

Using network equations the non-state variable ΔI_{qi} can be eliminated from (4.3). The linearized network equations are expressed as follows [51].

$$\Delta I = M_0 E_\Delta - j[\Delta \delta_\Delta M_0 - M_0 \Delta \delta_\Delta] E_0 \quad (4.4)$$

The machine is represented by simplified classical model so the voltage E behind the transient reactance is constant [12], hence $E_\Delta = 0$, (4.4) can be rewritten as

$$\Delta I = -j[\Delta \delta_\Delta M_0 - M_0 \Delta \delta_\Delta] E_0 \quad (4.5)$$

where $M_0 = T_0^{-1} Y T_0$ and Y is the admittance matrix reduced to the internal nodes of machines. The other variables are defined below:

$$\begin{aligned}
\Delta I_i &= \Delta I_{di} + j\Delta I_{qi}, I_{\Delta} = [\Delta I_1 \quad \Delta I_2 \quad \dots \quad \Delta I_n]^t \\
T_0 &= \text{diag}[e^{j\delta_{10}} \quad e^{j\delta_{20}} \quad \dots \quad e^{j\delta_{n0}}] \\
\delta_{\Delta} &= \text{diag}[\Delta\delta_1 \quad \Delta\delta_2 \quad \dots \quad \Delta\delta_n] \\
E_i &= 0 + jE_{qi}, E_0 = [E_1 \quad E_2 \quad \dots \quad E_n]^t
\end{aligned} \tag{4.6}$$

By equating the imaginary terms on both sides of (4.5), we obtain a linearized relationship between δ_{Δ} and $I_{q\Delta}$.

$$I_{q\Delta} = P\delta_{\Delta} = F \cdot X \tag{4.7}$$

where $I_{q\Delta} = [\Delta I_{q1} \quad \Delta I_{q2} \quad \dots \quad \Delta I_{qn}]^t$, $\delta_{\Delta} = [\Delta\delta_1 \quad \Delta\delta_2 \quad \dots \quad \Delta\delta_n]^t$ and matrix F can be obtained from equation (4.5).

Replacing $I_{q\Delta}$ in the swing equation (4.3) for machines with the linearized network equation (4.7) the following equation can be obtained.

$$\begin{aligned}
\dot{X} &= (C + DF)X \\
\text{or } \dot{X} &= AX
\end{aligned} \tag{4.8}$$

4.3.2.2 Weak Link Algorithm

The weak link idea [30] allows for the decoupling of systems by reorganizing the system matrix based on the relative coupling strength of the state variables which are associated with the machines. For purpose of demonstration, consider a system which we assume has only two coherent sets of generators. The system equation (4.8) is re-written as (4.9), with X_1 , and X_2 representing the state variables of each of the respective coherent areas.

$$\begin{bmatrix} \dot{X}_1 \\ \dot{X}_2 \end{bmatrix} = \begin{bmatrix} A_{11} & \varepsilon A_{12} \\ \varepsilon A_{21} & A_{22} \end{bmatrix} \begin{bmatrix} X_1 \\ X_2 \end{bmatrix} \tag{4.9}$$

In (4.9) ε is a positive number. When $\varepsilon \ll 1$ this gives rise to two weakly coupled subsystem with state variables X_1 and X_2 . From (4.9) it can be seen that a system structure yielding the minimum value of ε determines weakly coupled

subsystems with state vectors X_1 and X_2 . For a power system situation, the group of machines contained within A_{11} can be termed as weakly coupled with those in A_{22} , and vice-versa. Similarly, the machines contained in A_{11} are strongly coupled to all other machines in A_{11} (likewise for A_{22}).

The basic concept of the weak link method is to re-order the rows of A in (4. 8) so that the form (4. 9) is obtained with a small ε . Generalizing this to a multi-machine system, the structure depicted in Figure 4. 7 is obtained, where the coupling between the individual blocks \tilde{A}_{ii} is minimal, and the coupling within the blocks is strong.

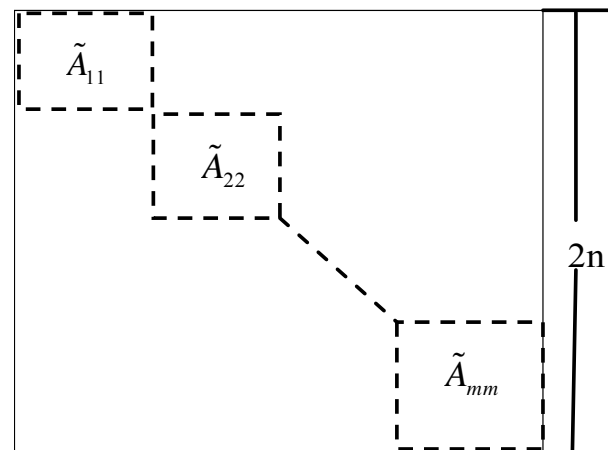


Figure 4. 7 Weakly Coupled Sub-systems

The more mathematics details and implementation procedures are illustrated in Appendix A using a simple eight bus system which is shown in Figure 4. 8.

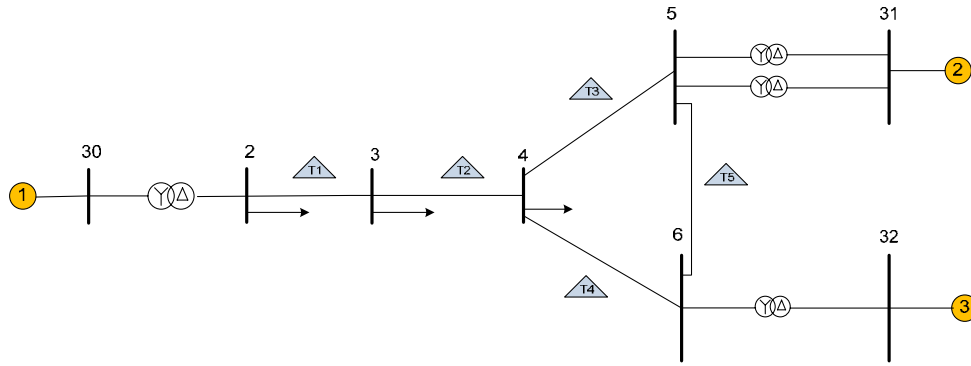


Figure 4.8 Eight Bus Test System

4.3.3 Two Time Scale Method (TS)

The Two Time Scale (TS) [31]-[35] coherency identification method is based on the comparison of the pattern of the synchronous machine's contributions to the eigenvectors of the lowest frequency inter-area system modes.

The physical relationship between the low frequency oscillations and weakly connected synchronous machines is used. It is known that low frequency oscillations are caused by groups of strongly interconnected synchronous machines oscillating against other strongly interconnected synchronous machines through a weak tie. The following sub-section is a brief description of implementation procedures of this method.

4.3.3.1 Implementations Procedures of the Two Time Scale (TS) Algorithm

The number of the coherent groups r is defined first. The system eigenvector matrix is inspected, and the r generators showing the most independent modes patterns are chosen to be the reference generators for each of the r coherent group. This procedure is explained using an example in the following subsection. Gaussian elimination with complete pivoting is used to get the reference generators. The remaining generators are placed into the coherent groups depending on the closeness of their oscillation modes to each the reference generators. A generator with an eigenvector pattern closest to a reference generator is grouped with that reference generator.

The following is the physical interpretation of the TS method. Each row of the eigenvector matrix U describes how the modes are distributed in a particular generator.

The r reference generators are most linearly independent for these r slowest modes. The coherency identification is described in more detail below: [31].

- 1) Choose the number of desired coherent groups r .
- 2) Compute the $n \times r$ eigenvector sub-matrix U , whose columns are the eigenvectors corresponding to the r smallest magnitude eigenvalues (smallest frequencies). These are essentially the inter-area modes that are seen at terminals of the external system.
- 3) Gaussian elimination with complete pivoting is applied to U in order to get T . The first r rows of the resulting matrix T correspond to the r required reference machines.
- 4) Rearrange the matrix U such that the first r rows correspond to the r reference machines shown as (4. 10).

$$U = [U_1 \quad U_2]^T \quad (4. 10)$$

where U_1 contains the first r rows and U_2 contains the remaining $n - r$ rows. Use (4. 11) to obtain the $(n - r) \times r$ matrix L . Each row of L is associated with a non-reference machine, while each column corresponds to a reference machine

$$L = U_2 U_1^{-1} \quad (4. 11)$$

- 5) Scan each row k (corresponding a non-reference generator) of L to obtain the largest element. The indices of this element identify which reference generator this generator is most coherent with. For example, if the largest element is $L_{k,p}$, it means that non-reference generator k belongs to the coherent group referenced by generator p .

Using this procedure, the coherent sets can be identified. In the following sub-section, a simple eight bus system shown in Figure 4. 8 is used to illustrate the implantation of this method.

4.3.3.2 An Eight Bus System Example with Two Time Scale (TS) Algorithm

In Figure 4. 8 , line T2 is a long line, T3 and T4 are short lines, it is institutive that generator 2 and 3 should form a coherent group. The following implementation of the TS method has verified this institutive assumption.

1) Formulate the system state matrix A . The size of A is supposed to be n .

Select the number of groups (r) to be determined. For the three machine test system, the number of groups is selected as 2, that is, $r = 2$.

2) Determine U , where U is a $n \times r$ matrix whose columns are the eigenvectors corresponding to the smallest eigenvalues of A

$$\text{For example, let } A = \begin{bmatrix} -11.075759 & 5.061610 & 6.014149 \\ 3.883401 & -13.504492 & 9.621091 \\ 2.890914 & 7.534051 & -10.424965 \end{bmatrix}$$

$$\text{The eigvalues are } \Lambda = [0 \quad -14.332597 \quad -20.672619]$$

$$\text{The right eigvector is } V_{right} = \begin{bmatrix} 0.577350 & 0.919097 & 0.065840 \\ 0.577350 & -0.167745 & -0.812713 \\ 0.577350 & -0.356541 & 0.578931 \end{bmatrix}$$

Since r has been chosen as 2, we form the submatirx U , which corresponds to the 2 slowest eigenvalues, ie; 0 and -14.3.

$$U = \begin{bmatrix} 0.577350 & 0.919097 \\ 0.577350 & -0.167745 \\ 0.577350 & -0.356541 \end{bmatrix}$$

3) Determine the reference synchronous machines for each group. This is achieved by applying Gaussian elimination with complete pivoting to U to get T . The first r rows of the resulting matrix (T) after the Gaussian elimination correspond to the r required reference machines. The row permutations introduced by the full pivoting procedure are tracked to identify the generators corresponding to the rows of T .

The Gaussian elimination procedure is illustrated on the three machine system example.

U is the following:

$$U = \begin{bmatrix} 0.577350 & 0.919097 \\ 0.577350 & -0.167745 \\ 0.577350 & -0.356541 \end{bmatrix} \begin{bmatrix} x_1 \\ x_2 \\ x_3 \end{bmatrix}$$

The largest number of U is the (1, 2) entry. The first and second columns are exchanged to obtain

$$\begin{bmatrix} 0.919097 & 0.577350 \\ -0.167745 & 0.577350 \\ -0.356541 & 0.577350 \end{bmatrix} \begin{bmatrix} x_1 \\ x_2 \\ x_3 \end{bmatrix}$$

Then the (1, 1) entry is used as the pivot to eliminate the remainder of the first column, resulting in

$$\begin{bmatrix} 0.919097 & 0.577350 \\ 0 & 0.682723 \\ 0 & 0.801319 \end{bmatrix} \begin{bmatrix} x_1 \\ x_2 \\ x_3 \end{bmatrix}$$

Now the largest number below the first row is the (3, 2) entry. We exchange the second and third row, resulting in

$$\begin{bmatrix} 0.919097 & 0.577350 \\ 0 & 0.801319 \\ 0 & 0.682723 \end{bmatrix} \begin{bmatrix} x_1 \\ x_3 \\ x_2 \end{bmatrix}$$

The largest number below the first row is the (2, 2) entry. The procedure terminates here because all the pivots have been found and the reference states are x_1 and x_3 . The whole process can be shown as following.

$$\begin{bmatrix} 0.919097 & 0.577350 \\ -0.167745 & 0.577350 \\ -0.356541 & 0.577350 \end{bmatrix} \begin{bmatrix} x_1 \\ x_2 \\ x_3 \end{bmatrix} \Rightarrow \begin{bmatrix} 0.919097 & 0.577350 \\ 0 & 0.682723 \\ 0 & 0.801319 \end{bmatrix} \begin{bmatrix} x_1 \\ x_2 \\ x_3 \end{bmatrix} \Rightarrow \begin{bmatrix} 0.919097 & 0.577350 \\ 0 & 0.801319 \\ 0 & 0.682723 \end{bmatrix} \begin{bmatrix} x_1 \\ x_3 \\ x_2 \end{bmatrix} = T \begin{bmatrix} x_1 \\ x_3 \\ x_2 \end{bmatrix}$$

The order of the state vector is now $[x_1 \ x_3 \ x_2]^T$. According to the number of groups ($r=2$) x_1 and x_3 in the state vectors are selected which are in correspond with generator #1 and #3. Hence it is clear the reference generator is #1 and #3.

4) Rearrange the matrix U such that the first r rows correspond to the r reference synchronous machines. This will result in the new matrix TT which can be partitioned as

$$TT = \begin{bmatrix} U_1 \\ U_2 \end{bmatrix} \quad (4.12)$$

U_1 contains the first r rows and U_2 contains the remaining $(n-r)$ rows. For the three machine example

$$TT = \begin{bmatrix} 0.577350 & 0.919097 \\ 0.577350 & -0.356541 \\ 0.577350 & -0.167745 \end{bmatrix}, U_1 = \begin{bmatrix} 0.577350 & 0.919097 \\ 0.577350 & -0.356541 \end{bmatrix}, U_2 = [0.577350 \quad -0.167745]$$

5) Form L , where

$$L = U_2 U_1^{-1} \quad (4.13)$$

L is of size $(n-r) \times r$. For this matrix, each row corresponds to a non-reference synchronous machine and each column corresponds to a reference machine.

6) Determine for each row of L , the index of the element with maximum modulus. This index gives the group with which the corresponding synchronous machine is coherent.

For the three machine example, L is shown in the Table 4. 1.

#1	#3	
0.148000979	0.851999021	#2

Table 4. 1 L Matrix of 8 Bus System

The reference generators are #1 and #3, it can be seen from L that #3 and #2 generators are coherent.

4.4 Application to IEEE (New England) 39 Bus System

This section continues the application of the developed method to the well known

IEEE 39 bus system. In comparison to the highly simplified eight bus system of section 4.3 this system shows multiple coherent groups. The New England Test System [21] shown in Figure 4. 9 is used as a study case for the two coherency identification approaches. And time domain simulation is employed as verification using TSAT software.

For the TS method, the L matrix is shown in Table 4. 2. Six reference machines are selected, namely #9, #5, #7, #10, #1 and #3. The groups of the remaining machines (i.e. #6, #8, #2 and #4) are decided according to the highest magnitude entry in Table 4. 2, from which the groups (6,7),(8,1),(2,3),(4,5) and (9) emerge. The coherency result is just the same as the WL method (see Appendix A).

#9	#5	#7	#10	#1	#3	
0.021654	0.11061	0.702407	-0.00665	0.092958	0.079024	#6
0.10926	0.014857	0.022322	-0.01356	0.853728	0.013391	#8
0.00677	-0.01114	-0.01577	0.182458	-0.11709	0.954767	#2
0.023241	0.681245	0.150351	-0.01349	0.082873	0.07578	#4

Table 4. 2 L Matrix of 39 Bus System

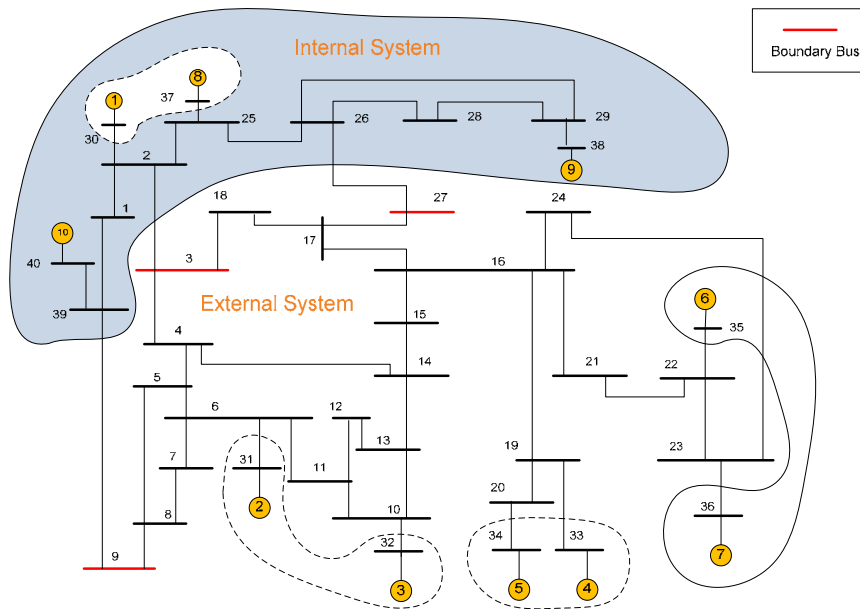


Figure 4. 9 Coherent Groups of IEEE 39 Test System

The validity of above approaches is confirmed by conducting a time domain simulation of the network using the commercial software TSAT. A fault is applied on bus 29 of duration of 6 cycles (100 *ms*) and the swing curves are shown in Figure 4. 10. The figure plots swing curves for machines (1, 8) and (2, 3). The machines groups can be seen to swing in unison, showing that they form two coherent sets. Each coherent group is indicated by a different curve type. The result clearly validates the coherency identification of the weak link method. Other machines are not shown, but when the full set of swing curves is plotted, the coherent grouping shown in Figure 4. 9 is seen to be correct. It is identical to the result given by the WL and TS methods.

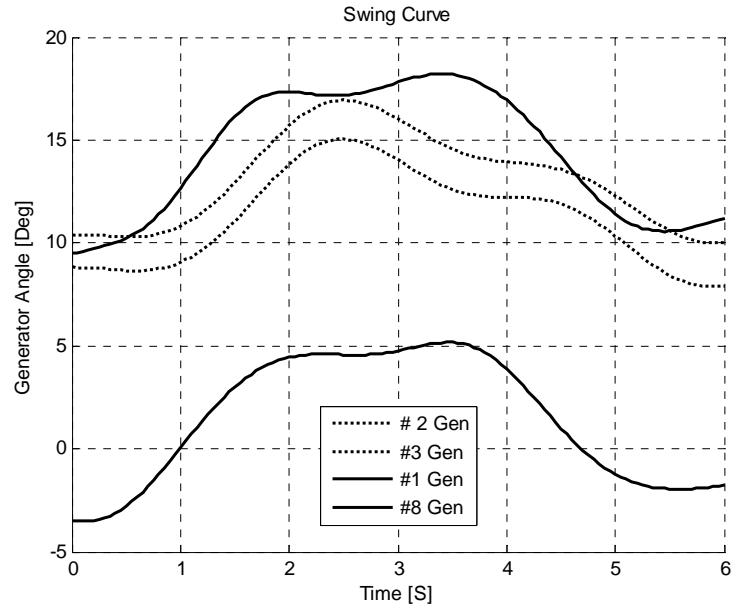


Figure 4. 10 TSAT Time Domain Simulation Results

Both WL and TS methods described above are fault independent techniques. The WL method is simpler to implement, but is less flexible as it does not allow specification of the number of coherent groups. The Two Time Scale (TS) method is more mathematically rigorous, and also permits specification of the number of coherent groups and hence permits the user to select the size of the equivalent. For these advantages the TS method is employed further in this research.

4.5 Coherency Based Network Reduction

Once the coherent groups of machines are identified using the TS (or WL) method the next task is to reduce the network. This process is introduced in this section.

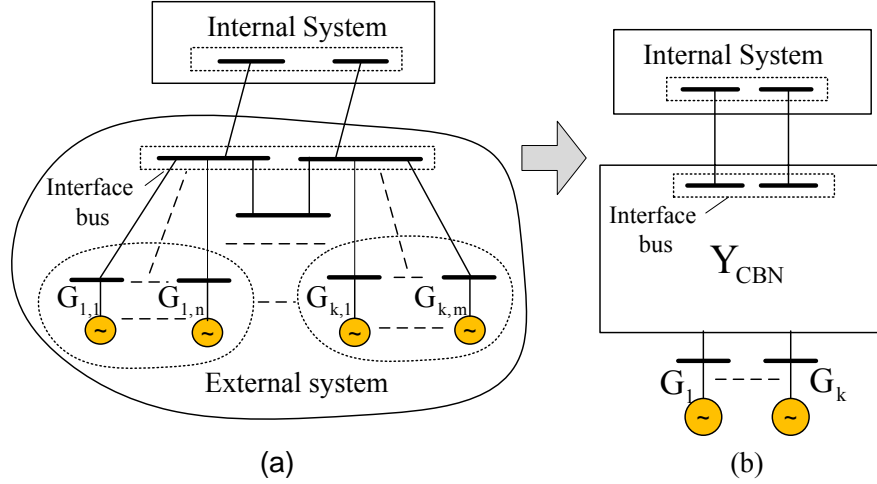


Figure 4.11 Coherency Based Bus Reduction

The generator terminal buses of the m individual machines $G_{k,1}, G_{k,2}, \dots, G_{k,m}$ in coherent group k are no longer available as these are replaced by an equivalent bus to which the equivalent generator G_k is connected as shown in Figure 4.11 (a) and (b). Instead, the single equivalent bus and the remaining network buses (referred to as boundary buses) now form a new network. After all coherent groups are thus reduced; a new network with a reduced admittance matrix Y_{CBN} consisting only of the equivalent generator terminal buses and the remaining buses of the external network is formed as shown in Figure 4.11 (b). The details of the above procedure are shown below.

For the external system, the subscript c denotes coherent generators terminal buses which are to be reduced, and b denotes the rest of the buses (boundary buses) of the external network. The network equation can be expressed as

$$\begin{bmatrix} \bar{I}_b \\ \bar{I}_c \end{bmatrix} = \begin{bmatrix} \bar{Y}_{bb} & \bar{Y}_{bc} \\ \bar{Y}_{cb} & \bar{Y}_{cc} \end{bmatrix} \begin{bmatrix} \bar{V}_b \\ \bar{V}_c \end{bmatrix} \quad (4.14)$$

Further, suppose that group b contains m buses and group c contains $n-m$ buses. Equation (4.14) can be expanded again to yield:

$$\begin{bmatrix} I_1 \\ \cdot \\ \cdot \\ \cdot \\ I_m \\ I_{m+1} \\ \cdot \\ \cdot \\ \cdot \\ I_n \end{bmatrix} = \begin{bmatrix} Y_{11} & \cdot & \cdot & \cdot & Y_{1m} & Y_{1(m+1)} & \cdot & \cdot & \cdot & Y_{1n} \\ \cdot & & & & \cdot & \cdot & & & & \cdot \\ \cdot & & & & \cdot & \cdot & & & & \cdot \\ \cdot & & & & \cdot & \cdot & & & & \cdot \\ Y_{m1} & \cdot & \cdot & \cdot & Y_{mm} & Y_{m(m+1)} & \cdot & \cdot & \cdot & Y_{mn} \\ Y_{(m+1)1} & \cdot & \cdot & \cdot & Y_{(m+1)m} & Y_{(m+1)(m+1)} & \cdot & \cdot & \cdot & Y_{(m+1)n} \\ \cdot & & & & \cdot & \cdot & & & & \cdot \\ \cdot & & & & \cdot & \cdot & & & & \cdot \\ \cdot & & & & \cdot & \cdot & & & & \cdot \\ Y_{n1} & \cdot & \cdot & \cdot & Y_{nm} & Y_{n(m+1)} & \cdot & \cdot & \cdot & Y_{nn} \end{bmatrix} \begin{bmatrix} V_1 \\ \cdot \\ \cdot \\ \cdot \\ V_m \\ V_{m+1} \\ \cdot \\ \cdot \\ \cdot \\ V_n \end{bmatrix} \quad (4.15)$$

Rewriting (4.15) for each bus $i = 1, \dots, n$

$$I_i = \sum_{k=1}^m Y_{ik} V_k + \sum_{k=m+1}^n Y_{ik} V_k \quad (4.16)$$

Where the first summation is over the group b and the second summation is over the group c .

The equivalent will be formed by replacing the coherent group of buses c with a single equivalent bus labeled t . Equation (4.15), which after reduction, will become:

$$\begin{bmatrix} I_1 \\ I_2 \\ \cdot \\ \cdot \\ \cdot \\ I_m \\ I_t \end{bmatrix} = \begin{bmatrix} Y_{11} & Y_{12} & \cdot & \cdot & \cdot & Y_{1t} \\ Y_{21} & & & & & \cdot \\ \cdot & & & & & \cdot \\ \cdot & & & & & \cdot \\ Y_{m1} & \cdot & \cdot & \cdot & \cdot & Y_{mt} \\ Y_{t1} & \cdot & \cdot & \cdot & \cdot & Y_{tt} \end{bmatrix} \begin{bmatrix} V_1 \\ V_2 \\ \cdot \\ \cdot \\ V_m \\ V_t \end{bmatrix} \quad (4.17)$$

In this equation the $(n-m)$ buses of the coherent group have been replaced by a single bus t .

A power matching technique is used to form the equivalent. The power flow at each of the boundary buses is conserved. Similarly, power production in the coherent group is conserved.

The first step in the derivation of the equivalent is the conservation of power at each

of the boundary nodes.

Equation (4. 15) is rewritten with $i = b$, a bus on the boundary.

$$I_b = \sum_{k=1}^m Y_{bk} V_k + \sum_{k=m+1}^n Y_{bk} V_k \quad (4. 18)$$

The power at bus b is given by

$$S_b = V_b I_b^* \quad (4. 19)$$

Where * denotes complex conjugate, substituting (4. 18) in (4. 19) yields

$$\begin{aligned} S_b &= \left(\sum_{k=1}^m V_k^* Y_{bk}^* + \sum_{k=m+1}^n V_k^* Y_{bk}^* \right) V_b \\ &= \sum_{k=1}^m V_k^* Y_{bk}^* V_b + \sum_{k=m+1}^n V_k^* Y_{bk}^* V_b \end{aligned} \quad (4. 20)$$

The first summation in (4. 20) is the contribution to the power at b by other buses in the boundary and the second summation is the contribution from the entire coherent group.

In the reduced network the entire coherent group will be replaced by a single bus t . The power at b will become:

$$S_b = \sum_{k=1}^m V_k^* Y_{bk}^* V_b + V_t^* Y_{bt}^* V_b \quad (4. 21)$$

V_t is the voltage at this equivalent bus and Y_{bt} is the bt^{th} term of the reduced bus admittance matrix.

Equation (4. 20) is equated to (4. 21) resulting in:

$$\begin{aligned} \sum_{k=1}^m V_k^* Y_{bk}^* V_b + \sum_{k=m+1}^n V_k^* Y_{bk}^* V_b &= \sum_{k=1}^m V_k^* Y_{bk}^* V_b + V_t^* Y_{bt}^* V_b \\ \Rightarrow \sum_{k=m+1}^n V_k^* Y_{bk}^* V_b &= V_t^* Y_{bt}^* V_b \end{aligned} \quad (4. 22)$$

Taking the conjugate of (4. 22) and dividing by V_t

$$Y_{bt} = \frac{1}{V_t} \sum_{k=m+1}^n V_k Y_{bk} = \sum_{k=m+1}^n \frac{V_k}{V_t} Y_{bk} \quad (4.23)$$

Equation (4.23) implies that the bt^{th} term of the bus admittance matrix is determined as soon as a voltage V_t is chosen for the equivalent. The voltage V_t is arbitrary but is chosen as some type of average of the voltage at the buses which are eliminated. The voltage magnitude was chosen as the average of the voltage magnitudes of the buses eliminated, and its angle was chosen as the average angle

$$|V_t| = \frac{1}{n-m} \sum_{k=m+1}^n |V_k| \quad (4.24)$$

$$\theta_t = \frac{1}{n-m} \sum_{k=m+1}^n \theta_k \quad (4.25)$$

The second step in the derivation of the equivalent is the conservation of power in the group of buses to be eliminated. For any 'c' bus in the coherent group, the total power of the coherent group is:

$$S_c = \sum_{c=m+1}^n V_c I_c^* \quad (4.26)$$

For each c the current I_c can be expanded using (4.18)

$$I_c = \sum_{k=1}^m Y_{ck} V_k + \sum_{k=m+1}^n Y_{ck} V_k \quad (4.27)$$

Substituting (4.27) into (4.26) results in:

$$S_c = \sum_{c=m+1}^n \left\{ \sum_{k=1}^m V_k^* Y_{ck}^* V_c + \sum_{k=m+1}^n V_k^* Y_{ck}^* V_c \right\} \quad (4.28)$$

Interchanging the order of summation yields:

$$S_c = \sum_{k=1}^m \sum_{c=m+1}^n V_k^* Y_{ck}^* V_c + \sum_{k=m+1}^n \sum_{c=m+1}^n V_k^* Y_{ck}^* V_c \quad (4.29)$$

Writing the same expression for the reduced network gives the following:

$$S_c = \sum_{k=1}^m V_k^* Y_{tk}^* V_t + V_t^* Y_{tt}^* V_t \quad (4. 30)$$

The first term in (4. 29) is the summation of the powers entering the coherent group from the boundary buses. Similarly the first term of (4. 30) represents powers entering the equivalent bus from the boundary buses. In order for the equivalent to show similar dynamic performance to its coherent component machines, these terms must be equal as shown in (4. 33). The second term in (4. 29) is the summation of the powers entirely internal to the coherent group and equivalent. Each group should have its power conserved; hence the second terms are equated shown as (4. 31):

$$V_t^* Y_{tt}^* V_t = \sum_{k=m+1}^n \sum_{c=m+1}^n V_k^* Y_{ck}^* V_c \quad (4. 31)$$

Dividing (4. 31) by $V_t^* V_t$ yields an expression for the self admittance of the equivalent:

$$Y_{tt} = \sum_{k=m+1}^n \sum_{c=m+1}^n \frac{V_k}{V_t} Y_{ck} \frac{V_c}{V_t^*} \quad (4. 32)$$

Returning to (4. 29) and (4. 30), the first terms are equated:

$$\sum_{k=1}^m \sum_{c=m+1}^n V_k^* Y_{ck}^* V_c = \sum_{k=1}^m V_k^* Y_{tk}^* V_t \quad (4. 33)$$

The index k in (4. 33) runs over the boundary buses. For any fixed k , $k = b$ say, an expression for the tb^{th} term of the bus admittance matrix is found:

$$\sum_{c=m+1}^n V_b^* Y_{cb}^* V_c = V_b^* Y_{tb}^* V_t \quad (4. 34)$$

Eliminating the common factor V_b^* , dividing by V_t and taking the conjugate results in:

$$Y_{tb} = \sum_{c=m+1}^n Y_{cb} \frac{V_c}{V_t^*} \quad (4. 35)$$

Comparing (4. 35) with (4. 23) shows that $Y_{tb} \neq Y_{bt}$. The magnitude is the same,

however, indicating that a pure phase shifting transformer has been introduced in the line from the equivalent bus t to each boundary bus b . The phase shift is half the angular difference of Y_{bt} and Y_{tb} .

Once one coherent group is considered, the extension to more groups is straightforward. The admittance elements between the coherent group and the boundary buses are the same with (4. 23) and (4. 35). And the self admittance of the coherent group is the same with (4. 32). The items between two coherent groups are the following:

It is assumed that buses of the coherent group $c1$ are from $m1$ to $n1$, and buses of group $c2$ are from $m2$ to $n2$. Y_{c1c2} and Y_{c2c1} are the line admittances. V_{c1} is the complex voltage of the bus in one coherent group. V_{c2} is the complex voltage of the bus in the other coherent group. The average voltage of $c1$ and $c2$ are V_{t1} and V_{t2} .

$$Y_{t1t2} = \sum_{c1=m1}^{n1} \sum_{c2=m2}^{n2} Y_{c1c2} \frac{V_{c1}}{V_{t1}} \frac{V_{c2}^*}{V_{t2}^*} \quad (4. 36)$$

$$Y_{t2t1} = \sum_{c2=m2}^{n2} \sum_{c1=m1}^{n1} Y_{c2c1} \frac{V_{c1}^*}{V_{t1}^*} \frac{V_{c2}}{V_{t2}} \quad (4. 37)$$

Summary of Procedures for Obtaining Coherency Based Reduced Network:

The entire process discussed above is summarized into its essential steps below. Buses $m+1, \dots, n$ will be reduced:

The voltage of the equivalent is

$$|V_t| = \frac{1}{n-m} \sum_{k=m+1}^n |V_k| \quad (4. 38)$$

$$\theta_t = \frac{1}{n-m} \sum_{k=m+1}^n \theta_k \quad (4. 39)$$

The bt^{th} term of the reduced bus admittance matrix is

$$Y_{bt} = \sum_{k=m+1}^n \frac{V_k}{V_t} Y_{bk} \quad (4. 40)$$

(b is a boundary node)

The tb^{th} term of the reduced bus admittance matrix is

$$Y_{tb} = \sum_{c=m+1}^n Y_{cb} \frac{V_c}{V_t^*} \quad (4.41)$$

(b is a boundary node)

The tt^{th} term of the reduced bus admittance matrix is (the self admittance of the equivalent)

$$Y_{tt} = \sum_{k=m+1}^n \sum_{c=m+1}^n \frac{V_k}{V_t} Y_{ck} \frac{V_c}{V_t^*} \quad (4.42)$$

The angle of the phase shifting transformer between t and b

$$\theta_{tb} = \frac{1}{2}(\beta_{bt} - \beta_{tb}) \quad (4.43)$$

Where β_{bt} is the angle of Y_{bt} and β_{tb} is the angle of Y_{tb} .

The $t_1 t_2^{th}$ and $t_2 t_1^{th}$ term of the reduced bus admittance matrix is

$$Y_{t_1 t_2} = \sum_{c_1=m_1}^{n_1} \sum_{c_2=m_2}^{n_2} Y_{c_1 c_2} \frac{V_{c_1}}{V_{t_1}} \frac{V_{c_2}}{V_{t_2}^*} \quad (4.44)$$

$$Y_{t_2 t_1} = \sum_{c_2=m_2}^{n_2} \sum_{c_1=m_1}^{n_1} Y_{c_2 c_1} \frac{V_{c_1}}{V_{t_1}^*} \frac{V_{c_2}}{V_{t_2}}$$

The resistance and reactance of the line from t to b is

$$R + jX = \frac{-1 \angle \theta_{tb}}{Y_{tb}} \left(\frac{-1 \angle -\theta_{tb}}{Y_{tb}} \right) \quad (4.45)$$

4.6 Transient Stability Analysis (TSA) Equivalent with the FDNE

From section 4.5, the entire admittance matrix of the external system has been reduced to Y_{CBN} as shown in Figure 4.12 according to the coherency bus reduction. Now this reduced admittance Y_{CBN} can be used to get the TSA equivalent of the external system.

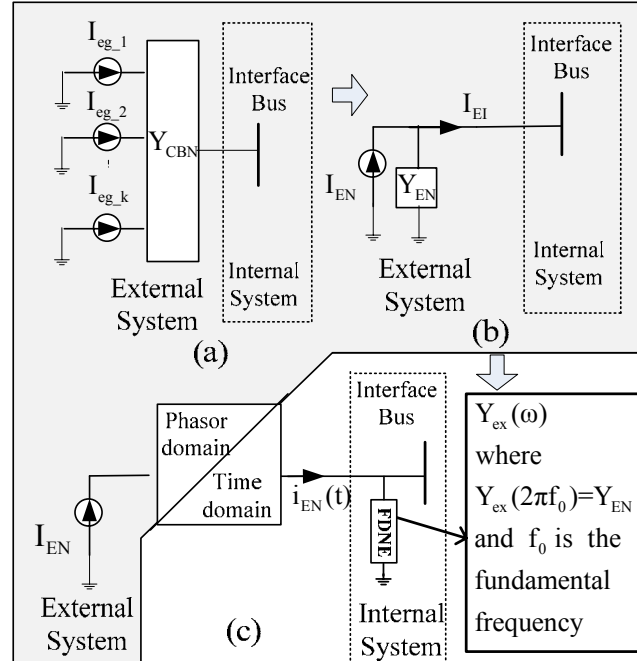


Figure 4.12 TSA Equivalent of the External System

As shown in Figure 4.12 (a) using the terminal voltages as the inputs the injection currents I_{EGk} to the network Y_{CBN} in each equivalent generator G_k can be determined by the generator state equation [7]. Once these currents are known, seen from the internal system the external system can be converted to a Norton-equivalent (I_{EN} and Y_{EN}) as shown in Figure 4.12 (b). For simplicity only one port is illustrated, but the actual procedure develops a multi-port equivalent.

The current I_{EN} in the Norton current source is injected into the EMT solution of the internal system. Note that the Norton impedance Y_{EN} in the TSA solution is essentially the fundamental frequency representation of the FDNE included in the EMT solution. Hence it is correct to inject only the current I_{EN} in the Norton source and not the interface current I_{EI} as shown in Figure 4.12 (b) and (c). The details of the above procedure are shown below.

From the point of equivalent, our concerns are the quantities of the boundary seen from the internal system. The new external system admittance can be divided into four parts as follows:

$$Y_{eq} = \begin{bmatrix} Y_{II} & Y_{IE} \\ Y_{EI} & Y_{EE} \end{bmatrix} \quad (4.46)$$

Where the sub matrix indices I run through the sequence of interface buses, and the indices E run through the sequence of buses in the external system that are not interface buses. The relationship between the voltages and currents in the external system is:

$$\begin{bmatrix} I_{I-external} + I_{I-internal} \\ I_E \end{bmatrix} = \begin{bmatrix} Y_{II} & Y_{IE} \\ Y_{EI} & Y_{EE} \end{bmatrix} \begin{bmatrix} V_I \\ V_E \end{bmatrix} \quad (4.47)$$

Where $I_{I-external}$ is the injection current vector of the equipments (generators and nonlinear loads) of the external system which are directly connected to the boundary buses. $I_{I-internal}$ is the (known) current vector from the internal system. As shown below, the second row of (4.47) can be rearranged as (4.48) to express the voltage-current relationships at the interface buses.

$$[V_E] = [Y_{EE}]^{-1} [I_E] - [Y_{EE}]^{-1} [Y_{EI}] [V_I] \quad (4.48)$$

Substitution of (4.48) into the equation obtained by expanding the first row of (4.47) gives (4.49):

$$\begin{aligned} & [I_{I-external} + I_{I-internal}] \\ &= [Y_{II}] [V_I] + [Y_{IE}] [Y_E]^{-1} [I_E] - [Y_{IE}] [Y_E]^{-1} [Y_{EI}] [V_I] \\ &\Rightarrow [I_{I-internal}] + \left\{ [I_{I-external}] - [Y_{IE}] [Y_{EE}]^{-1} [I_E] \right\} \\ &= \left\{ [Y_{II}] - [Y_{IE}] [Y_E]^{-1} [Y_{EI}] \right\} [V_I] \end{aligned} \quad (4.49)$$

Seen from the internal system, equation (4.49) is a Norton equivalent as shown in Figure 4.12 (b). The Norton admittance matrix is

$$Y_{EN} = \left\{ [Y_{II}] - [Y_{IE}] [Y_E]^{-1} [Y_{EI}] \right\} \quad (4.50)$$

The Norton equivalent current vector is

$$I_{EN} = \left\{ [I_{I-external}] - [Y_{IE}] [Y_{EE}]^{-1} [I_E] \right\} \quad (4.51)$$

This current is the one to be injected into the internal system. The current source is

converted into three phase instantaneous values ($i_{EN}(t)$) and interfaced to the EMT model of the internal network which includes the high frequency FDNE equivalent as shown in Figure 4. 12 (c).

To calculate the Norton equivalent current vector, $[I_E]$ should be multiplied by $[Y_{IE}][Y_E]^{-1}$. It should be noted that only when bus k is connected to a generator or a nonlinear load that $I_{Ek} \neq 0$, thus only part of the $[Y_{IE}][Y_E]^{-1}$ needs to be stored and used in the calculation.

At the interface buses, which are interfaces of internal and external systems as shown in Figure 4. 12, the EMT solution of the internal network receives inputs in the form of injected currents from the TSA solution of the external network. Also at these interface buses the TSA solution of the external network receives inputs in the form of injected currents from the EMT solution of the internal network. It should be noticed that the shaded area in Figure 4. 12 is in the phasor domain while the non-shaded area is in the time domain.

A data conversion block as shown in Figure 4. 12 (c) transforms data between EMT instantaneous and TSA phasor domain values. This conversion can be achieved by calculating the RMS value of the voltage[13], discrete Fourier transformation (DFT) [15] or curve fitting techniques[14][16][17]. These approaches work well in the steady status. But, during transients after a fault is cleared, these methods has difficulties getting the correct phasor quantities immediately. At least one cycle of data is needed to produce the correct phasor quantities.

It should be noticed that the major factor affecting electromechanical oscillation is the transfer of energy, i.e. real power. Based on this point a power balance method is employed to implement the conversion block. Besides steady status this method also works well in the transient after faults. The detailed procedure for this method is available in literature [18] and is also briefly described in section 6.2.

Chapter 5: Aggregation of Generating Units

The last step of the coherency-based dynamic technique is aggregating each group of coherent generators and their controls into a single equivalent. As we know from coherent groups, not all generators and their controls (exciters, governors and stabilizers) are of the same type. So how to aggregate all these coherent generators into an equivalent one becomes a problem.

There are several methods to do this. Basically, these methods can be divided into two categories. The first one uses nonlinear optimization methods. It can provide satisfactory results and handle different types of generators and controls. The disadvantage is that, computationally, it is a time consuming process. This optimization based technique is introduced in section 5.1.

The second method is referred to as the direct aggregation technique which does not require nonlinear optimization. This method assumes that all coherent machines have identical structures. Since there is no time consuming optimization process, it is faster than optimization based techniques. As each machine in the coherent group is assumed to have the same type of control structure, this method produces satisfactory results with the same quality as produced by optimization based methods. The disadvantage is that it can only deal with generators having identical control structures. If the coherent group contains different types of generators and controls, it has to be divided into sub groups in order that each sub group is made up with the same type structure. This direct technique is introduced in section 5.2.

5.1 Optimization Based Aggregation Techniques

In these techniques, a suitable objective function is used that captures the behaviors of the system. This objective function is a measure of the mismatch between the reduced model and the detailed model.

The general idea of these techniques is the construction of a target function built from variables in the full and reduced models. Then a nonlinear optimization technique is used to find the equivalent parameters of the reduced model by obtaining the minimum of the

target function. This process can be done either in the frequency or time domain. These techniques are introduced below.

5.1.1 Frequency Domain Optimization

This method is used in the software package DYNRED [29]. The assumptions are made that the coherent generating units are on a common bus, with the same terminal voltage \bar{V}_T , and have the same speed ω .

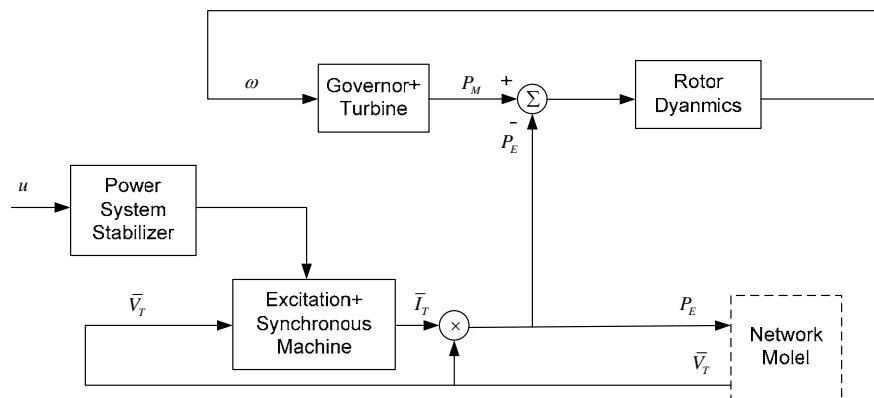


Figure 5. 1 Generating Unit Model

The block diagram of Figure 5. 1 represents the functional relations between the mechanical and electrical output of an individual generating unit with its speed ω and terminal voltage \bar{V}_T being considered as input variables.

An identical structure as in Figure 5. 1 is assumed for the model of the equivalent generating unit, with the equivalent mechanical power replaced by the total mechanical power and the equivalent electrical power by the total electrical power output for a group.

The objective of the method is to specify the parameters of this equivalent model given the model of each individual unit. This will be done by considering separately the rotor dynamics, the governor and turbine model, the synchronous machine model, the excitation system model and the power system stabilizer model.

The assumption is now made that the linear and nonlinear characteristics of the equivalent models can be identified separately as shown below.

The linear parameters of the equivalent model are numerically adjusted to obtain a minimal error between its transfer function and the weighted sum of the transfer functions of the individual units. The error to be minimized is the sum of the squares of the magnitude of the relative difference, for specified discrete frequencies.

For example, by taking into account each individual synchronous machine's contribution to the equivalent excitation system, the transfer function of the equivalent exciter can be expressed as

$$G_E(s) = \frac{\Delta e_{FD}}{\Delta V_T} = \sum W_j(s) \cdot G_{Ej}(s) \quad (5.1)$$

$G_E(s)$ is the summation of the weighted transfer function of the individual exciter gains. $G_{Ej}(s)$ is the individual exciter gain. The term $W_j(s)$ is a “weighting-factor” [29] which is proportional to the MVA rating of the machine [54]. The resulting block diagram of the equivalent exciter is shown in Figure 5. 2.

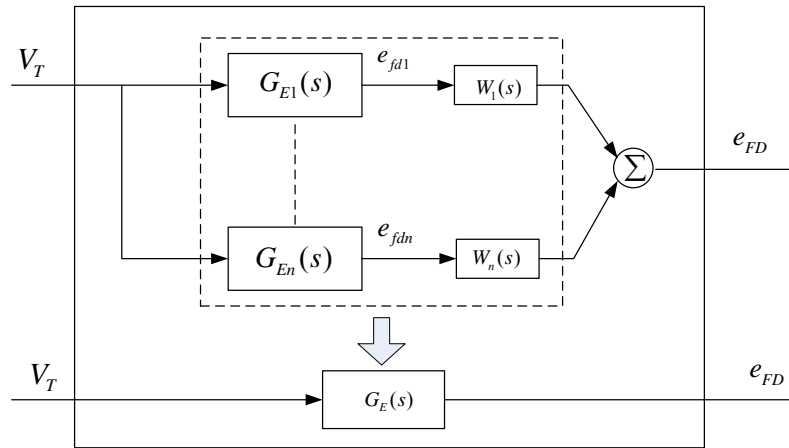


Figure 5. 2 Resultant Exciter by Weighting Individual Exciters

In the above method the resultant exciter transfer function is of a very large order (typically equal to $n \cdot m$ assuming n exciters of order m each). For practical reasons, it is convenient to represent the above sum in (5. 1) as a fitted lower order exciter model (such as the simplified IEEE type 1 excitation system), as shown in Figure 5. 3. The

procedure for doing this is shown next.

For discrete complex frequencies $j\omega_i$, the weighted transfer function $W_j(s) \cdot G_{Ej}(s)$ of the individual exciter is calculated and summed-up. The term of this summation is defined as $G_E(s)$ shown in (5. 1). Typical values are assigned to the unknown parameters of the equivalent exciter (such as the simplified IEEE type 1 excitation system shown in Figure 5. 3) and the equivalent transfer function $G_{IEEE1}^*(j\omega_i)$ is calculated.

The target function $\sum_i \frac{|G_{IEEE1}^*(j\omega_i) - G_E(j\omega_i)|^2}{|G_E(j\omega_i)|^2}$ is calculated. Then a nonlinear

optimization method is used to correct the unknown parameters in order to obtain the minimal of the target function. Using this method, the linear equivalent exciter parameters K_E^*, T_E^* shown in Figure 5. 3 can be obtained. The additional parameters S_{EMAX}^* and V_{RMAX}^* represent the contribution of nonlinear effects – the saturation of core and the limit of the exciter. In this thesis the Matlab function (lsqnonlin) [55] was used to achieve this.

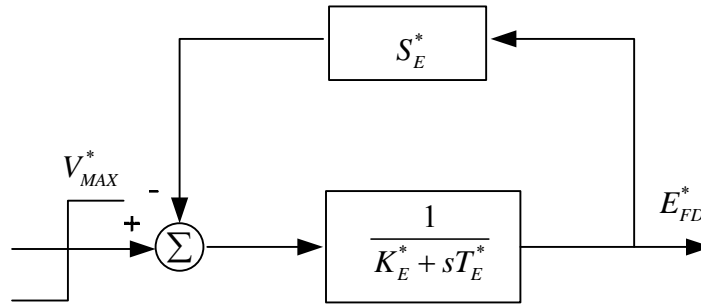


Figure 5. 3 Simplified Equivalent Exciter Model

Although the above method gives the equivalent exciter parameters K_E^* and T_E^* , which are based on the linear model, it still does not provide equivalent values for the non-linear parameters such as limits S_{EMAX}^* and V_{RMAX}^* . Assuming the same structure for the equivalent model as in Figure 5. 3, the equivalent regulator limit V_{RMAX}^* is

calculated assuming a step input equal to the regulator limit is applied simultaneously to each exciter system. It is shown in Figure 5. 4.

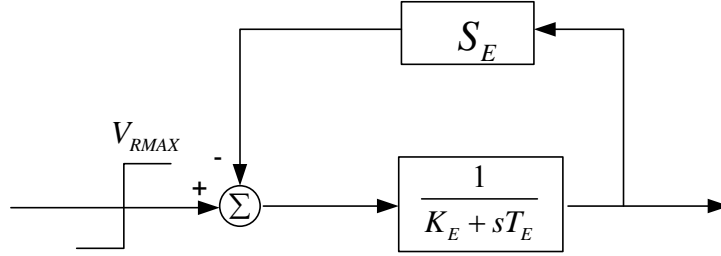


Figure 5. 4 Simplified exciter model for large step input

For such a step input, the output is

$$e_{FD}(s) = \frac{1}{s} \sum_j \left(\frac{V_{RMAXj} / (K_{Ej} + S_{Ej})}{1 + sT_{Ej} / (K_{Ej} + S_{Ej})} \right) \cdot W_j(s) \quad (5. 2)$$

Using the initial value theorem

$$\lim_{t \rightarrow 0^+} \frac{de_{FD}}{dt} = \sum_j \frac{V_{RMAXj}}{T_{Ej}} \cdot W_j(s = \infty) \quad (5. 3)$$

For the equivalent model in Figure 5. 3, a step input V_{RMAX}^* should produce an output V_{RMAX}^* / T_E^* . Equating V_{RMAX}^* / T_E^* with (5. 3) and noting that the parameter T_E^* is already known from fitting the linear transfer function, this gives

$$V_{RMAX}^* = T_E^* \left(\sum_j \frac{V_{RMAXj}}{T_{Ej}} \cdot W_j(s = \infty) \right) \quad (5. 4)$$

Using the final value theorem the E_{FDMAX}^* can be determined in (5. 5).

$$\lim_{t \rightarrow \infty} e_{FD}(t) = \sum_j \frac{V_{RMAXj}}{K_{Ej} + S_{EMAXj}} \cdot W_j(0) = E_{FDMAX}^* \quad (5. 5)$$

For the equivalent model there should be the same limit structure

$$\frac{V_{RMAX}^*}{K_E^* + S_{EMAX}^*} = E_{FDMAX}^* \quad (5.6)$$

Since V_{RMAX}^* , E_{FDMAX}^* and K_E^* are already known from (5.6) the S_{EMAX}^* can be determined. This completes the equivalent exciter transfer function.

5.1.2 Time Domain Optimization [54][56]

The method in this section is more complicated, and was not used in the thesis. This section is presented as background information only.

An alternative method to the frequency domain equivalent method of the previous section is the time domain optimization. As shown in Figure 5.5, the equivalent parameters are determined at the minimum of the target function using certain nonlinear optimization techniques. The target function must be properly selected, which penalizes any essential difference in the behavior of the full and reduced models.

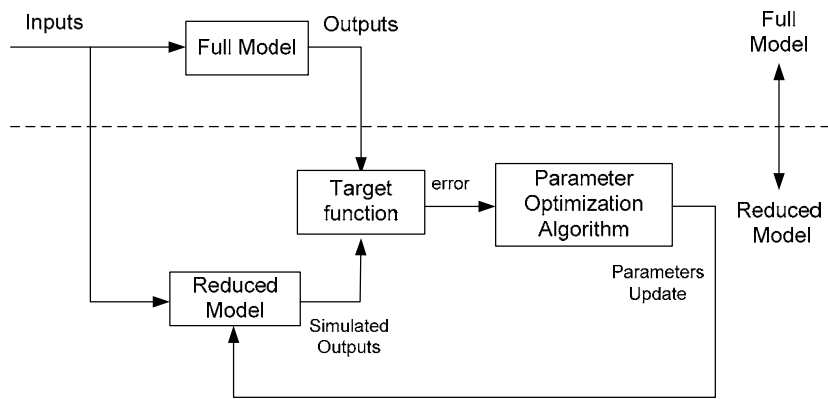


Figure 5.5 Time Domain Simulation Method

The above technique is used to get the equivalent model parameters in [54][56]. As shown in Figure 5.6, the full model of the coherent area is replaced with a reduced model. A nonlinear optimization technique is used to tune the parameters of the equivalent model parameters in order to make the boundary quantities of the full and reduced models, such as $I_1 \dots I_k$, $V_{b1} \dots V_{bk}$ etc, as close as possible.

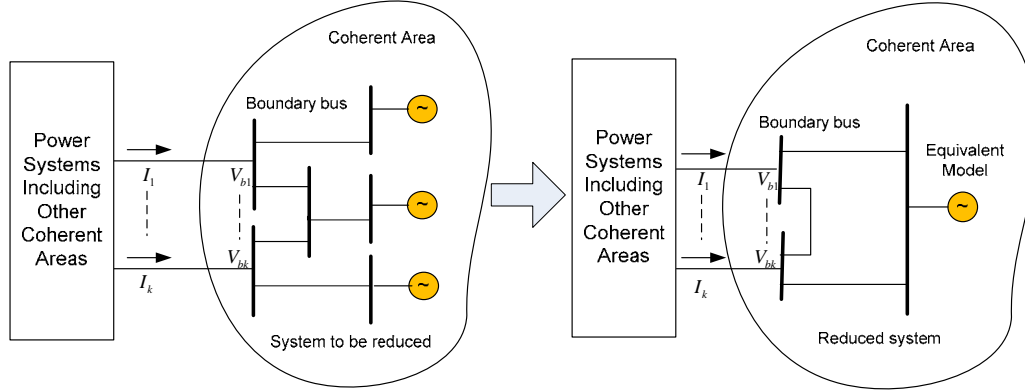


Figure 5.6 Coherent Area Input-Output Model

The following is an illustration of this technique showing how to get the equivalent exciter parameters [54].

A nonlinear input-output model for a coherent area i can be expressed as

$$\dot{x}_i = f_i(x_i, V_i, I_i) \quad (5.7)$$

$$0 = g_i(x_i, V_i, I_i) \quad (5.8)$$

The state vector x_i contains the entire generator and exciter state variables.

The current injection vector I_i

$$I_i = [I_1 \quad I_2 \quad \dots \quad I_k]^T \quad (5.9)$$

is the input, and the boundary bus voltage vector V_{bi}

$$V_{bi} = [V_{b1} \quad V_{b2} \quad \dots \quad V_{bk}]^T \quad (5.10)$$

which is a sub-vector of the entire system bus voltage vector V_i , is the model output.

The nonlinear vector function f_i represents the dynamics of the generators and exciters present in the area i . The network equations are represented by the vector of the nonlinear function g_i . Disturbances applied in the study area will affect the current injections I_i , which will perturb the coherent area from its equilibrium condition. The resulting boundary bus voltages will then affect the power flows between the coherent

area and the rest of the system, which will lead to further variations in I_i .

The exciter aggregation problem is formulated as follows. A typical exciter topology is assumed for the equivalent aggregate exciters; for example, the topology shown in Figure 5. 3. The parameters of this exciter are somewhat arbitrarily selected. For example, they may be the parameters of the highest MVA rating generator's exciter (The optimization process modifies these starting values to arrive at the final values to be used in equivalent). The resultant reduced system equations with the aggregate exciter connected to the aggregate generator are now as in (5. 11) and (5. 12).

$$\dot{x}_{ri} = f_{ri}(x_{ri}, V_{ri}, I_i, \alpha_i) \quad (5. 11)$$

$$0 = g_{ri}(x_{ri}, V_{ri}, I_i) \quad (5. 12)$$

where the state vector x_{ri} has a smaller dimension than that of x_i , and the bus voltage vector V_{ri} could have a dimension that is different from that of V_i . However, the dimensions of the current injection vector and the boundary bus voltage vector remain unchanged. The excitation parameters are contained in the vector α_i . The objective of the exciter aggregation problem is to tune α_i so that the error between boundary bus voltages V_{rbi} of the reduced model (5. 11) , (5. 12) and the same boundary bus voltages V_{bi} of the full model (5. 7), (5. 8) for a selected set of disturbances in the study area is as small as possible. This is achieved by minimizing the objective function $\sum_i (V_{rbi} - V_{bi})^2$ using a suitable nonlinear optimization method.

The method reported as an alternative only optimizes the exciter parameters. In reality even the MVA averaged generator model could have been made for part of the optimization. However, as the machine structures in coherent area are similar, this is not seen to be necessary.

Sometimes a simple MVA-averaged procedure is also used for equivalent exciters if an optimization program is unavailable. The time domain optimization method and a MVA-weighted method for exciter equivalents are compared to obtain the exciter parameters [54] shown in Figure 5. 7. It is concluded that the most important parameter is

the regulator gain K_A . The results show that the MVA based method provides close to optimal K_A . Thus it may not be always necessary to use optimization method to obtain the equivalent parameters.

This method is considerably complex. The purpose of the thesis was to develop an equivalent method that was accurate when viewed from the internal system terminals, and this level of detail was thought to be not necessary. Later testing of the equivalent confirmed this idea. Time domain fitting may be more relevant when the aim is to have a reduced order system model for TSA model, which is not the objective here.

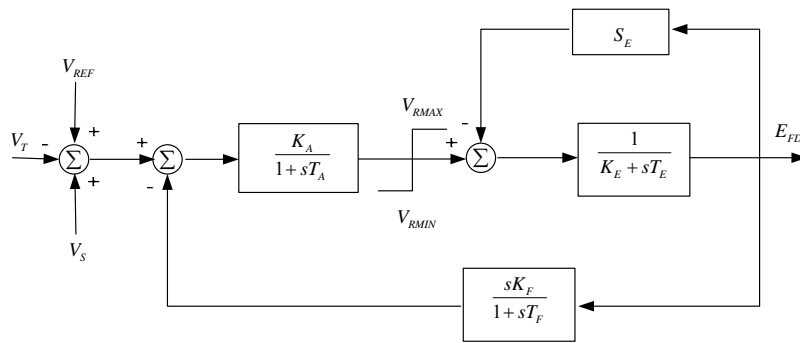


Figure 5.7 IEEE Type1 Excitation System Model

5.2 Direct Aggregation Techniques

As mentioned in the beginning of Chapter 5, there are basically two categories for generating unit aggregation. The first one is the nonlinear optimization based technique introduced in section 5.1. The second one can be referred to as the direct aggregation technique which is discussed in this section.

The method of synchronic modal equivalencing (SME), structure preservation and logarithmic average can be classified as direct aggregation techniques. They are generally simpler than the optimization techniques of the previous section. However they are more suited when all machines have identical controller structures, and hence were considered too simplistic for the current power system network. They are described here as background information.

5.2.1 Synchronic Modal Equivalencing Approach

This approach is used for detailed model aggregation of generators. Using small signal analysis, the generator with the greatest participation factor in the inter-area modes is represented as the reference generator and the remaining generators in the coherent group are simply replaced by injected currents [57][58]. It is shown in Figure 5. 8.

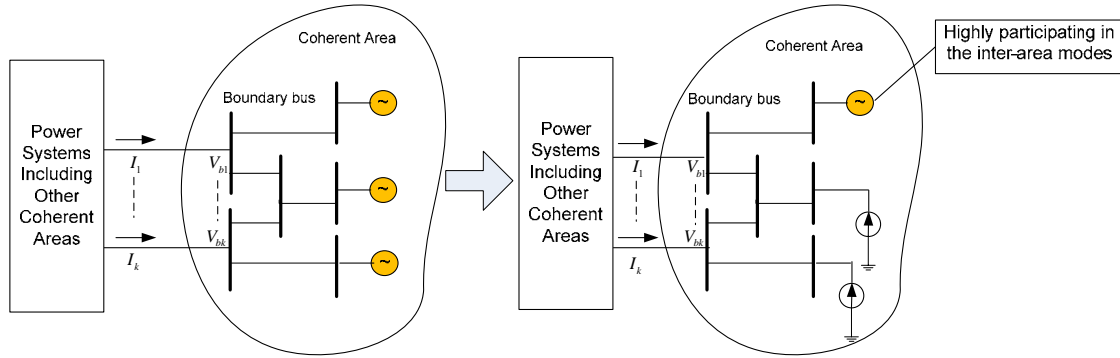


Figure 5. 8 Scheme of Synchronic Modal Equivalencing Approach

The reference generator is the one which highly participates in the inter-area modes. That means the reference generator has higher effects on the inter area than the non-reference generators. So the reference generator is kept in a detailed model. The dynamics of the remaining external area non-reference generators are replaced by purely algebraic equations and represented by controlled current injections.

5.2.2 Structure Preservation Algorithm

A structure preservation algorithm was developed in [59] and improved in [60]. It is based on the structure preservation of the coefficient matrices in the time domain representation of synchronous machines. The parameters of the aggregated model are obtained by the application of the principle of linear aggregation in time domain.

Additional details of this approach are available in [59] [60].

5.2.3 The Logarithmic Average Method

In the DYNEQ program the method of logarithmic average [21] is used. As with other direct aggregation techniques this method only handles the same type of generator

control.

This method replaces many similar dynamic elements with one “log average” element of the same structure. Within each coherent group of generating units, the individual machines are aggregated to form an equivalent machine; individual excitation systems are aggregated to form an equivalent excitation system, and individual governors are aggregated to form an equivalent governor. The coherency-based network reduction places all machines in each coherent group at each equivalent bus.

5.2.4 Aggregation Method for the Generator and Its Controls in the Proposed Work

As mentioned in section 3.8.1 and 3.8.2 there are several approaches to aggregate the generating units. The “direct method” [21][57]-[60] preserves the structure of the state matrices of the generator and its control. The approach assumes the same structure for the controllers of each machine, and aggregates these using a weighted average based on each machine’s MVA or some other simple averaging approach. Although this is extremely straightforward, it does not allow variable control structures in the aggregate machines.

In the practice of the power systems, the above assumption of similar structures in the coherent group is generally valid for the generators. So in the research a direct technique is used to aggregate the generators, i.e., the generator structures are assumed to be identical, which is the fact in practice. However, for the same kind of generator different kinds of controls could be used. Hence an optimization based method is employed in the proposed work to develop the equivalent controller described in section 5.1.1 earlier.

5.2.4.1 Aggregation of the Coherent Machines

The result of the machine aggregation is an equivalent machine with parameters representative of the individual machines in the coherent group. The procedure is outlined below.

The rating of the equivalent generator is taken to be the sum of the ratings of the individual generators being aggregated. It can be expressed as (5. 13)

$$MVA_e = \sum MVA_i \quad (5.13)$$

The inertia of the equivalent generator is assumed to be the sum weighed by the individual rating the coherent generators being aggregated shown as (5.14).

$$H_e = \frac{\sum H_i MVA_i}{MVA_e} \quad (5.14)$$

During the aggregation, all machine parameters must be expressed on a common MVA base. Coherent generators are assumed to have identical terminal voltages. Therefore, they can be relocated at a single equivalent bus; the magnitude and angle of the equivalent bus are chosen as the averages of the individual coherent generators.

Resistances and reactance are added in parallel. Equivalent time constants are found by taking the log average of the corresponding time constants. The equivalent saturation is found by taking the log average of the saturation factors.

In this research, the IEEE type of generator structure [11] is assumed for the aggregating generators.

5.2.4.2 Aggregation of the Controllers with the method of 5.1.1

Although the optimization based procedure is slower than the direct methods, this is not a major concern for the proposed work, because it can be conducted off-line. Once the aggregate controls and machine are determined, they are downloaded into the real-time equivalent model for conducting real-time simulations.

The approach used in this paper was originally proposed in [28] and described in section 5.1.1. In the proposed work a similar idea is used but with simplified procedures. The general idea is that a non-linear optimization algorithm is used to determine the equivalent controllers. It can aggregate different controller types. In this approach, an aggregate frequency response characteristic is created by doing a weighted MVA average of the individual controller frequency response characteristics. The frequency range of interest is typically 0.01 Hz to 5 or 10 Hz. Assuming a certain structure for the equivalent controller, parameters for this structure are selected that result in a frequency response characteristic that best fits the above aggregated characteristic. This is done using a non-linear optimization formulation. In this work, the Matlab nonlinear

least-squares solver (lsqnonlin) is used, and the objective function that is minimized (optimized) is the sum of squares of the fitting error at different frequency points.

The implemented procedure does not consider controller non-linearities such as limits. However, many of the limits in the individual controllers are based on maximum power ratings, etc., and can be added into the equivalent by summing individual ratings. Internal limits (e.g. integrator maxima, etc.) cannot be aggregated. Typical values are selected based on the type of equivalent controller structure selected.

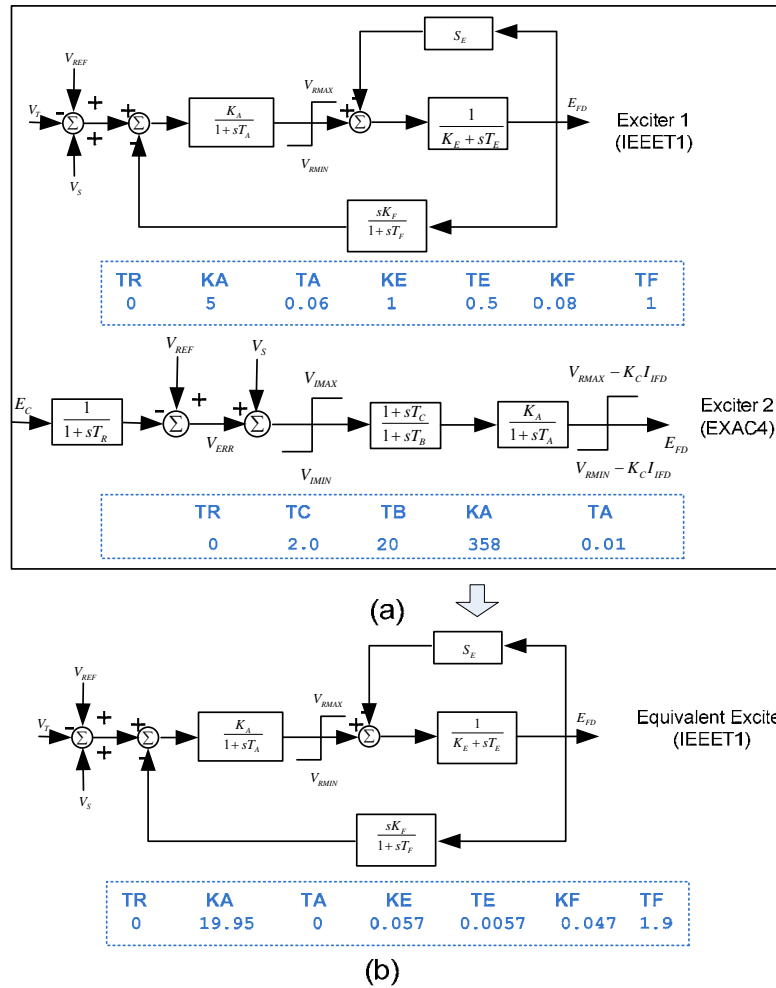


Figure 5.9 Aggregation of the Exciters

The approach can be demonstrated by an example of aggregating two different types of exciter structures shown in Figure 5. 9 (a), namely, the IEEE T1 and EXAC4 [11] exciters. The parameters for the two are also in the figure. Figure 5. 9 (b) shows the

equivalent exciter and its parameters assuming an IEEE-T1 structure. The frequency response plots (magnitude and phase) of the aggregate characteristic and the equivalent controller are shown in Figure 5. 10 and indicate a good agreement.

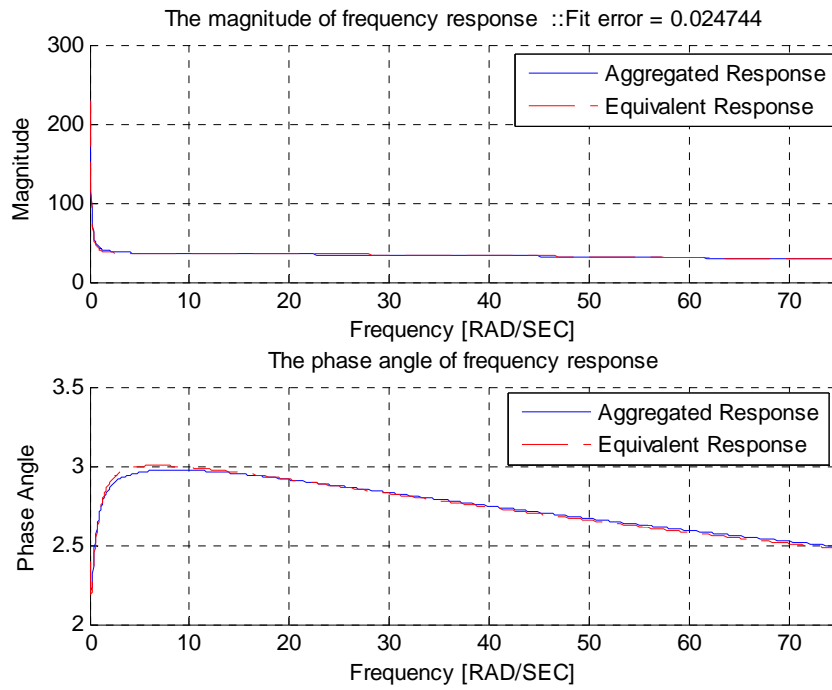


Figure 5. 10 Aggregated and Equivalent Frequency Response

Chapter 6: Implementation Structure of the proposed Equivalent

As discussed in the Chapter 1 Lin et al [18] developed an equivalent in which the high frequency behavior is represented by a FDNE and the low frequency behavior is represented by a full TSA model. The FDNE considerably reduced the size of the real-time EMT model. The TSA block, however, was still modeled in full and not as an equivalent, resulting in a very large model for the electromechanical part of the simulation. Although this approach reduced the computational hardware required for simulating a large system significantly, it was still impractical to model large systems with thousands of buses.

The discussion of the previous chapter shows that it is possible to make an equivalent even for the TSA part. The low frequency dynamic characteristics are represented by a reduced equivalent TSA solution block, in which the external network is modeled by equivalent generators derived from a coherency based analysis. This approach further reduces the size of the modeled network in comparison to the earlier “two-part equivalent” approach of Lin et al [18]. This block interfaces to the EMT solution through a controlled current source, in a manner similar to that in [18]. This chapter describes the implementation of this scheme.

6.1 Schematic Structure of the Proposed Equivalent

The schematic structure in this work is similar as [18] and shown in Figure 6. 1. The system consists of a detailed model for the internal system and an equivalent model for the external system. The FDNE is actually an equivalent impedance placed inside the internal system and represents the high frequency behavior of the external system. The blocks included in the dotted box are the reduced TSA model of the external system obtained after coherency-based reduction.

The schematic blocks are described below.

Block “A” measures the injection currents from the detailed RTDS model (internal system modeled with the EMT full model) to the external system, and converts them

from three phase instantaneous values to fundamental frequency positive sequence phasor values.

The phasor signals are sent to the reduced TSA network solution block “B”. This block implements the coherency based reduced model of the original network as a TSA model. The terminal voltages (phasor values) of the generators (including both individual and equivalent generators) in the external system are calculated.

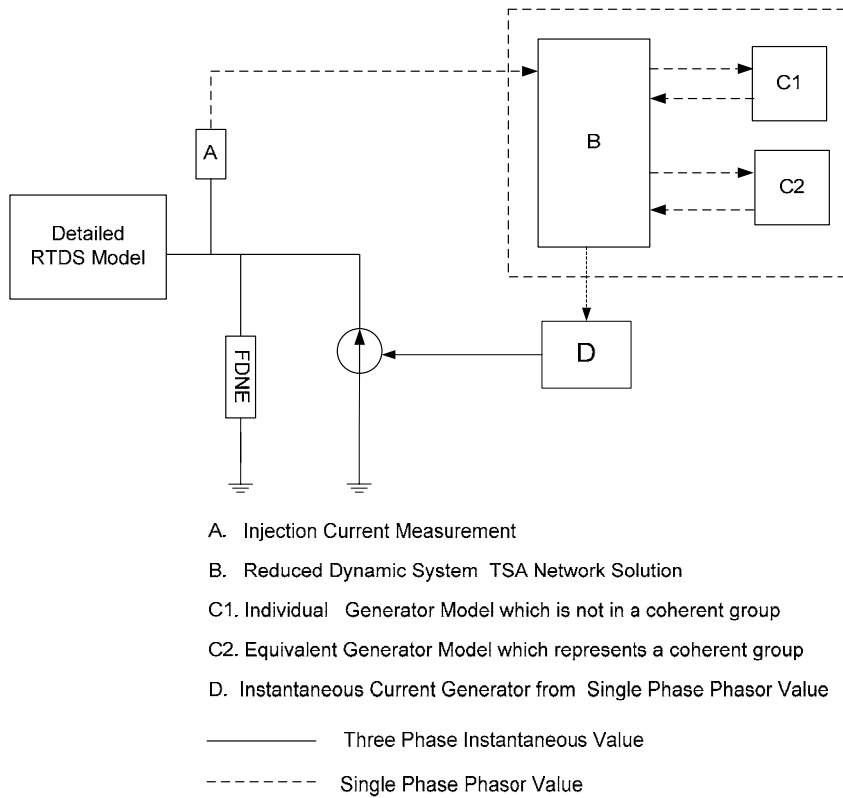


Figure 6.1 General Structure of the Equivalent Scheme

When the coherency procedure is applied, some generators cannot be aggregated to any coherent group, or alternatives, we can say they form a coherent group of one machine. Block “C1” represents the generators which are not in any coherent groups and are thus not aggregated. Block “C2” represents generators which are in coherent groups and needed to be modeled as an aggregation. Both generator models (individual and equivalent) use the terminal voltages as the inputs of their state equation solvers, and

calculate the currents (phasor values) that they inject into the external network.

The current injections of the generators and other dynamic or nonlinear equipment in the external system block “D” are used to calculate the equivalent current (phasor value) as seen from the interface bus, and to generate the signals to control the three phase current source. The three phase current source reproduces the electromechanical dynamic response of the external system.

The signal flow of the proposed scheme is shown in Figure 6. 2. It can be seen that in the conversion block, the internal system instantaneous currents from EMT solution are converted to phasor values. The method is described in a later section. Then these phasor values are used for obtaining the controlled currents which represent the low frequency dynamics of the external system. Finally these controlled currents are converted back to instantaneous values and used in the EMT simulation in the RTDS platform.

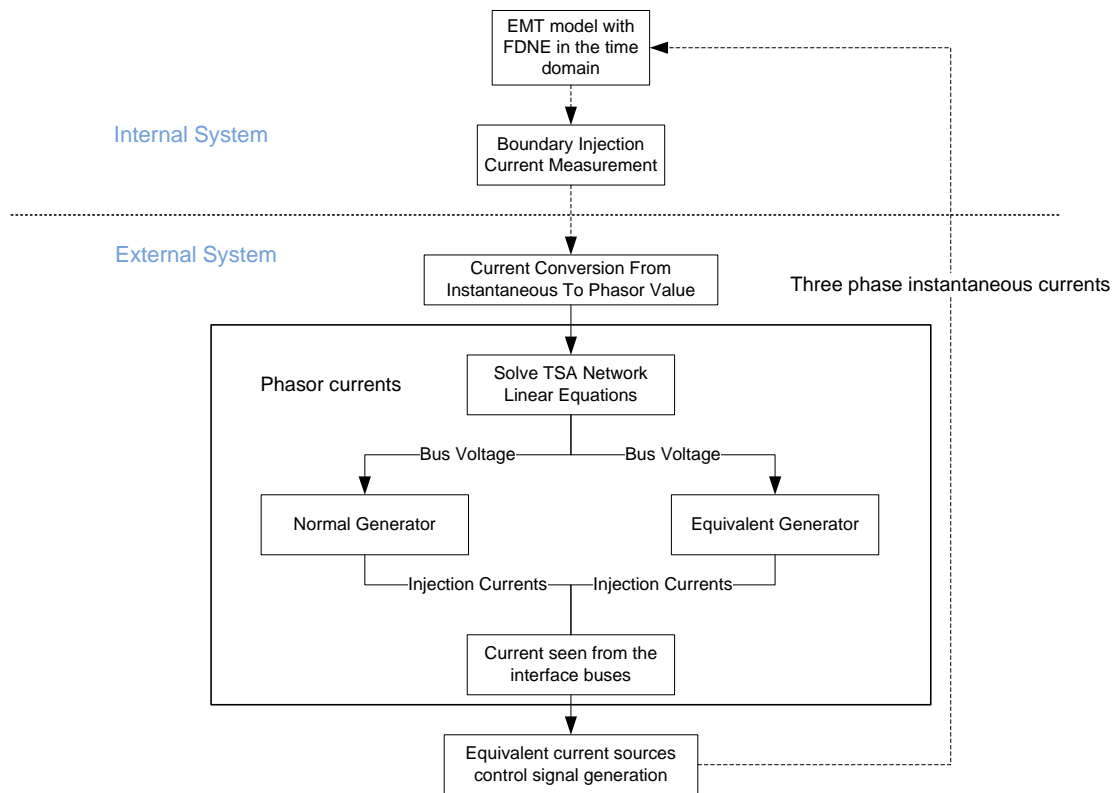


Figure 6. 2 Signal Flow of the Proposed Scheme

The proposed scheme is implemented on the RTDS by using standard RTDS control components and the “user defined component” (UDC), facilities available in RTDS [8]. This facility permits RTDS users to build their own components according to their personal needs. The blocks in Figure 6. 2 can be individually constructed as user defined control models in the RTDS.

6.2 Boundary Data Conversion

Fundamental frequency phasor voltages and currents are needed in a reduced TSA type solution for the external system. In the EMT type solution of the internal system, all the currents and voltages vary continuously with time. Thus the conversion between these two kinds of quantities becomes an important task. This technique presented below was originally introduced by Lin et al [18] and is briefly presented here for completeness.

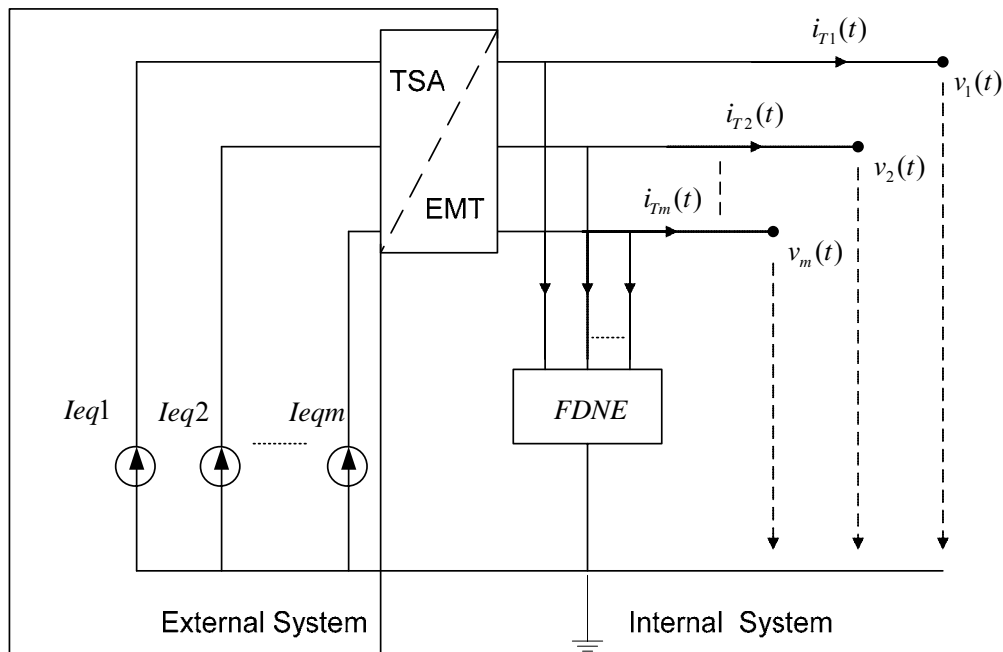


Figure 6. 3 Multi-port Norton Equivalent Circuit

It is assumed that the external system which has m ports as in Figure 6. 3. In this research it is represented by a multi-port frequency dependent network equivalent (FDNE) and multiple equivalent current sources which are generated by the coherency-based TSA

solution (phasor domain) and then converted to time domain (instantaneous value).

For the first FDNE part, the frequency domain admittance response of the external system is acquired and a rational function is found in the s-domain using the vector fitting technique. This technique ensures that the frequency domain response of the fitted function is close to the frequency domain response of the external system. Finally, the s-domain admittance is readily converted into the standard Norton equivalent representation common in most EMT programs, which consists of a fixed conductance in parallel with a history current source [10]. The FDNE part does not take the current generated by the external system generators into account. These are handled by the reduced TSA part, which generates phasor domain values for the injected currents. To interface these phasor domain values to the time domain simulation of the EMT solution, these values must be converted to their instantaneous values as in Figure 6. 3.

Also an appropriate process is required to represent the instantaneous internal system quantities in the phasor domain for use by the TSA solution. Extracting the fundamental phasor quantities from the time domain instantaneous waveform using a method such as discrete Fourier transformation (DFT) is a way doing this. This works well in the steady state. However, during transients such as fault clearing, this method has difficulties getting the correct phasor quantities immediately. The DFT method requires at least one cycle of data to produce the correct phasor quantities. After a fault is cleared, the bus voltages in an EMT simulation immediately recover to near normal values. But the DFT cannot immediately produce the correct phasor value since it takes about one cycle for the phasor representation to its normal value.

It should be noted that the major factor affecting electromechanical oscillation is the transfer of energy, i.e. real power. In the TSA solution, all of the voltages and currents are assumed to be at the fundamental frequency, purely sinusoidal, and perfectly balanced. Similarly, the network is only represented by the fundamental frequency positive sequence parameters. During transients, especially large transients, many other frequency components arise including zero sequence and negative sequence components. Such “non-standard” components may transfer real power and hence can affect the oscillations of the generators in the external system. Thus, if the conversion only aims to extract the

‘accurate’ fundamental frequency positive sequence magnitude and phase angle of the injection currents and to apply them to a positive sequence fundamental frequency external system model, it cannot correctly represent how the internal system affects the electromechanical transients of the external system. Instead the objective of the conversion should be to find the phasor values of the injection currents which results in the same amount of real power transfer at the internal and external system interface as it is real power that affects the rotor accelerations.

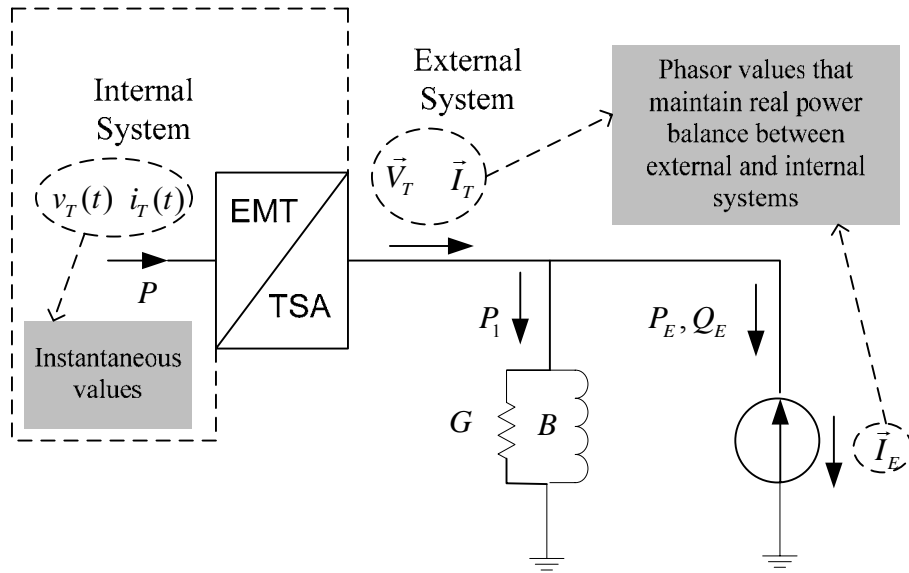


Figure 6.4 Instantaneous and phasor value conversion

Figure 6. 4 shows the conversion mechanism as seen at the fundamental frequency and positive sequence. The positive sequence values $G + jB$ of the FDNE $Y(\omega)$ at fundamental frequency are known as:

$$\begin{aligned} G &= \text{Re}(Y(\omega_f)) \\ B &= \text{Im}(Y(\omega_f)) \end{aligned} \tag{6.1}$$

where ω_f is the fundamental frequency.

\vec{I}_E is the phasor current $[I_{eq1}, I_{eq2}, \dots, I_{eqm}]$ from Figure 6. 3 which is computed in the reduced TSA solution. Then it is converted to instantaneous current form

$(i_{Ea}(t), i_{Eb}(t), i_{Ec}(t))$ and injected into the internal system at the border. The implement details are listed in Figure 6. 5.

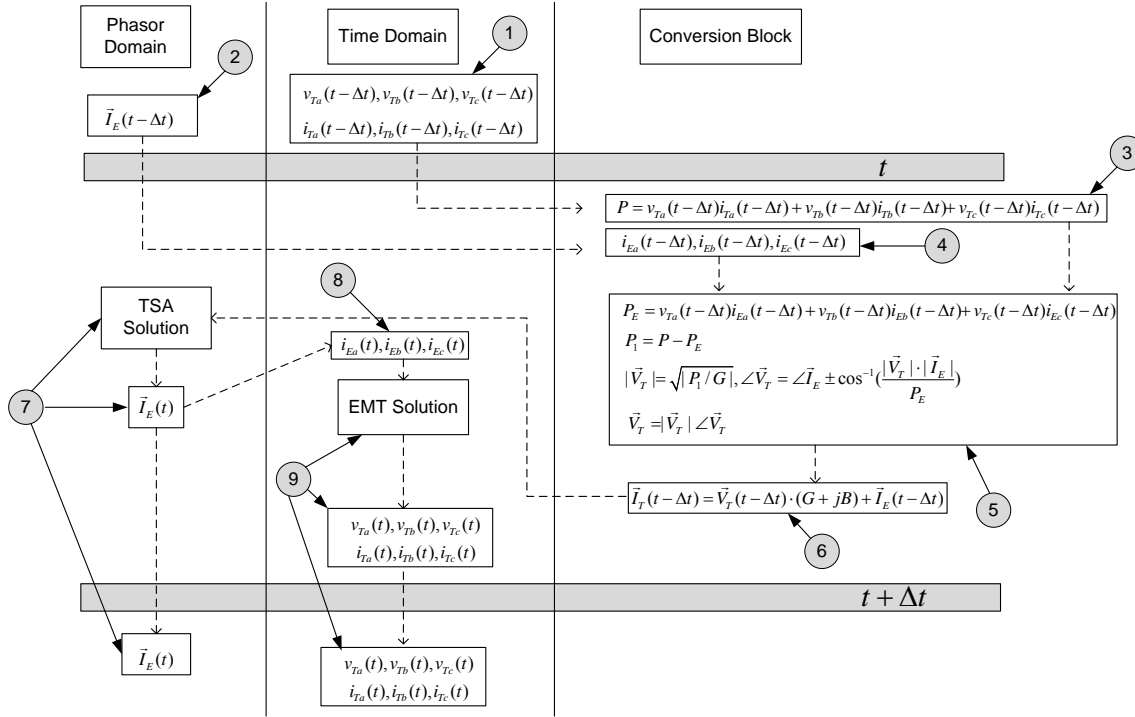


Figure 6.5 Implementation of the EMT/TSA conversion

For the TSA solution, we need to know the phasor values of the terminal (boundary bus) voltages and currents \vec{V}_T and \vec{I}_T . Their phasor values are unknown and need to be calculated and used as the inputs to the reduced TSA solution block. The instantaneous terminal voltages $v_T(t-\Delta t) = [v_{Ta}(t-\Delta t), v_{Tb}(t-\Delta t), v_{Tc}(t-\Delta t)]$ and current $i_T(t-\Delta t) = [i_{Ta}(t-\Delta t), i_{Tb}(t-\Delta t), i_{Tc}(t-\Delta t)]$ are known from the previous time-step $(t-\Delta t)$ of the EMT solution for the internal system shown in step ① of Figure 6. 5. The phasor value ($\vec{I}_E(t-\Delta t)$, step ② in Figure 6. 5) of the controlled three-phase current source is calculated in the TSA program with a relatively small time-step (equal to or smaller than 2 ms), and even its value is actually calculated in the previous time-step, it can be considered to be the same in the present time-step. The instantaneous values of the corresponding three-phase currents $(i_{Ea}(t), i_{Eb}(t), i_{Ec}(t))$ are thus calculated by expressing

the phasor values in time domain form shown as step ④.

In order to calculate \vec{V}_T , the instantaneous three phase real power P and P_E are calculated using (6. 2) and shown in step ③ of Figure 6. 5 , which is valid during both the steady state and the transient state:

$$P = v_{Ta}(t - \Delta t)i_{Ta}(t - \Delta t) + v_{Tb}(t - \Delta t)i_{Tb}(t - \Delta t) + v_{Tc}(t - \Delta t)i_{Tc}(t - \Delta t) \quad (6. 2)$$

$$P_E = v_{Ta}(t - \Delta t)i_{Ea}(t - \Delta t) + v_{Tb}(t - \Delta t)i_{Eb}(t - \Delta t) + v_{Tc}(t - \Delta t)i_{Ec}(t - \Delta t) \quad (6. 3)$$

P is the real power which flows into the external system. P_E is the real power which flows through the controlled current source. P_1 is the real power which flows through the FDNE. In order to obtain a solution which maintains real power balance on either side of the TSA/EMT interface, the following condition must be satisfied:

$$P_1 = P - P_E \quad (6. 4)$$

The magnitude of \vec{V}_T can be derived from P_1

$$|V_T| = \sqrt{|P_1 / G|} \quad (6. 5)$$

Since \vec{I}_E is known, the relative angle between \vec{V}_T and \vec{I}_E can be derived from P_E ,

$$|\angle \vec{V}_T - \angle \vec{I}_E| = \cos^{-1} \left(\frac{|\vec{V}_T| \cdot |\vec{I}_E|}{P_E} \right) \quad (6. 6)$$

Equation (6. 6) does not show in which quadrant \vec{V}_T lies with \vec{I}_E as the reference. This can be derived from the knowledge of the sign of Q_E , which is the reactive power flowing through the controlled current source. The three phase reactive power equation in steady states is:

$$Q_E(t - \Delta t) = \frac{1}{\sqrt{3}} \left[\begin{array}{l} v_{Ta}(t - \Delta t)(i_{Eb}(t - \Delta t) - i_{Ec}(t - \Delta t)) + \\ v_{Tb}(t - \Delta t)(i_{Ec}(t - \Delta t) - i_{Ea}(t - \Delta t)) + \\ v_{Tc}(t - \Delta t)(i_{Ea}(t - \Delta t) - i_{Eb}(t - \Delta t)) \end{array} \right] \quad (6. 7)$$

This equation is not accurate during transients. But this is not critical since only the

sign of Q_E is needed for determining the quadrant of \vec{V}_T . Equations (6. 4)-(6. 7) are implemented in the step ⑤ of Figure 6. 5.

Now $\vec{I}_E(t-\Delta t)$ is known, $\vec{V}_T(t-\Delta t)$ can be finally derived and hence $\vec{I}_T(t-\Delta t)$ can be calculated (step ⑥ in Figure 6. 5).

$$\vec{I}_T(t-\Delta t) = \vec{V}_T(t-\Delta t) \cdot (G + jB) + \vec{I}_E(t-\Delta t) \quad (6. 8)$$

These quantities $\vec{V}_T(t-\Delta t)$ and $\vec{I}_T(t-\Delta t)$ ensure real power balance, because (6. 4) was used in their derivation. Hence rotor acceleration calculated in TSA program will also include real power injection from harmonic frequency components of $v_T(t-\Delta t)$ and $i_T(t-\Delta t)$.

The calculated $\vec{I}_T(t-\Delta t)$ is fed into the reduced TSA solution (described in section 6.3) so that the new phasor value of the external system current injection $\vec{I}_E(t)$ can be calculated. Then $\vec{I}_E(t)$ is converted into the time domain form and fed into the EMT solution to get the $v_T(t)$ and $i_T(t)$ for the subsequent timestep shown in step ⑦-⑨ in Figure 6. 5.

For multi-port cases, a similar process is used; the only difference is that the matrix form of (6. 8) is applied. This method is very simple, but as can be seen in the next chapter, it works well during the unbalanced faults and other distorted waveform conditions.

6.3 TSA Solution

Once \vec{I}_T (which is the phasor value of the currents injected from the internal system) is determined as described in the previous section, it can be used as the input to the TSA network solution block. It is assumed that the TSA network has been reduced using the coherency based equivalencing approach described in section 4.5.

The TSA network solution block uses the following linear equation [12] to determine the unknown voltages V . It is assumed that current injections are known.

$$Y \cdot V = I \quad (6.9)$$

In (6.9), Y is the admittance matrix of the external system. I is the injection current vector, which is the input of the block. V is the bus voltage vector of the external system, which is to be solved and outputted. Matrix Y and the V and I vectors are all complex (phasor).

Since the external equivalent is developed on the assumption of an unchanging network, the Y matrix is constant. This fact greatly simplifies the solution process and makes it very fast. The straight forward way of solving (6.9) is to inverse matrix Y

$$V = Y^{-1} \cdot I = Z \cdot I \quad (6.10)$$

Where Z is the impedance matrix of the external system, and it is also constant. Consequently, the inversion can be done off-line and only the Z matrix is stored and used in the RTDS simulation. The inversion process therefore does not contribute to the CPU time of the real time algorithm.

For a power system, Y is a very sparse matrix, while Z is a full matrix. So storing Z is not efficient and the multiplication is very time consuming, which makes (6.10) successfully applicable only to very small systems.

Sparse matrix techniques have been widely employed in power system calculations. In this research, a mature and widely used sparse matrix technique is employed [62].

Using LU factorization, Y matrix can be factorized into four matrix: L, U, P and Q .

$$P \cdot Y \cdot Q = L \cdot U \quad (6.11)$$

L is a unit lower triangular matrix, U is an upper triangular matrix, P is a row permutation matrix, Q is a column reordering matrix. L and U maintain the sparse characteristic of matrix Y .

Equation (6.9) can be rewritten as:

$$P^{-1} \cdot L \cdot U \cdot Q^{-1} \cdot V = I \quad (6.12)$$

Equation (6.12) can be solved in four steps:

$$\overset{*}{I} = P \cdot I \quad (6.13)$$

Equation (6.13) only reorders the injection current vector I .

$$L \cdot T = \overset{*}{I} \quad (6.14)$$

Equation (6.14) can be solved with a forward substitution process. Some of the entries of $\overset{*}{I}$ are nonzero (The nonzero entries of $\overset{*}{I}$ are associated with the buses connected to nonlinear loads, generators and other dynamic equipments). Also, most entries of L are zero. So in the forward substitution process, there are many zero multiply zero or nonzero multiply zero operations, which can be ignored. This can be known beforehand with the knowledge of the sparse structure of L and $\overset{*}{I}$. Thus only a small part of L should be stored and used. This is called ‘Fast Forward Substitution’.

$$U \cdot \overset{*}{V} = T \quad (6.15)$$

$$V = Q \cdot \overset{*}{V} \quad (6.16)$$

As in (6.13), (6.16) is only a reorder process. Equation (6.15) can be solved with a backward substitution process. Only some entries of $\overset{*}{V}$ are of interest (‘target’ entries, those associated with the buses connected to nonlinear loads, generators and other dynamic equipment). Because most entries of U are zero, it is not necessary to calculate the whole $\overset{*}{V}$ vector. Only ‘useful’ entries of $\overset{*}{V}$ are needed to be calculated, i.e. only those entries $\overset{*}{V}_k$ which multiply a non-zero k^{th} column of Q . Only the nonzero entries of U which are associated with these ‘useful’ entries of $\overset{*}{V}$ are used in the calculation. Thus only a small part of U should be stored and used. This is called ‘Fast Backward Substitution’.

Since the Y matrix is constant, the factorization (6.11) is done off-line using a standard function of MATLAB. The UDC code for the process from (6.13) to (6.16) can be optimized and will require minimum memory and computational resource since the

structures of all the matrices and vectors are known.

6.4 Example

This section exemplifies the procedure described in the above section using a simple 8 bus 2 generator system shown in Figure 6. 6.

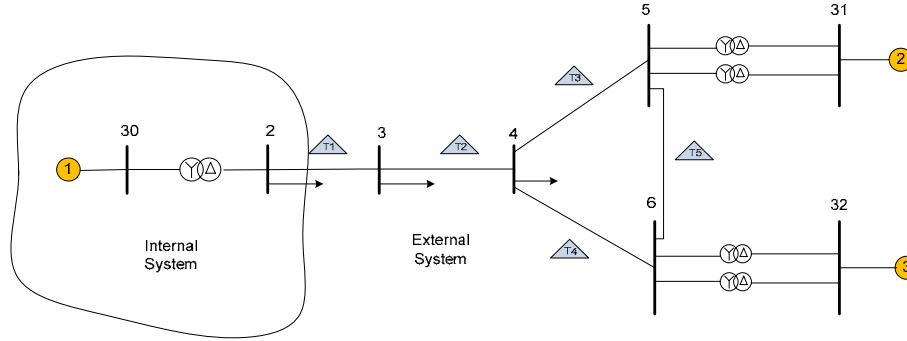


Figure 6. 6 Eight Bus and One Port System

In the system shown in Figure 6. 6, the internal system consists of 2 buses and 1 generator and the external system consists of 6 buses and 2 generators. Because line T2 is a long line, T3 and T4 are short lines, it is intuitive that generator 2 and 3 should form a coherent group. A program was also developed to implement the coherency identification using Weak Link (WL) and Two Time Scale (TS) methods described in section 3.3. This program confirms the intuitive assumption.

In order to construct the proposed equivalent in the RTDS the process listed below is applied:

- 1) The power flow data, dynamic data and the boundary separating internal and external areas are read from the data files. Power flow and dynamic data files are in PSSE data formats (.raw and .dyr). The area definition file is in a custom format.
- 2) For the full external system without any reduction, using method mentioned in section 3.2 to get the frequency dependent Norton Admittance matrix $Y_{ex}(j\omega)$. Then $Y_{ex}(j\omega)$ is implemented as a FDNE and put on the interface bus of the internal system as part of the EMT simulation.

- 3) From the external network, the coherency groups are found using methods described in section 4.3.3. In the example, there is only one coherency group and it consists of #2, #3 generators.
- 4) The coherency buses are reduced and a new admittance Y_{CBN} of the external system as discussed in section 4.5 is formed.
- 5) As discussed in section 5.2.4, #2, #3 generators can be aggregated to an equivalent generator. The equivalent generator and the reduced admittance Y_{CBN} are solved to form the current injection which represents the electromechanical behaviors.
- 6) Steps 2),3), 4), and 5) can be synthesized in a RTDS UDC, which is a C-like language in the RTDS to help users to form their own models as illustrated in Figure 6.7 .

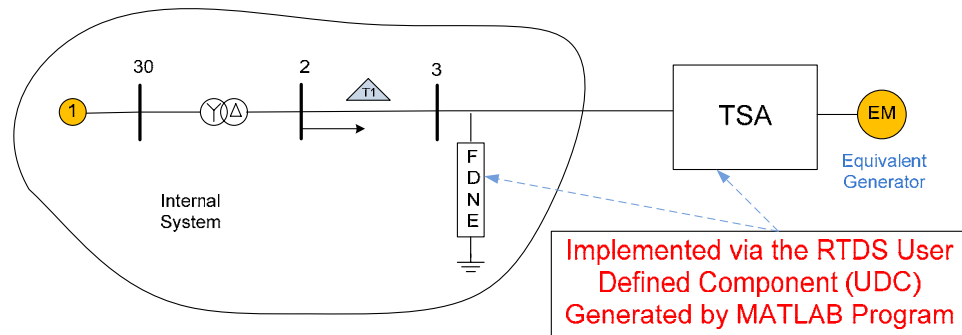


Figure 6.7 Scheme of coherency-based TSA in RTDS

Figure 6.8 shows a screen capture of the RTDS GUI, with the dotted components representing the FDNE and coherency based TSA solutions. The currents of TSA solution for \vec{I}_E are calculated and injected to the internal system as a current source.

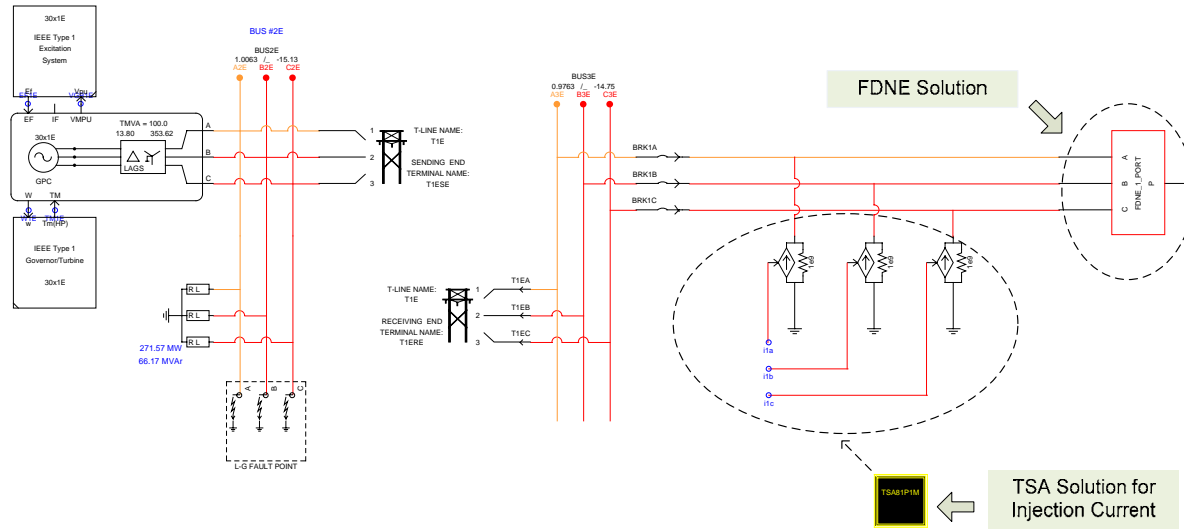


Figure 6.8 The Implementation of the Scheme in RTDS

The coherency-based TSA solution is implemented by “the dynamic hierarchy” component (Hierarchy is a graphic component available in RSCAD, the software behind the RTDS. Hierarchy is used for schematically separating the user’s circuit diagram into a number of blocks [8]). The coherency-based TSA solution block generates the signals to control the three phase current source.

As shown in Figure 6.9, there are three parts inside the dynamic hierarchy required for modeling the TSA solution shown in Figure 6.8. The “injection current conversion” part has been described in section 6.2. The “current control signal generation” part is a simple three phase sinusoidal signal generator. The major part is the “coherency-based TSA solution”, which contains the coherency-based TSA type network solution model and TSA type equivalent generator models (Figure 6.9 only shows one equivalent generator). Each equivalent generator and its equivalent exciter and governor is separately modeled. They are set up and connected through the RSCAD graphic user interface as is done for other ordinary RTDS components. It should be noted that from the view point of the RTDS, the coherency-based TSA type generator model is actually implemented as a control system block. A circuit model for this equivalent does not exist, as the TSA solution represents a phasor domain (approximate) solution, whereas the remainders (i.e., internal systems) are modeled in full detail, as a circuit.

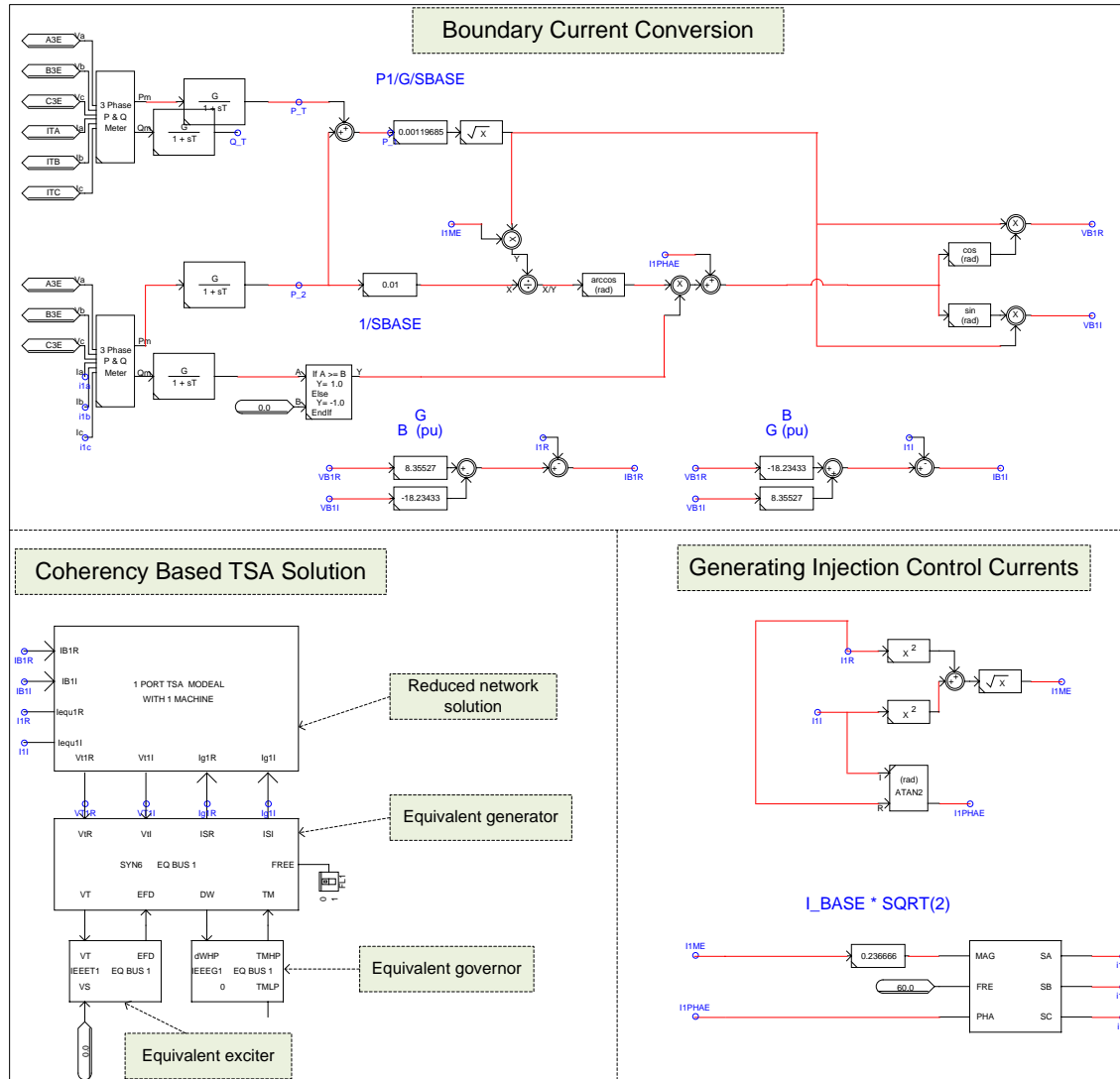


Figure 6.9 Implementation of coherency-based TSA in RTDS

Chapter 7: Simulation Cases and Validations for the Proposed Equivalent on the RTDS Platform

This chapter describes simulation examples and validation to demonstrate the applications of the approach are also presented.

The proposed equivalent has been implemented on the RTDS platform. In order to verify this technique, firstly the full system is simulated in the RTDS in full detail using an electromagnetic transient (EMT) simulation model. Then the external system is replaced with the proposed equivalent, maintaining the detailed EMT model for the internal network.

The proposed reduction consists of replacing the coherent generators with equivalent generators and then representing the whole external system with a FDNE part and a coherency-based TSA part as described before.

7.1 Simulation Results For The Eight Bus System

The simulation results of the 8 bus system of Figure 6. 6 which was described in detail in section 6.4 are shown below. A three phase ground fault of 100 *ms* duration is applied to #2 bus. Plots Figure 7. 1 and Figure 7. 2 for the three phase voltages at buses 2 and 3 are shown for detailed and equivalent models. The two curves are virtually identical and appear as one, and hence validate the proposed equivalencing approach.

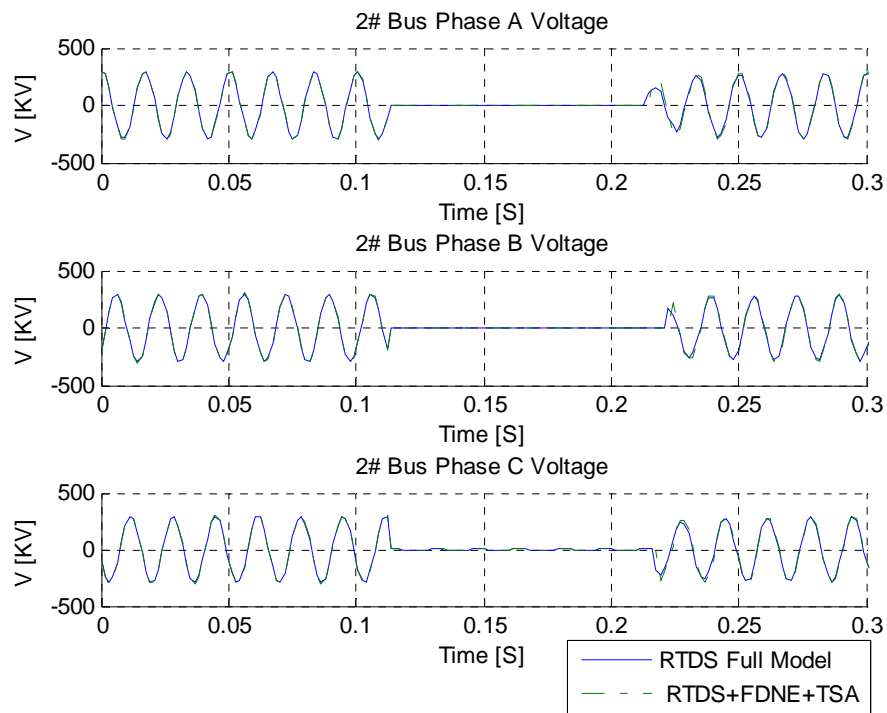


Figure 7.1 Simulation Results of #2 Bus Voltage

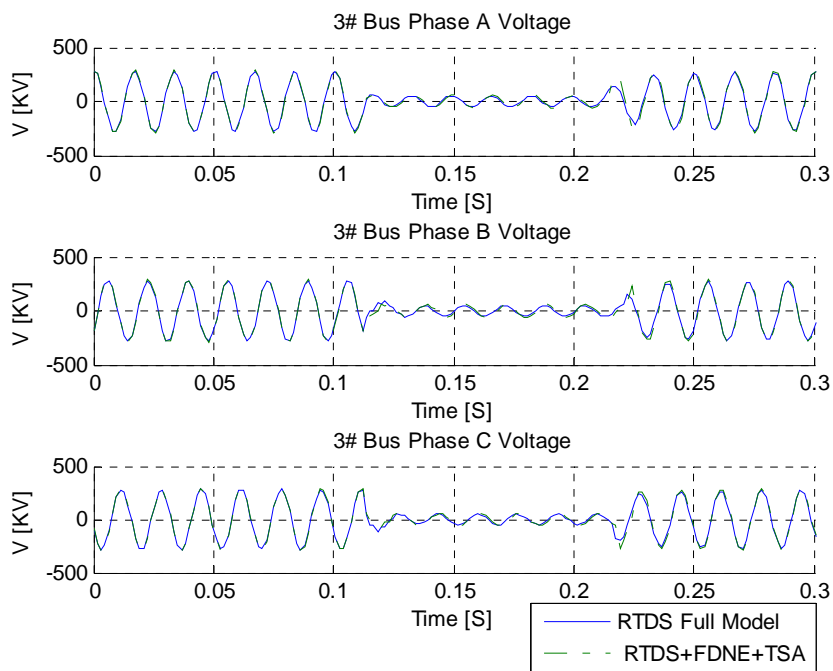


Figure 7.2 Simulation Results of #3 Bus Voltage

If the equivalent external system is exactly representing the full external system, the power generated by the #1 generator in the internal system for the full and equivalent models should be identical. Figure 7. 3 below shows the active and reactive power of #1 generator for the full and equivalent system respectively. They show essentially the same dynamic response after the three phase ground fault.

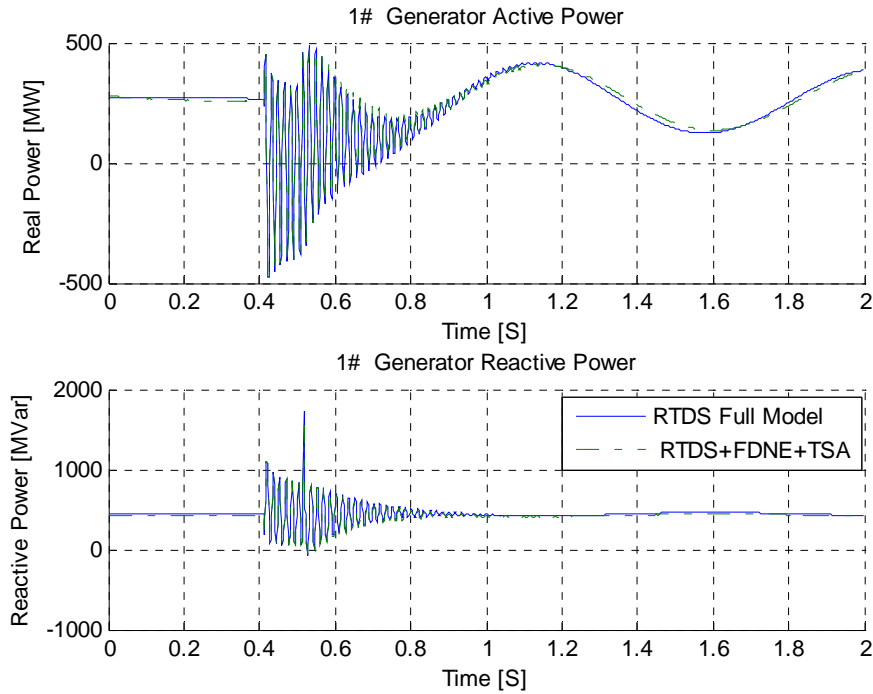


Figure 7.3 Simulation Results of #1 Generator Power

7.2 Test Systems and Validation

The previous example included only a small eight bus system. In this section the developed equivalent (FDNE+Coherency-based TSA) was applied to four different test systems. These included i) The well-known 39 bus New England system ; ii) a modified 39 bus system with an HVDC infeed with coupling between the dc line and an adjacent ac line; iii) a 108 bus AC system; IV) a 2300 bus AC/DC system.

The first three test systems could be modeled in full detail on the real time simulator (RTDS), and thus could be used as comparison benchmarks for the equivalent. The fourth system was represented using the developed equivalent only, as it is too large to be modeled in full EMT detail in real time at a reasonable cost. It is estimated that it would

require in excess of 130 RTDS racks, and for comparison the world largest RTDS installation in 2009 was 28 racks. Systems in this size can realistically only be included on a real time simulator using an equivalent approach such as the one in this thesis.

7.2.1 Simulation of a 39-Bus AC System Using Two Port Equivalent

This test system is the well-know New England Test System shown in Figure 7. 4. It is divided into two internal systems (solid colour shading) and an external system. The coherent group is shown by the areas with dotted shading. The equivalent is thus a two port equivalent (with each port being a three phase connection) as it interfaces to two separated internal systems.

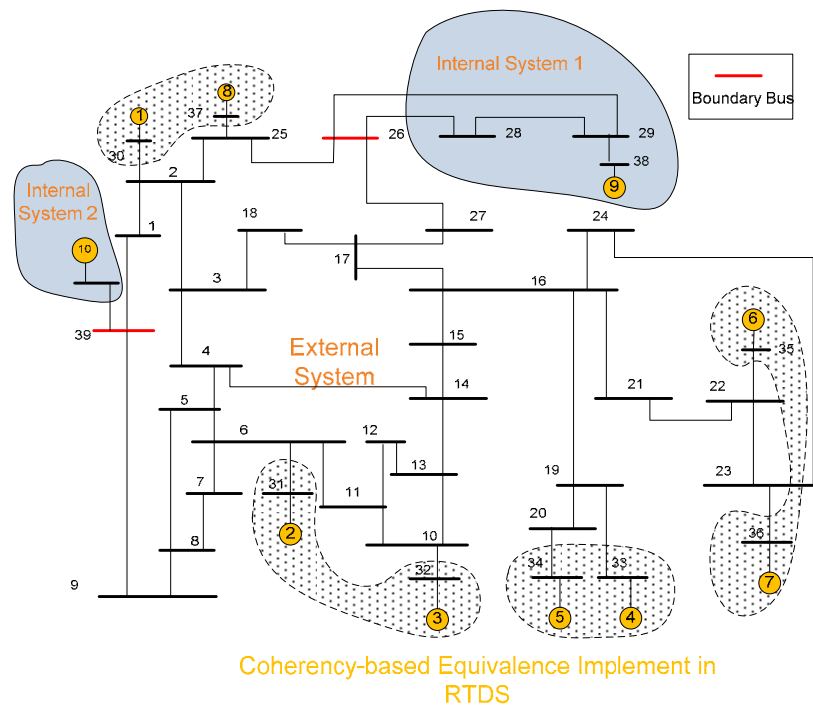


Figure 7. 4 The New England IEEE 39 Bus test system

From the coherency identification results obtained in section 4.3 it can be seen that the 10 machines shown in Figure 7. 4 fall into 6 coherent groups (9), (8, 1), (10) (2, 3), (5, 4) (7, 6). There are 4 coherent groups for the external system (the two single machine groups (9) and (10) are in the internal system). These groups are enclosed by the dotted lines in Figure 7. 4.

As mentioned in section 4.1, the high frequency behavior of the network is

represented in the equivalent by a FDNE(see Figure 4.1). As the system has two three-phase interface buses, the size of the FDNE admittance matrix is of dimension 6×6 . Once the FDNE is determined in transfer function form, it becomes directly implementable as an admittance in the EMT model of the internal system [50]. The full equivalent is the combination of the FDNE with the coherent TSA equivalent.

A three phase ground fault of 6 cycles (100 ms) duration on #28 bus in Figure 7. 4 is simulated. The simulation results of the full and reduced system are shown in Figure 7. 5- Figure 7. 7.

Figure 7. 5 shows the three phase voltage of the #29 bus of the internal system. The plots show the results for the complete model implemented in full EMT detail (RTDS FULL MODEL), which provides the benchmark, and the proposed equivalent (RTDS+Coherency-based TSA). The two curves are nearly identical and appear as one, indicating that the proposed method provides an accurate equivalent of the external system.

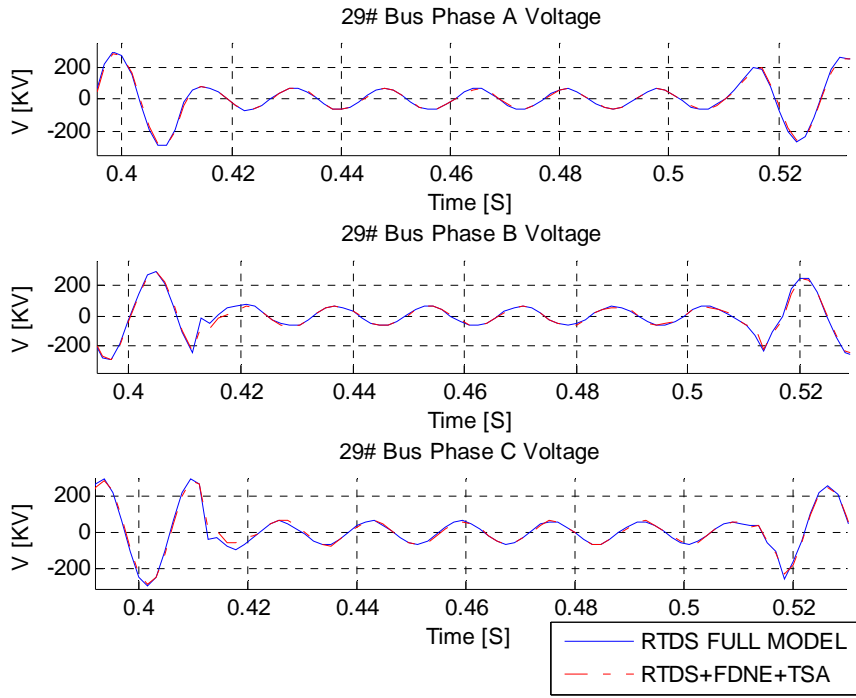


Figure 7. 5 Simulation Results of #29 Bus Voltage

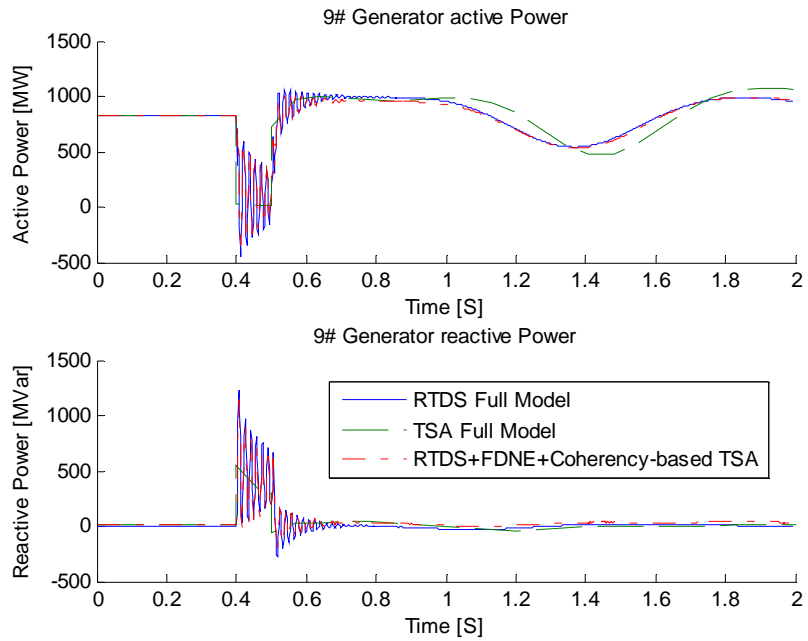


Figure 7.6 Simulation Results of #9 Generator Power

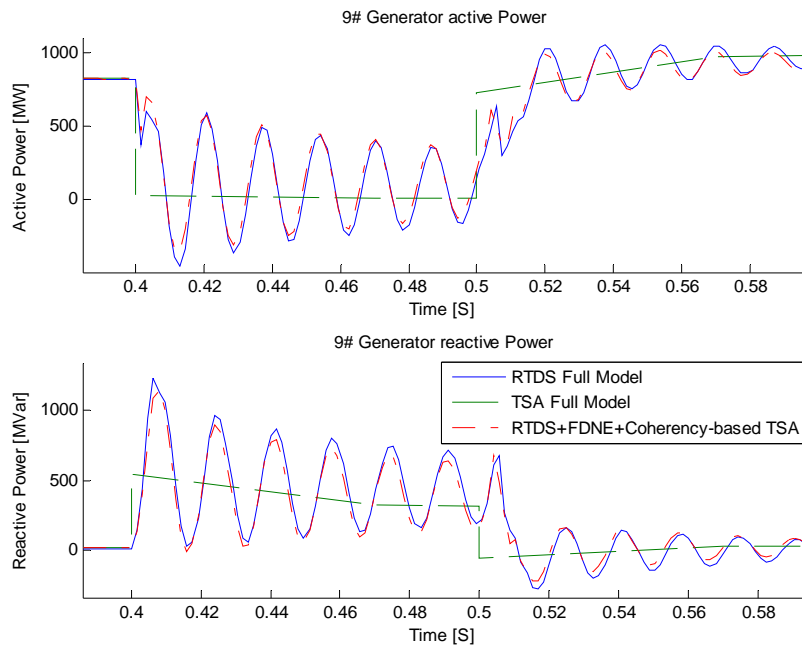


Figure 7.7 The Transient of #9 Generator

Figure 7.6 shows the active and reactive power of #9 generators. Figure 7.7 shows a close-up of Figure 7.6 showing the first 12 cycles after the fault. As an additional

comparison a pure TSA type simulation which completely ignores electromagnetic transients is also modeled (TSA Full Model). Comparison between the benchmark (RTDS FULL MODEL) and the proposed equivalent (RTDS+Coherency-based TSA) is very close, both for the faster transients as well as for the rotor oscillations. The pure TSA model (TSA Full Model) does not consider the electromagnetic transients and hence shows a more or less averaged transient.

In order to investigate the modeling approach under unbalanced conditions, a single phase (A) ground fault of 6 cycles (100 *ms*) duration on #28 bus in Figure 7. 4 is simulated. The simulation results of the full and reduced system are shown in Figure 7. 8 - Figure 7. 9.

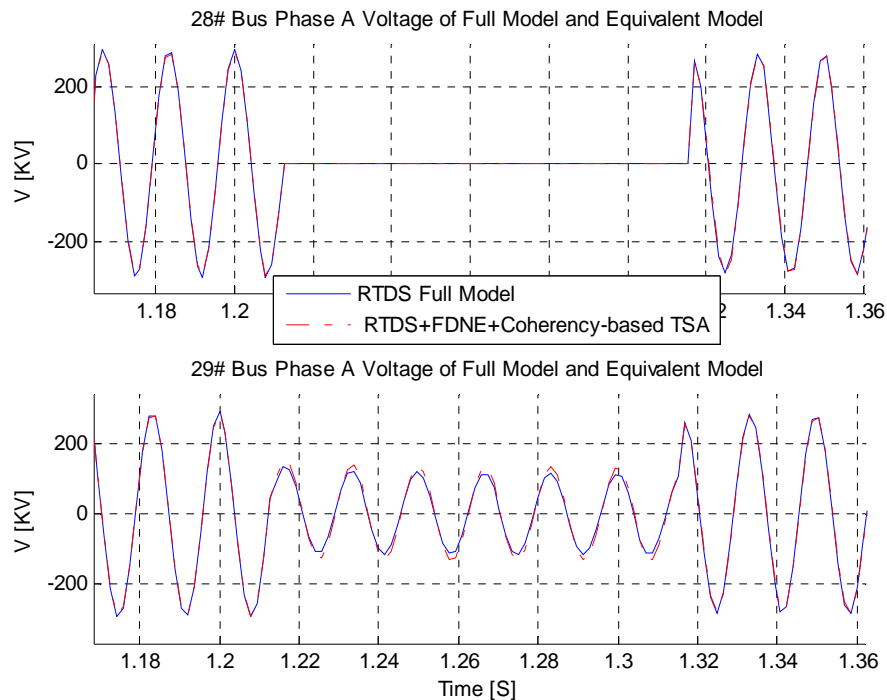


Figure 7. 8 Simulation Results of #28, #29 Bus Voltage

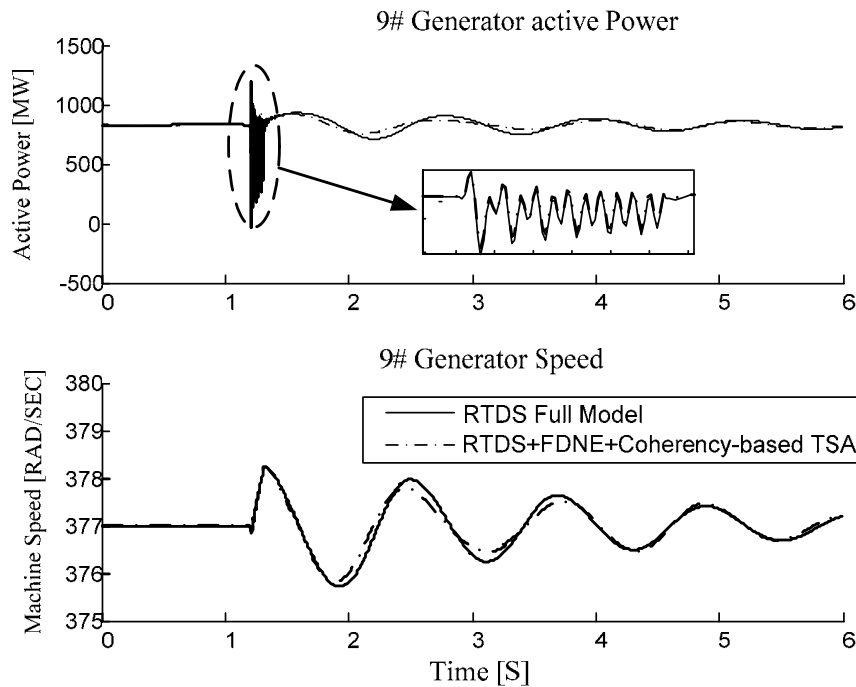


Figure 7.9 Simulation Results of #9 Generator

Figure 7.8 shows the phase (A) voltage of buses #28 and #29 in the internal system. The plots are for the complete (benchmark) model implemented in full EMT detail (RTDS FULL MODEL) and the proposed equivalent model (RTDS+FDNE+Coherency-based TSA). The two curves are nearly identical indicating that the proposed method provides an accurate equivalent of the external system. In Figure 7.9 the plots of active power and speed of #9 generator in the internal system also show an excellent agreement.

The above comparisons confirm that the proposed equivalent exhibits behaviors that are essentially identical to the detailed RTDS model. It can be concluded that the proposed equivalent can preserve both high and low frequency behaviors of the full system. The pure TSA simulation neglects the high frequency transients behaviors and only consider the low frequency behaviors.

7.2.2 Simulation of 39 bus system with coupled AC/DC lines

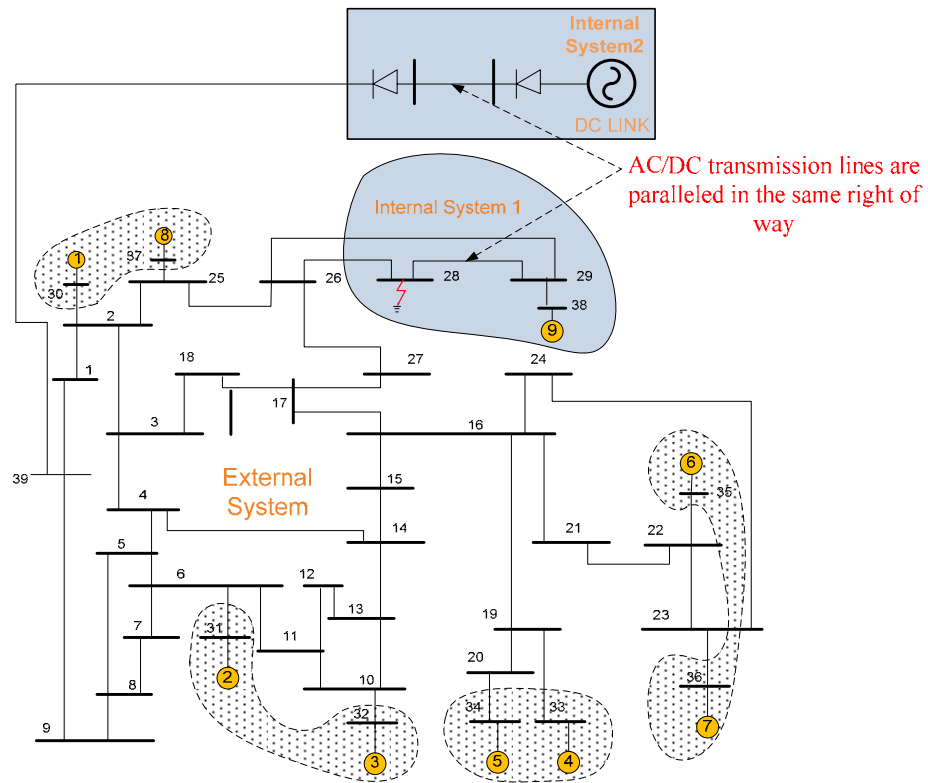


Figure 7.10 The Ac/Dc Coupling System

This case, shown in Figure 7.10, considers an HVDC infeed into the previous 39 bus network. Also, it is assumed that the dc line shares a common right of way with one of the lines in the 39 bus system. A two phase (A, B) ground fault of 9 cycles (150 ms) duration on bus 28 is simulated which is shown in Figure 7.11.

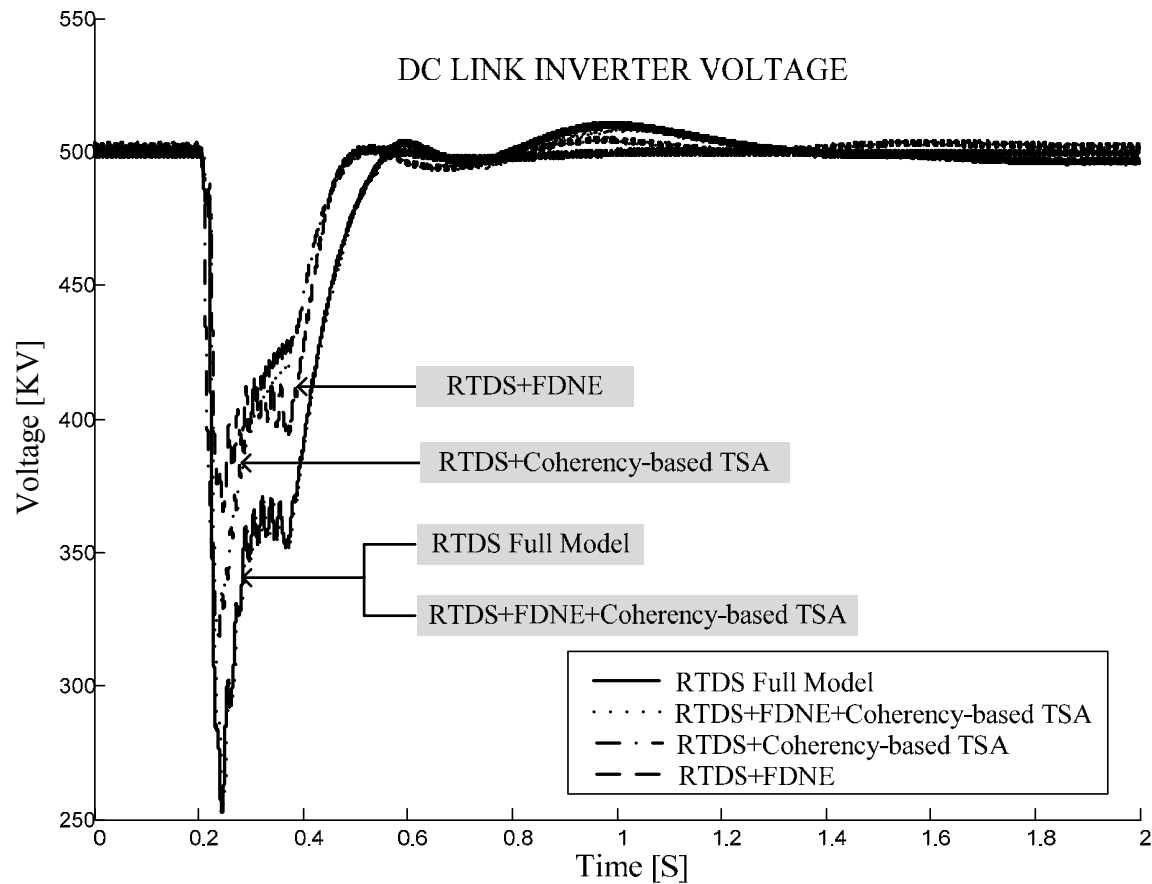


Figure 7.11 DC Link Voltage of AC/DC Coupling System

The DC link inverter side voltage is shown in Figure 7. 11. Four curves are shown. In Figure 7. 11 the first is a full detail EMT implementation (RTDS FULL MODEL), the next is the proposed equivalent representation of the external system (RTDS+FDNE+Coherency-based TSA), the third uses an equivalent for the external system that ignores the FDNE and only considers the reduced TSA solution (RTDS+Coherency-based TSA), and the fourth only includes the FDNE solution of the external system while neglecting the reduced TSA solution (RTDS+FDNE). Both internal and reduced external systems are simulated using the time step $50 \mu s$.

Results from Figure 7. 11 show that as in previous case the proposed equivalent gives the closest near identical fit to the benchmark (RTDS FULL MODEL). Ignoring either the FDNE part or the TSA part results in less accurate simulation.

7.2.3 Simulation of a 108 bus System Using One Port Equivalent

A 108-bus system is tested to verify the accuracy of the proposed equivalencing method with reduced RTDS hardware. The system is divided into two parts. The internal system (2 generators, 4 transformers and 1 transmission line) is modeled in full detail and connected to a one port external system equivalent shown in Figure 7. 12. The equivalent has 19 generators and here they are aggregated to 5 equivalent generators and included in the coherency-based TSA solution. The RTDS full model simulation is run on six RTDS racks, with the detailed model using $50 \mu s$ time step. The reduced system is run on one RTDS rack with internal system modeled with EMT detail and external system with the proposed equivalent. The simulation time step still can be $50 \mu s$ for both internal and external system.

A single phase to ground fault is applied inside the internal system for $100 ms$, two rotor speed curve of generator #20 and generator #21, which are in the internal system, are shown in Figure 7. 13.

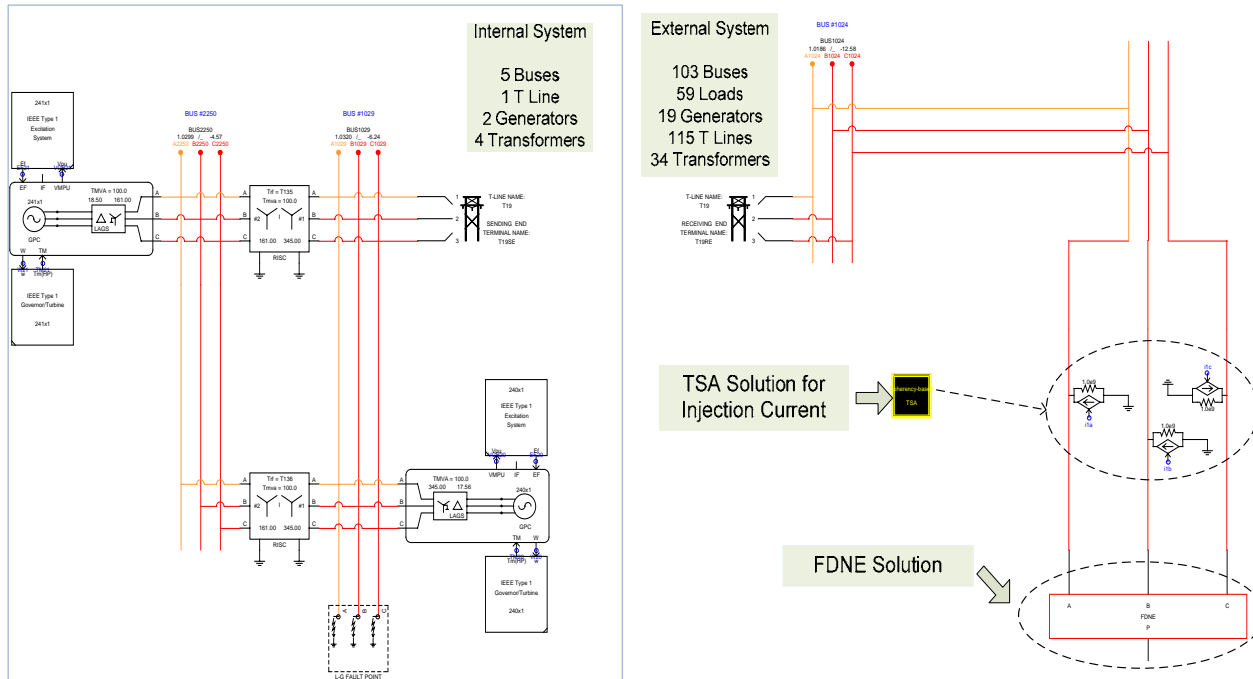


Figure 7. 12 One Port Equivalent in RTDS for a 108 Bus System

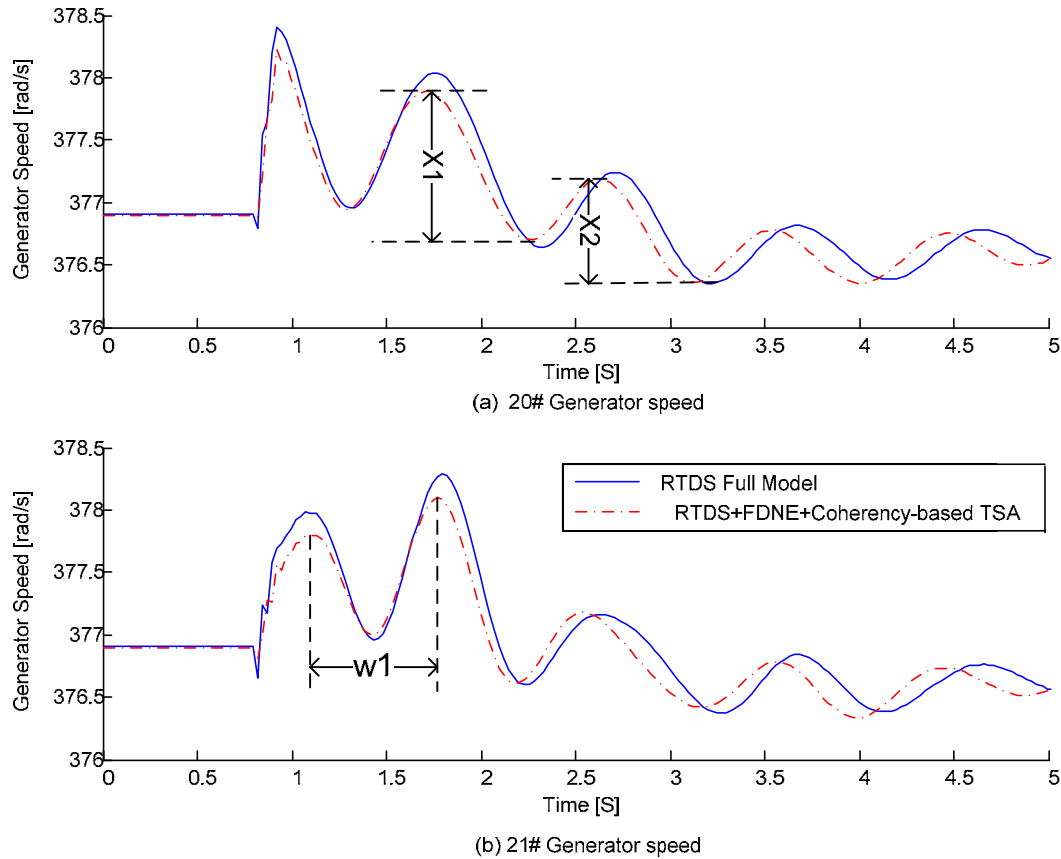


Figure 7.13 Generator Speed

The curves in Figure 7.13 show similar oscillation frequencies and damping for the full RTDS and the proposed equivalent models. For a more quantitative measure of the accuracy, a comparison can be made between the error in damping (i.e. the decay of the waveform) and the error in oscillation frequency. Damping can be estimated as the ratio of the peak-to-peak swings in two consecutive cycles (e.g. x_2/x_1 for the proposed equivalent in Figure 7.13 (a)). The oscillation frequency can be directly calculated as the reciprocal of the period (e.g. w_1 for the proposed equivalent in Figure 7.13 (b)). The damping and frequency values as well as the percentage errors for generators 20 and 21 are shown in Table 7.1. The maximum damping error is 4.05 % and the frequency error is 9.1%.

	damping (full RTDS model)	damping (equivalent model)	frequency (full RTDS model)	frequency (equivalent model)	error (damping)	error (frequency)
G 20#	0.667	0.64	1.055 Hz	1.15 Hz	4.05%	9.1%
G 21#	0.533	0.516	1.221 Hz	1.299 Hz	3.2%	6.04%

Table 7. 1 Generator Speed Curve Data

The 108 bus 21 generator system which was the limit of what could be modeled in full EMT detail with the RTDS resources (6 racks) available to the authors, and hence was the largest system to be fully validated. Simulations showed excellent agreement between the detailed simulations and the one's using the proposed equivalent. The next example which has 2300 three-phase buses shows the true power of the approach, but for this case, detailed EMT validation becomes impossible.

7.2.4 Simulation of a 2300 Bus System Using One Port Equivalent

A 2300 bus system, which is partly shown in Figure 7. 14, is used here in order to demonstrate the capability of the proposed equivalencing method of handling super large system with reduced RTDS hardware. The system has one internal system which connects to the external system through the boundary transmission line T1473_674. There are two generators (G_21138, G_72266) and a HVDC line (D12473_11473) in the internal system. The external system has 2292 buses, 802 loads, 137 generators which have been aggregated to 30 equivalent generators, 142 shunts, 1006 transmission lines and 1338 transformers. The full system is simulated using TSAT with the time step of 5 *ms* since the entire system is too large for the RTDS to run the EMT simulation. For the reduced model, the internal system and reduced external system are both run in the RTDS using two racks with the time step of 50 μs .

A three phase 12 cycles (200 *ms*) ground fault was applied at bus 1473. In a subsequent simulation, a three phase ground fault with the same duration was applied on bus 18473, which is closer to the HVDC inverter bus.

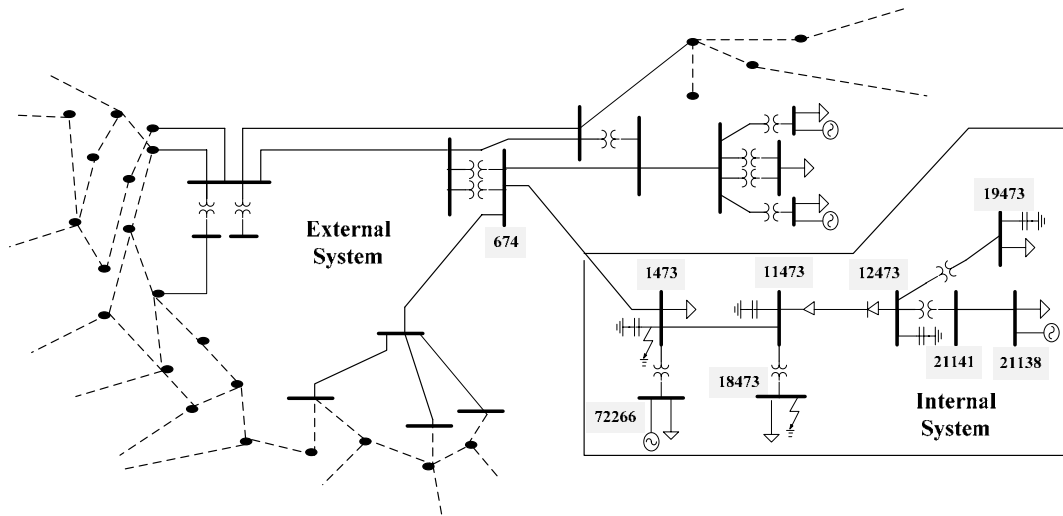


Figure 7.14 2300 Bus System

It can be concluded that if the equivalent is a correct representation of the external system the dynamic behavior of the boundary transmission line T1473_674 for both full and reduced model should be the same when the fault is in the internal system. The active and reactive power of T1473_674 for the first scenario has been shown in Figure 7.15. Here the authors are grateful to the Alberta ISO for providing the original data which was modified to derive this 2300 bus system.

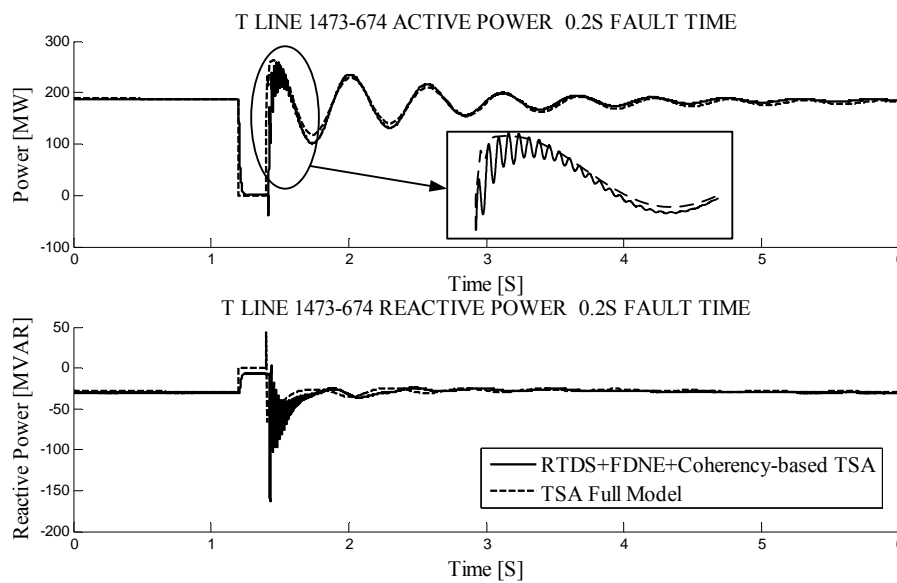


Figure 7.15 T Line Power with Fault on Bus 1473

It is obvious that the proposed equivalent can essentially reproduce the dynamic behaviors of the external system. It is also interesting to note that in the TSA full model the high frequency transient (electromagnetic) has been neglected while in the proposed equivalent this transient during the fault process are still captured.

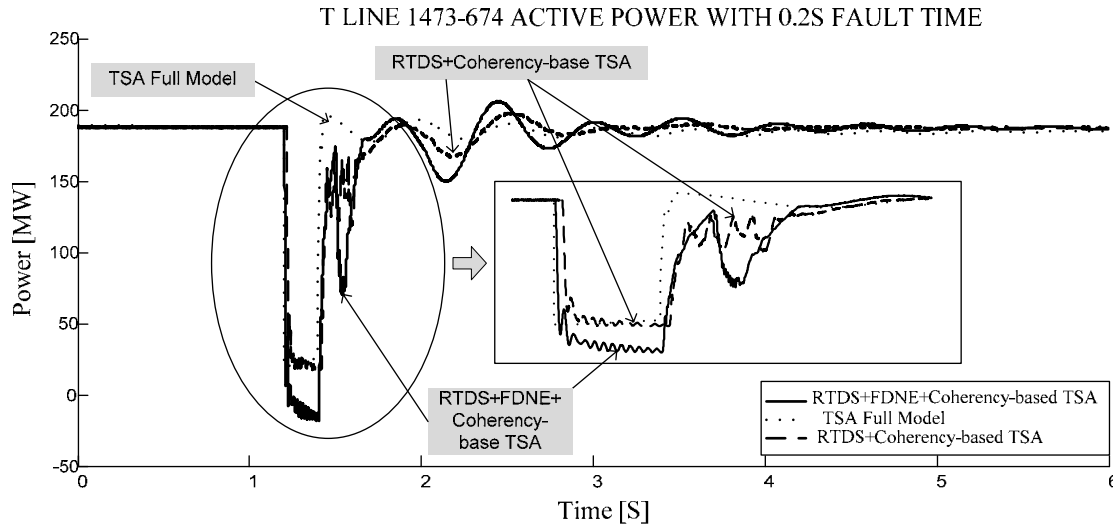


Figure 7.16 T Line Power with Fault on Bus 18473

For the second fault which was closer to the inverter on bus 18473, some difference was observed between the proposed equivalent based model and the TSA full model as shown in Figure 7.16. The reason for this is that there is a commutation failure during recovery which is clearly captured by the proposed equivalent based model, but is not able to be accurately simulated on the purely phasor based TSA representation used in the comparison. After about 3s post-fault, the two curves merge because the transient initiated by the commutation failure decays and only the inter-area low frequency modes remain.

Also plotted in Figure 7.16 are the simulation results obtained with the RTDS+Coherency-based TSA only model, in which a series R-L representation with the correct fundamental frequency impedance is used instead of a detailed FDNE. With this approach, there is an observable difference between the high frequency transients. This shows that the more detailed FDNE does make a significant difference to the impact of

the external system on the internal system.

Although the largest system size used was 2300 bus system, there is no preset limit to the size of the external system, and the approach is capable of handling tens of thousands of buses.

7.2.5 The Efficiency of the Proposed Algorithm

Traditionally in non-real time simulation programs, the increase in efficiency of an equivalencing algorithm is judged by the speedup in computation time. However, in this case the equivalent and the full models are both running in real time (in synchronism with a real time clock) and have the same computation times. Instead, a better index for the efficiency would be the comparison of the hardware resources required for the two models.

When an RTDS rack is populated with the latest generation GPC (giga-processor card) from the available RTDS inventory, it is capable of solving 66 nodes (22 three phase busses) in one rack. Each rack is normally used to model a cluster of network nodes that is isolated from the other nodes in a network via transmission line models. Transmission lines do not allow voltages/currents at one end to reach the other than faster than the speed of light in a vacuum (300 m/us or 15 km per 50 us timestep). This allows independent parallel simulations of each of the node clusters. As most networks are self-similar in structure, the distribution of clusters and transmission lines is roughly similar regardless of the size. This is an observation borne from experience. Hence, the size of the simulation hardware required also scales proportionally to the network size.

For a 2300 bus system which is described in the previous section, it is estimated that $\frac{2300}{22} \approx 105$ racks are needed to simulate the full system. This is not practical since the largest user of RTDS in the world as of the year 2010 has 33 racks.

In comparison, the proposed equivalencing algorithm requires only two racks to simulate the detailed internal system and the equivalent external system in real time. This indicates the efficiency of the proposed equivalencing algorithm.

Chapter 8: Conclusion and Future Work

In this Chapter, a summary of the contributions in this thesis is presented and some directions for future work are proposed.

In many power system studies, it is a common practice to partition the study system into an internal and external system. The internal system is of greater interest and is modeled with all its components represented in complete detail. Faults or other disturbances are applied within this internal system. The remainder of the study system can be modeled as an external system which is a simplified equivalent. This reduces the external system to a manageable and affordable model.

In earlier work in this area, Lin et al [18] developed a two part equivalent in which the high frequency behaviour of the reduced network was implemented using a multi-port Frequency Dependant Network Equivalent (FDNE); whereas the low frequency electro-mechanical behaviour was implemented by conducting a transient stability solution on the unreduced network. The FDNE considerably reduced the size of the network to be represented by the real-time EMT model. The TSA block, however, was still modeled in full and not as an equivalent, resulting in a very large model for the electromechanical part of the simulation. Although this approach reduced the computational hardware required for simulating a large system significantly, it was still impractical to model large systems with thousands of buses.

In the course of this thesis, an improved wide-band multi-port equivalent for the real time simulator (RTDS) was proposed to enable the RTDS to handle very large systems (thousands of buses) with reasonable hardware cost. The proposed equivalent has been extensively validated with several test systems and shows that from the point of view of the internal system, both high and low frequency behaviors are accurately modeled.

8.1 The Contribution Toward the Reduced Transient Stability Analysis (TSA) Equivalent Model

The coherency approach is based on the empirical observation that following a disturbance certain groups of generators tend to swing together. This technique has been

tested on large systems of 11,028 bus bars and 2,553 generators [36]. It has been found to be cost - efficient and reasonably accurate. The coherency technique does not need any special interfacing with the internal system model, because the equivalent is in the form of a model of an actual physical component as used in stability programs. However previous coherency based model was not directly applicable to RTDS because it did not consider electromagnetic transients.

The proposed approach improves the previous work of Lin et al [18] by determining approaches to further reduce the low frequency TSA model into a simpler equivalent using coherency-based techniques. To obtain the coherency-based TSA equivalent, the sets of coherent generators of the external system are identified and aggregated into equivalent generators. A reduced TSA model is thus obtained. Solution of this model provides values for the interface Norton-current sources which are injected into the EMT model of the internal system.

Several test systems described in detail in the previous chapter have been employed to validate the proposed technique. The very simple eight bus system is used to illustrate the mechanism of the proposed technique. The simulation results between the benchmark (RTDS FULL MODEL) and those with the proposed equivalent are very close, and hence validate the proposed equivalencing approach.

As a standard IEEE benchmark testing system, the well-known New England 39 bus system, along with a modified 39 bus system with an HVDC infeed with coupling between the dc line and an adjacent ac line, are used to validate the accuracy of the proposed procedure. The simulation results have shown that the proposed equivalent can essentially reproduce both the faster transients as well as for the rotor oscillations. Furthermore the simulation results of the modified 39 bus system have illustrated both FDNE and reduced TSA solution contribute to the accuracy of the proposed equivalencing technique.

The capacity of the proposed equivalencing algorithm for modeling very large network was validated by employing a 108 and a 2300 bus system. Simulations show excellent agreement between the detailed simulations and those using the proposed equivalent. At the same time those simulations also show the proposed equivalent is

capable of reducing the RTDS hardware to an affordable number. The entire system was represented very economically using just 2 RTDS racks. It is estimated that without the equivalent, the simulation would have required more than 100 racks.

From the validation results it can be concluded that the proposed procedure can greatly reduce the computational effort in the representation of the external system and allows the RTDS to handle very large system with much less hardware. The proposed equivalent shows that in the point view of the internal system, both high and low frequency behaviors are accurately modeled. Although the largest system size used was 2300 bus system, there is no preset limit to the size of the external system, and the approach is capable of handling tens of thousands of buses. The test results have shown that this approach breaks the size-barrier for real-time simulators by enabling the consideration of very large systems with thousands of buses with an affordable hardware cost.

8.2 The Contribution toward the FDNE with Passivity Enforcement

The FDNE is a multi-port admittance matrix with rational polynomial elements (in the Laplace or s-domain) embedded into the EMT solution. The frequency response characteristic of this admittance closely matches the frequency response behavior of the entire external network (not the reduced external network, and ignoring non-linearities) over the selected frequency range (typically from a tens of Hz to several kHz). The FDNE can be calculated by fitting a known or derived frequency response plot of the entire external network's admittance as seen from the interface terminals. This FDNE is then included in the EMT solution.

In reality passive elements in the power system must absorb real power. That means the equivalent for the systems should always be passive. However, inherent approximations in the fitting process may cause some passivity violations at certain frequency ranges [49].

The earlier approach of Lin et al [18] to ensuring passivity of the FDNE was to identify frequency regions of passivity violation and then do a more refined and tighter fitting in those regions. While this eliminated many of the passivity violation cases, it was not foolproof. This thesis adopts an alternate improved formulation based on [49], which

enforces passivity using linearization and constrained optimization. A frequency scan of the fitted function is carried out and if the scan shows any eigenvalues of negative real parts, the coefficients of the elements of the fitted function are perturbed till the violations disappear. An optimization problem is formulated in which the objective function is a combination of fitting error and passivity constraint violation. Solving the problem yields a passive fitted function with an acceptable fitting error.

However, this optimization method has the disadvantage that passivity violation needs to be relatively small. Hence this thesis developed a more practical passivity enforcement procedure described in section 3.7.3 which combined the constrained optimization approach [49] and the above mentioned experienced procedures. Validated from those testing systems described in previous chapter this procedure was found to work very well and can essentially assure the passivity of the FDNE model in the EMT simulation.

8.3 Directions for Future Research

- 1) In the previous work of Lin [18], the PSSE format power flow and dynamic data are used to get the frequency response of the external system. In this proposed equivalencing work the frequency response is obtained with the same method. This method is easy to be implemented and the PSSE format is a widely used one. Other methods on obtaining frequency response of the external network could be further investigated. For the same external network the frequency response using different algorithm could be compared in order to pick up one which can get the closest frequency response.
- 2) In future research, larger systems could be investigated to find the maximum limits of the algorithm. Realistic system data for such larger systems were not available to the author, and is hence left for future work.
- 3) It would be interesting to investigate the fast controllable devices that may react on the events in the internal system (e.g. SVC keeping constant voltage, CSC keeping constant power flow etc.) which have not been considered in the proposed equivalencing method. How to model these devices is a challenging problem. If these devices have intermediate speeds of response, then they could be included in the proposed equivalent in a manner similar to generator controllers. Otherwise

other solutions should be investigated and then include these solutions in the proposed equivalent.

- 4) In the 2300 bus validation case an approximate calculation is used to find how much RTDS hardware resource is needed to simulate the entire system. In the future RTDS implementation of the proposed equivalent the optimization of the computation processors should be investigated in order to find out the best distribution of computation processors for the proposed equivalent.

APPENDIX A: WEAK LINK METHOD

(A1) Theory of Weak Link Method

Equation (4. 9) in section 4.3.2.2 is applicable to a system consisting of only two weakly coupled subsystems. However, extending this idea further for the case of a system consisting of m weakly coupled subsystems, it is desired that the state variables X_1, X_2, \dots, X_n in (4. 8) are regrouped to generate a new matrix A in which the block diagonal sub-matrixes $\tilde{A}_{ii}, i = 1, 2, \dots, m (m < n)$ for m groups are weakly coupled with each other as illustrated by Figure 4. 7 in section 4.3.2.2.

The coupling between two subsystems comprising of different groups of machines is measured in terms of a ‘coupling factor’ [30]. It is assumed that an arbitrary system is divided into two sub-systems, such that the first subsystem consists of $2n_1$ states of n_1 machines and the second subsystem contains $2n_2$ states of the n_2 remaining machines. The coupling factor S is then defined as in (A-1). It is the ratio of the sum of absolute value norms of the off diagonal sub-matrixes (shaded areas in Figure A-1) and the sum of absolute value norms of the diagonal (shaded) sub-matrixes. As is evident, $S = 0$ means that the matrix is strictly block diagonal. A large S means that the shaded areas are densely populated.

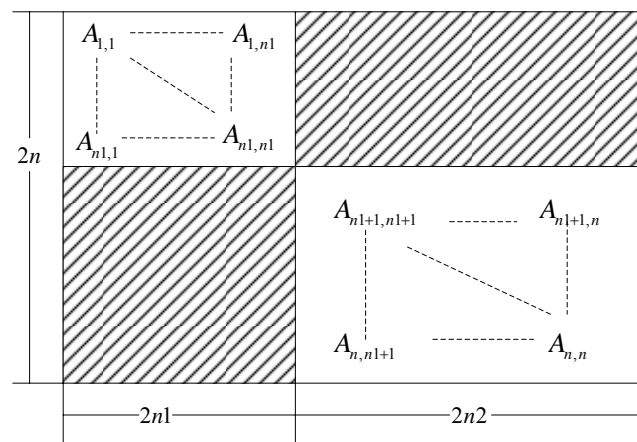


Figure A-1 System Matrix

$$\begin{aligned}
SNUM &= \sum_{j=nl+1}^n \sum_{i=1}^{nl} |A_{ij}| + \sum_{j=1}^{nl} \sum_{i=nl+1}^n |A_{ij}| \\
STOT &= \sum_{j=1}^n \sum_{i=1}^n |A_{ij}|, \quad SDEN = STOT - SNUM \\
S &= SNUM / SDEN
\end{aligned} \tag{A- 1}$$

To implement this technique firstly the coupling between each machine and the rest of the system is calculated. The machine that has the weakest S with the rest of the system becomes the first machine of the new ordered array L of machines.

The next step is to find the machine to be placed in the second position of the ordered array L . To do this, all the two machine subsystems consisting of the first machine in the ordered array L and each of the remaining machines are formed. Then, the two machine subsystem that has the weakest S to the rest of the system is identified. That machine, which has not been already placed in the ordered array, is now placed the second position of the ordered array L . This form of ordering of machines goes on until all machines are ordered. Subsequent subsystems will consist of machines already placed in the ordered array L and one of the remaining machines. The state variable matrix A is now re-ordered with the new sequence L .

Once, the ordering is done, let $S(m)$ represent the coupling factor considering the first m machines in the reordered A matrix, with the remaining $(n-m)$ machines. $S(m+1)$ represents the new coupling factor when the next machine is added to the set of m . If the coupling factor $S(m+1)$ is smaller than $S(m)$, it means that the $(m+1)$ th machine is strongly coupled to the first m machines, as including it together with the first m machines, makes the resultant set more decoupled from the remainder of the network. On the other hand, if the $S(m+1)$ is larger than $S(m)$, it implies that the $(m+1)$ th machine is more strongly coupled with the remaining machines than with the group of first m machines. This provides a natural method of grouping the machines.

(A2) Implementation Algorithm of Weak Link Method

In order to explain the implementation of the weak link method, a system with n state variables (machines) is illustrated as Figure A-2.

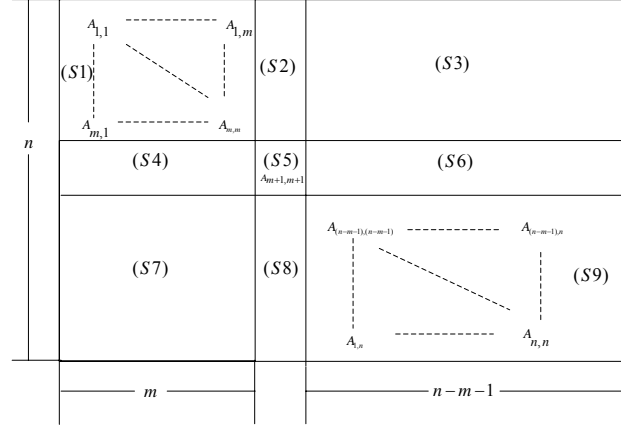


Figure A- 2 Implementation of Weak Link Method

An arbitrary subsystem $N1$ is defined which contains m machines namely $L(1), L(2), \dots, L(m)$. $s(1), \dots, s(9)$ are the norms of the elements of the sub matrixes shown in Figure A-2. The coupling factor [30] of subsystem $N1$ can be defined as

$$S(m) = \frac{[(s2) + (s3) + (s4) + (s7)]}{[(s1) + (s5) + (s6) + (s8) + (s9)]} \quad (\text{A- 2})$$

Then the $m+1$, namely $L(m+1)$ machine is added to the subsystem $N1$ and hence the new subsystem of $N1'$ is formed. The rest of $(n-m-1)$ machines are defined as subsystem $N2$, which contains the remaining $(n-m-1)$ machines. The coupling factor of subsystem $N1'$ can be calculated as

$$S(m+1) = \frac{[(s3) + (s6) + (s7) + (s8)]}{[(s1) + (s2) + (s4) + (s5) + (s9)]} \quad (\text{A- 3})$$

The strength of the coupling of the additional machine $L(m+1)$ in the subsystem $N1$ can be measured in terms of the change in the value of S due to the inclusion of this machine.

$$\begin{aligned} \Delta S(m) &= S(m+1) - S(m) \\ &= \frac{[(s3) + (s6) + (s7) + (s8)]}{[(s1) + (s2) + (s4) + (s5) + (s9)]} - \frac{[(s2) + (s3) + (s4) + (s7)]}{[(s1) + (s5) + (s6) + (s8) + (s9)]} \end{aligned} \quad (\text{A- 4})$$

From (A-4) it can be seen that if machine $L(m+1)$ has a stronger coupling with $N2$, then $\Delta S(m)$ is positive. If machine $L(m+1)$ has stronger coupling with $N1$, then

$\Delta S(m)$ is negative. This variation in the coupling factor is illustrated in the plot of $s(m)$ against the machine number $L(m)$. This plot is called a ‘coupling graph’.

Change in the slope of S at the inclusion of machine $L(m)$ in the coupling graph can be represented by $\Delta^2 S(m)$, where

$$\Delta^2 S(m) = \Delta S(m) - \Delta S(m-1) \quad (\text{A-5})$$

If $\Delta^2 S(m) > 0$ then machine $L(m+1)$ is weakly coupled to $L(m)$.

If $\Delta^2 S(m) < 0$ then machine $L(m+1)$ is strongly coupled to $L(m)$.

Equation (A-5) also indicates that the points of relative minima of the coupling graph mark the end of weakly coupled groups as mentioned earlier. Using (A-5), a ‘grouping bar chart’ plot of $\Delta^2 S(m)$ against the machine number $L(m)$ can be obtained. In this kind of figure, a negative value of $\Delta^2 S(m)$ after a positive value of $\Delta^2 S(m)$ marks the beginning of a group. The next positive $\Delta^2 S(m)$ determines the last machine in this group that is strongly coupled.

(A3) An Eight Bus System Implementation Example of the Weak Link Method

A computer algorithm, based on the coupling factor S , for arranging the machines in order of their relative coupling within the system is explained below. A system with 3 machines and 8 buses is shown in Figure 4. 8 and is used as an example to illustrate this approach.

This method rearranges the synchronous machines according to their relative coupling factor. That is, the synchronous machines in the system state matrix are reordered to reflect their strength of coupling with other machines.

First the coupling between each machine and the rest of the system is calculated. The synchronous machine that has the weakest coupling with the rest of the system becomes the first machine of the ordered array L of synchronous machines.

The next step is to find the synchronous machine to be placed in the second position of the ordered array L . To do this, all the two machine subsystems consisting of the first

machine in the ordered array L and each of the remaining machines are formed. Then, the two machine subsystem that has the weakest coupling to the rest of the system is identified. That synchronous machine, which has not been already placed in the ordered array, is now placed into the second position of the ordered array. This form of ordering of the synchronous machines goes on until all the generators are ordered. Subsequent subsystems will consist of machines already placed in the ordered array and one of the remaining machines. The following are procedures for the computer algorithm [29].

- 1) Form the system state matrix (A). M is the size of the state matrix A . For the eight bus system, the state matrix A is shown in Table A-1.

0	376.9911	0	0	0	0
-0.02938	0	0.013426	0	0.015953	0
0	0	0	376.9911	0	0
0.010301	0	-0.03582	0	0.025521	0
0	0	0	0	0	376.9911
0.007668	0	0.019985	0	-0.02765	0

Table A- 1 State Matrix of the Eight Bus System

- 2) Calculate $STOT$. $STOT$ is the norm of the state matrix A and is defined in (A-1).

For the test system, $STOT = 1.131e+003$

- 3) Calculate for $j = 1, M$

$$Sum(j) = \sum_{i=1}^M (|A_{ij}| + |A_{ji}|); i \neq j. \quad (A- 6)$$

$Sum(j)$ is the off-diagonal term of the element A_{jj} . For the test system the result is shown in Table A-2.

0.047349	0.069233	0.069127
----------	----------	----------

Table A- 2 Off Diagonal Summation of the State Matirx

For all $j = 1, M$ find minimum of $Sum(j)$ and store the minimum in $S_{\min}(1)$ and its index j in $I_{\min}(1)$

$$S_{\min}(1) = 0.047349, \quad I_{\min}(1) = 1$$

5) Calculate for all $j = 1, M$ and $j \neq I_{\min}(1)$, the following:

$$S_{\min i}(j) = S_{\min}(1) + Sum(j) - 2[A(j, I_{\min}(1)) + A(I_{\min}(1), j)] \quad (\text{A-7})$$

For the case $j = 2$, shown in Figure A-3.

(S1) $A_{1,1}$	(S2)	(S3)
(S4)	(S5) $A_{2,2}$	(S6)
(S7)	(S8)	(S9) $A_{3,3}$

Figure A-3 Calculation of Coupling Factor

From step 4, $I_{\min}(1) = 1$, $S_{\min}(1) = S(2) + S(3) + S(4) + S(7)$

From step 3, $Sum(2) = S(4) + S(6) + S(2) + S(8)$

$$A(j, I_{\min}(1)) + A(I_{\min}(1), j) = A(2, 1) + A(1, 2) = S(2) + S(4)$$

From (A-6)

$$\begin{aligned} S_{\min i}(j) &= S_{\min i}(2) \\ &= S_{\min}(1) + Sum(2) - 2[A(2, 1) + A(1, 2)] \\ &= S(2) + S(3) + S(4) + S(7) + S(4) + S(6) + S(2) + S(8) - 2S(2) - 2S(4) \\ &= S(3) + S(6) + S(7) + S(8) \end{aligned}$$

$S_{\min i}(2)$ is just the numerator of the ‘coupling factor’ of the two machine system which contains #1 and #2 generator.

In this way, the previous calculation results are used for get a new coupling factor. This saves computation resource and time.

6) For all $j = 1, M$ and $j \neq I_{\min}(1)$, find the minimum of $S_{\min i}(j)$ and store the

value in $S_{\min}(2)$ and its index j in $I_{\min}(2)$.

For the three machine example, $j = 2$ and $S_{\min}(2) = 0.069127$

7) Repeat step 5 and 6 until all machines have been ordered in arrays S_{\min} and I_{\min} . The process is described below:

For all $j \neq I_{\min}(1), I_{\min}(2), \dots, I_{\min}(R)$, where R is the number of machines processed so far;

$$S_{\min} i(j) = S_{\min}(R) + Sum(j) - 2[A(j, I_{\min}(R)) + A(I_{\min}(R), j)]$$

Find the minimum of $S_{\min} i(j)$ and store the value in $S_{\min}(R+1)$ and its index j in $I_{\min}(R+1)$. If $R+1 = M$ then stop.

For the three machine example

$$S_{\min} = 0.0473488, 0.0691268, 0.0472428$$

$$I_{\min} = 1, 2, 3$$

8) Calculate the following:

$$S(R) = S_{\min}(R) / (STOT - S_{\min}(R))$$

$$\Delta S(R) = S(R+1) - S(R) \quad (A-8)$$

$$\Delta^2 S(R) = \Delta S(R) - \Delta S(R-1)$$

where:

$STOT$ is the norm of the state matrix A

$S(R)$ is the coupling factor at the inclusion of the R^{th} synchronous machine

$\Delta S(R)$ is the slope of $S(R)$ at the inclusion of synchronous machine $R+1$. Also $\Delta S(M) = 0$ where M is the index number of the last synchronous machine.

$\Delta^2 S(R)$ is the rate of change of $\Delta S(R)$ at the inclusion of machine R .

To identify strongly coherent synchronous machines $\Delta^2 S(R)$ is used. A negative rate of change in the slope following a positive rate of change in the slope marks the beginning of a strongly coherent group of synchronous machines. The next positive $\Delta^2 S$

marks the last synchronous machine of the group. Single machine groups are identified by a positive $\Delta^2 S$ that does not mark the end of a strongly coherent group. The rate of change in slope of the first machine of the ordered array is not clearly defined by this method. If the $\Delta^2 S$ of the second machine is negative, then the first machine may be taken as part of the first group. If the $\Delta^2 S$ of the second machine is positive, then the first and second machines are single groups.

For the three machine example system, the ‘coupling graph’ is shown in Figure A-4.

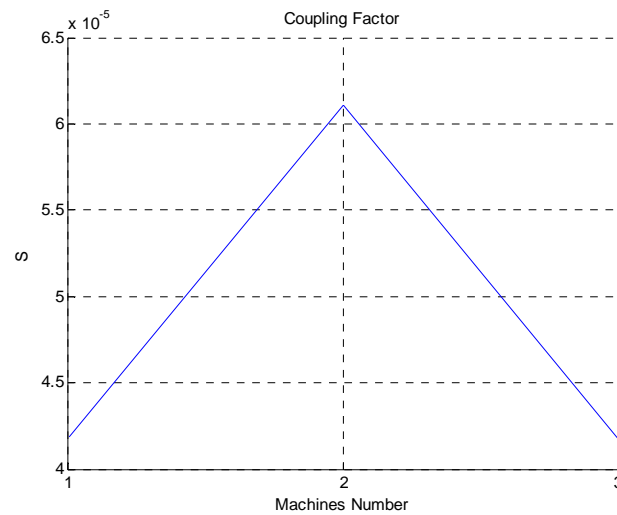


Figure A- 4 Coupling Graph of 3 Machine System

From the graph it is observed that if the #2 machine is added to the group which only contains the #1 machine, the coupling factor increases. This shows the #2 generator has a strong coupling with the remaining part of the network, #3 generator, and a weak coupling with the #1 generator.

The ‘grouping bar chart’ plot of $\Delta^2 S(m)$ versus the machine number $L(m)$ is shown in Figure A-5. It also shows that the #2 generator has weak coupling with the #1 generator and strong coupling with the #3 generator.

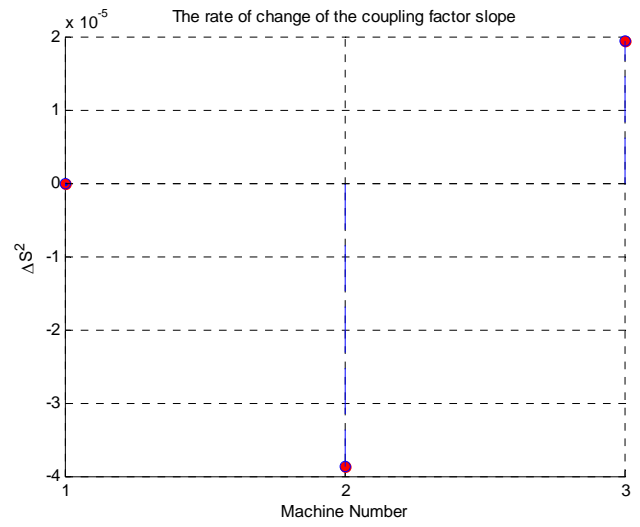


Figure A- 5 Grouping Bar Chart of 3 Machine System

References

- [1] IEEE/CIGRE Joint Task Force on Stability Terms and Definitions, "Definition and Classification of Power System Stability", *IEEE Trans on Power system*, Vol. 19, No. 2, pp.1387-1401, May. 2004
- [2] J.Arrillaga, N.Watson, Power Systems Electromagnetic Transients Simulation, *The Institution of Engineering and Technology, London, 2002*
- [3] Kuffel, R. Giesbrecht, J. Maguire, T., Wierckx, R.P., McLaren, P.G., "A fully digital power system simulator operating in real time", *Electrical and Computer Engineering, 1996. Canadian Conference , Volume 2, 26-29 May 1996 Page(s):733 - 736 vol.2*
- [4] P.Forsyth, R.Kuffel, R. Wierckx et al, "Comparison of Transient Stability Analysis and Large-Scale Real Time Digital Simulation", *Power Tech Proceedings, 2001 IEEE Porto*
- [5] P.G McLaren, R.Kuffel, R.Wierckx et al, "A Real Time Digital Simulator For Testing Realys", *IEEE Trans on Power Delivery, Vol.7, No. 1, pp.207-213, Jan. 1992*
- [6] Forsyth, P., Maguire, T., Kuffel, R., "Real time digital simulation for control and protection system testing", *Power Electronics Specialists Conference, 2004. PESC 04. 2004 IEEE 35th Annual , Volume 1, 20-25 June 2004 Page(s):329 - 335*
- [7] A.M. Gole, Power Systems Transient Simulation, Course Notes, *University of Manitoba, 2005.*
- [8] RTDS Manual Set, *RTDS Technologies Inc., Winnipeg, 2009*
- [9] A. M. Gole et al, "Guidelines for modeling power electronics in electric power engineering applications", *IEEE Trans on Power Delivery, vol.12, No.1, pp.505514, Jan. 1997.*
- [10] H.W.Dommel, "Digital Computer Solution of Electromagnetic Transients in Single and Multi-phase Networks", *IEEE Trans on Power Apparatus and Systems, vol.PAS-88, No.4, pp.388-399, Apr.1996.*
- [11] PSS/E™ 30.2 Manual Set, *Power Technologies International, Siemens Power Transmission & Distribution, Inc., November 2005, Schenectady*
- [12] P. Kundur, Power System Stability and Control, *McGraw-Hill, New York, 1994.*
- [13] M. D. Heffernan, K. S. Turner, J. Arrillaga and C. P. Arnold, "Computation of AC-DC System Disturbances, Parts I, II and III", *IEEE Trans on Power Apparatus and systems, vol. PAS-100, No.11, pp. 4341-4363, Nov. 1981.*
- [14] J. Reeve and R. Adapa, "A New Approach to Dynamic Analysis of AC Network Incorporating Detailed Modeling of DC Systems, Part I and II", *IEEE Trans on Power Delivery, vol.3, No.4, pp.2005-2018, Oct. 1988.*
- [15] X. Wang, P. Wilson and D. Woodford, "Interfacing Transient Stability Program to EMTDC Program", *International Conference on Power System Technology, 2002. Proceedings. PowerCon 2002.*
- [16] G. W. J. Anderson, N. R. Watson, C. P. Arnold and J. Arrillaga, "A New Hybrid Algorithm for Analysis of HVDC and FACTS Systems", *International Conference on Energy Management and Power Delivery, 1995. Proceedings of EMPD '95., 1995.*

- [17] H. Su, K. W. Chan, L. A. Snider and J-C. Soumagne, "Advancements on the Integration of Electromagnetic Transients Simulator and Transient Stability Simulator", *International Conference on Power Systems Transients Montreal, Jun. 19-23, 2005*.
- [18] Xi Lin, Gole A.M., Ming Yu, "A Wide-Band Multi-Port System Equivalent for Real-Time Digital Power System Simulators", *IEEE Transactions on Power Systems, Volume 24, Issue 1, Feb. 2009 Page(s):237 - 249*
- [19] B.Gustavsen, A.Semlyen, "Rational Approximation of Frequency Domain Responses by Vector Fitting", *IEEE Trans on Power Delivery, Vol.14,No.3,pp.1052-1061,Jul. 1999*
- [20] L. Wang, M. Klein, S. Yirga, P. Kundur, "Dynamic Reduction of Large Power System for Stability Studies", *IEEE Trans. Power Systems, vol.12, No.2, pp.889-895, May 1997*.
- [21] Coherency Based Dynamic Equivalents for Transient Stability Studies, *EPRI 904 Final Report, January 1975*
- [22] Perez-Arriaga, I.J., "Selective Modal Analysis with Applications to Electric Power Systems", Ph.D. Thesis, *Electrical Engineering, Massachusetts Institute of Technology, June 1981*.
- [23] Perez-Arriaga, I.J., Verghese, G.C. and Schweppe, F.C., "Selective Modal Analysis with Applications to Electric Power Systems, Part 1: Heuristic Introduction," *IEEE Transaction on Power Apparatus and system, Vol. PAS-101, No 9, September 1982*
- [24] Verghese, G.C., Perez-Arriaga, I.J., and Schweppe, F.C., "Selective Modal Analysis with Applications to Electric Power Systems, Part II: The Dynamic Stability Problem," *IEEE Transaction on Power Apparatus and system, Vol. PAS-101, No 9, September 1982*
- [25] J. M. Undrill, A. E. Turner, "Construction of Power System Electromechanical Equivalents By Modal Analysis", *IEEE Trans, Vol, PAS-90, Sept,1971, pp:2049-2059*
- [26] Price, W.W.; Roth, B.A., "Large-Scale Implementation of Modal Dynamic Equivalents", *IEEE Transactions on Power Apparatus and Systems, Volume PAS-100, Issue 8, Aug. 1981 pp:3811 – 3817*
- [27] R. Podmore, "Identification of Coherent Generators for Dynamic Equivalents", *IEEE Trans on Power Apparatus and systems, vol. PAS-97, No.4, pp.1344-1354, July 1978*.
- [28] R.Podmore, "Development of Dynamic Equivalents for Transient Stability Studies", *EPRI Report EL-456,1977*
- [29] P. Kundur, G.J. Rogers, D.Y. Wong, J. Ottevangers, and L.Wang, "Dynamic Reduction", *EPRI TR-102234 Volume 1, Project 2447-01 Final Report, April 1993*
- [30] R. Nath, S. S. Lama, K. S. Prakasa Rao, "Coherency Based System Decomposition into Study and External Areas", *IEEE Trans on Power Apparatus and systems, vol. PAS-104, No.6, pp.1443-1449, June 1985*.
- [31] J. R. Winkelman, J. H. Chow, B. C. Bowler et al, "An Analysis of Interarea Dynamics of Multi-Machine Systems", *IEEE Trans on Power Apparatus and systems, vol. PAS-100, No.2, pp.754-763, Feb.*
- [32] P. V. Kokotovic, J. J. Allemong, J. R. Winkelman, J. H. Chow, "Singular Perturbation and Iterative Separation of Time Scales," *AUTOMATICA, Vol. 16, No. 1, January 1980, pp. 23-33*.
- [33] Winkleman, J.R., Chow, J.H., Allemong, J.J. and Kokotovic, P.V. "Multi-Time Scale Analysis of Power System", *AUTOMATICA, Vol. 16, pp. 35-43*.

- [34] J. H. Chow, "Time-scale Modeling of Dynamic Networks with Applications to Power Systems", *Springer-Verlag, New York, 1982*.
- [35] S.B. Yusuf, G.J. Rogers, R.T.H. Alden, "Slow Coherency Based Network Partitioning Including Load Buses", *IEEE Trans on Power systems, vol.8, No 3, August 1993*.
- [36] William W. Price, Joe H. Chow, Allen W. Hargrave, Brian J. Hurysz, Peter M. Hirsch, "Large-scale system testing of a power system dynamic equivalencing program", *IEEE Trans on Power Systems, vol.13, No.3, August 1998*.
- [37] Yao-nan Yu, El-Sharkawi M.A., "Estimation of External Dynamic Equivalents of a Thirteen-Machine System", *IEEE Trans on Power Apparatus and Systems, Volume PAS-100, Issue 3, March 1981 pp:1324 - 1332, Digital Object Identifier 10.1109/TPAS.1981.316605*
- [38] Ju, P., Ni, L.Q., Wu, F., "Dynamic equivalents of power systems with online measurements. Part 1: Theory", *Generation, Transmission and Distribution, IEE Proceedings, Volume 151, Issue 2, 2 March 2004 Page(s):175 -178*
- [39] Ju, P., Li, F., Yang, N.G., Wu, X.M., He, N.Q., "Dynamic equivalents of power systems with online measurements Part 2: Applications", *Generation, Transmission and Distribution, IEE Proceedings, Volume 151, Issue 2, 2 March 2004 Page(s):179 - 182*
- [40] Stankovic, A.M., Saric, A.T., "Transient power system analysis with measurement-based gray box and hybrid dynamic equivalents", *Power Systems, IEEE Transactions on Volume 19, Issue 1, Feb. 2004 Page(s):455 - 462*
- [41] S.Geeves, "A Modal-Coherency Technique for Deriving Dynamic Equivalents", *IEEE Transaction on Power systems, vol.3, No 1, February 1998*.
- [42] A.S.Morched, J.H.Ottevangers, L.Marti, "Multi-Port Frequency Dependent Network Equivalents for the EMTP", *IEEE Trans on Power Delivery, vol.8, No.3, pp.1402-1412, Oct.1993*
- [43] N.R.Watson, J.Arrillaga, "Frequency-Dependent A.C. System Equivalents for Harmonic Studies and Transient Converter Simulation", *IEEE Trans on Power Delivery, vol.3, No.3, pp.1196-1203, Jul.1988*
- [44] Marti, L., "Low-Order Approximation of Transmission Line Parameters for Frequency-Dependent Models", *IEEE Trans on Power Apparatus and Systems Volume PAS-102, Issue 11, Nov. 1983 Page(s):3582-3589*
- [45] Noda, T., "Identification of a multiphase network equivalent for electromagnetic transient calculations using partitioned frequency response", *IEEE Trans on Power Delivery, vol.20, Issue 2, Part 1, April 2005 Page(s):1134-1142*
- [46] Noda, T., "A Binary Frequency-Region Partitioning Algorithm for the Identification of a Multiphase Network Equivalent for EMT Studies", *IEEE Trans on Power Delivery, vol.22, No.2, April 2007*
- [47] J.Hong, J.Park, "A time-domain approach to transmission network equivalents via Prony analysis for electromagnetic transients analysis", *IEEE Transaction on Power systems, vol.10, No 4, pp.1789-1797, November 1995*.
- [48] B. Gustavsen, "Improving the Pole Relocating Properties of Vector Fitting", *IEEE Transactions on Power Systems, Vol 21, No 3, July 2006*
- [49] Bjorn Gustavsen, "Enforcing Passivity for Admittance Matrices Approximated by Rational Functions", *IEEE Transactions on Power Systems, Vol 16, No 1, February 2001*

- [50] H.W. Dommel, *Electromagnetic Transients Program Reference Manual (EMTP Theory Book)*. Portland, OR, U.S.A.: BPA, 1986
- [51] Power System Control and Stability, Second Edition, P.M. Anderson, A.A. Fouad
- [52] W.W. Price, E.M. Gulachenski, P. Kundur, F.J. Lange, G.C. Loehr, B.A. Roth, R.F. Silva, "Testing of the modal dynamic equivalents technique", *IEEE Trans on Power Apparatus and Systems*, vol. PAS-97, pp:1366-1372, July/August 1978.
- [53] A. J. Germond, R. Podmore, "Dynamic Aggregation of Generating Unit Models", *IEEE Trans on Power Apparatus and Systems*, vol. PAS-97, No.4, pp.1060-1069, July 1978.
- [54] R. J. Galarza, J. H. Chow, W. W. Price et al, "Aggregation of Exciter Models for Constructing Power System Dynamic Equivalents", *IEEE Trans on Power Systems*, vol.13, No.3, pp.782-788, Aug. 1998.
- [55] Matlab R2007a Help Documentation, The MathWorks, Inc.
- [56] Lei, X., Povh, D., Ruhle, O., "Industrial approaches for dynamic equivalents of large power systems", *Power Engineering Society Winter Meeting, 2002. IEEE, Volume 2, 27-31 Jan. 2002 Page(s):1036 - 1042 vol.2*
- [57] Ganesh N. Ramaswamy, Luis Rouco, Ollivier Fillatre, George C. Verghese, "Synchronic Modal Equivalentencing (SME) for Structure-Preserving Dynamic Equivalents", *IEEE Trans on Power Systems*, Vol. 11. No. 1, February 1996
- [58] G.N.Ramaswamy, C.Evrard,G.C.Verghese, O.Fillatre, B.C.Lesieutre, "Extensions, simplifications,and tests of synchronic modal equivalentencing(SME)", *IEEE Trans.Power System*,vol.12,no. 2,pp.896-905,May 1997
- [59] R.Nath , S.S. Lamba, "Development of coherency-based time domain equivalent model using structure constraints", *Proc.Inst.Elect.Eng.*,vol.133,no.4,pt.C,pp.165-175,May 1986
- [60] M.Larbi Ourari, Louis-A.Dessaint, Van-Que Do, "Dynamic Equivalent Modeling of Large Power Systems Using Structure Perservation Technique", *IEEE Trans on Power Systems*,Vol.21,No.3,August 2006
- [61] "Computer Representation of Excitation Systems", IEEE COMMITTEE REPORT, *IEEE Transactions on Power Apparatus and Systems*,vol.PAS-87, No.6.June 1968
- [62] W.F Tinney, V. Brandvajn, S.M. Chan, "Sparse Vector Methods", *IEEE Trans on PAS*, Vol.PAS-104,. No. 4, Feb 1985